

**Design of a Low Head Pico Hydro Turbine
for Rural Electrification in Cameroon**

by

Bryan Patrick Ho-Yan

**A Thesis
presented to
The University of Guelph**

**In partial fulfilment of requirements
for the degree of
Master of Applied Science
in
Engineering and International Development**

Guelph, Ontario, Canada

© Bryan Patrick Ho-Yan, April, 2012

ABSTRACT

DESIGN OF A PICO HYDRO TURBINE FOR RURAL ELECTRIFICATION IN CAMEROON

**Bryan Patrick Ho-Yan
University of Guelph, 2012**

**Advisor:
Professor W. D. Lubitz**

Rural areas of Cameroon have limited to no availability of grid-supplied electricity, however many locations have significant hydro potential. Pico hydro (less than 5 kW generation capacity) has been identified as a promising means for rural electrification.

Tests of previously implemented designs and field research in Cameroon were conducted to contextualize the design process. Field research involved end-user and artisan interviews, market research, site investigations, and artisan collaboration. Findings were used to select an axial flow propeller for the improved turbine. Detailed design used turbomachinery theory towards the development of a locally manufactured low head pico hydro turbine for rural electrification. A propeller turbine with complex blade geometries was designed but simplified to incorporate flat blade geometries to better suit the local manufacture capabilities. A prototype turbine was built and tested. The flat blade propeller turbine performed reasonably well, but was unable to achieve desired power generation targets with predefined head and flow rate conditions.

Dedication and Acknowledgements

This thesis is dedicated to my wife, Annie, who has never stopped encouraging me throughout this endeavour and constantly inspires me through her love and integrity. And also to my daughters, Blythe and Abbey, for keeping me on my toes and inspiring me to never stop learning.

I would like to express my gratitude to my graduate advisor, Dr. William David Lubitz for the opportunity to define my research and run with it. Through his guidance and openness he has strengthened this work. My appreciation also goes to Dr. Warren Stiver for his insights and strong support for this project.

This research would not exist without the leadership and hard work of Johannes Hertlein, Cornelia Ehlers, and Edwin Njongo of GREEN STEP e.V. I am always amazed by their enthusiasm and their ability to make things happen. My appreciation goes to them for showing me the beauties of Cameroon.

Many thanks go to Dr. Stephan Krebs, Johannes Urban, Petra Kuerzinger, Gerald Schickhuber, and Björn Pucher for sharing their invaluable ideas with me.

I must acknowledge my friends and research colleagues in Engineering and International Development specifically Qiyue Song, Rajendra Sapkota, and Murray Lyons for their help with research and the test rig setup, and Joel Citulski, Graham Aikenhead, Maxime Moisan, Nitin Seth, and Stephanie Shaw for going through this whole adventure with me.

I am grateful for the technical and administrative support from the University of Guelph staff, namely Ken Graham, Steve Wilson, Barry Verspagen, Nate Groendyck, John Whiteside, Mary Payne, Phil Watson, Lucy Cremasco, Alex Galvez, Martha Davies, and Laurie Gallinger.

And a final thank you to my professors at the University of Guelph for opening my eyes to the complexities of development from all disciplines and perspectives and for teaching me about how little we know.

This research was supported by the Natural Sciences and Engineering Research Council (NSERC) Chair in Environmental Design Engineering at the University of Guelph.

Table of Contents

Dedication and Acknowledgements	iii
Nomenclature	viii
Glossary of Terms	xi
1.0 Project Environment.....	1
1.1 Rural Electrification.....	1
1.1.1 The Current State of Rural Electrification.....	1
1.1.2 Rural Electrification Options	2
1.1.3 Benefits of Rural Electrification.....	2
1.1.4 Applications of Rural Electrification.....	4
1.1.5 Challenges of Rural Electrification.....	5
1.2 Cameroon	5
1.2.1 Geography	6
1.2.2 History	6
1.2.3 Corruption.....	7
1.2.4 Economics	8
1.2.5 Energy.....	8
2.0 Pico Hydro.....	10
2.1 Pico Hydro for Development	10
2.2 General Pico Hydro Principles.....	13
2.3 System Components.....	14
2.3.1 Forebay	14
2.3.2 Penstock.....	14
2.3.3 Turbine.....	15
2.3.4 Draft Tube.....	16
2.3.5 Electrical System	17
2.4 Pico Hydro Turbine Technology.....	17
2.4.1 High Head.....	17
2.4.2 Medium Head	19
2.4.3 Low Head	21
2.5 Pico Hydro in Cameroon.....	27
2.6 Turbine Theory	27
2.6.1 Specific Speed and Specific Diameter.....	27
2.6.2 Euler Turbomachinery Equation.....	30
2.6.3 Velocity Diagrams	31
2.6.4 Blade Cascade Geometry.....	33
3.0 Problem Statement	34
3.1 Problem Statement and Significance	34
3.2 Affiliates	35
3.3 Scope of Work	37
4.0 Baseline Investigation	38
4.1.1 Baseline Construction - Firefly.....	39
4.1.2 Baseline Test Apparatus	40
4.1.3 Baseline Test Method	41
4.1.4 Baseline Test Results.....	42
4.1.5 Baseline Test Discussion	43
5.0 Technology Selection and Concept Designs	45
5.1 Technology Selection.....	45

5.2	Concept Design	49
5.2.1	Cross-flow Concept Design	50
5.2.2	Propeller Turbine Concept Design	52
5.2.3	Concept Design Summary	54
6.0	Cameroon Field Research	55
6.1	End-user and Artisan Interviews	56
6.1.1	Household Information	57
6.1.2	Annual Income and Livelihoods	58
6.1.3	Energy Expenditure	60
6.1.4	Electrical applications	61
6.1.5	Perceived primary concern	65
6.2	Market Research	66
6.3	Installation Site Visit	66
6.4	Craftsmen Collaboration	76
6.5	Field Research Discussion	88
7.0	Detailed Design	90
7.1	Runner Design	91
7.1.1	Tip Diameter	91
7.1.2	Hub-Tip Diameter Ratio	94
7.1.3	Design Velocity Diagrams	96
7.1.4	Number of Blades and Space-Chord Ratio	98
7.1.5	Incidence and Deviation Angle	100
7.1.6	Flat Blade Design	103
7.2	Flat Blade Runner Performance Prediction	104
7.3	Stator Design	107
7.4	Inlet Basin	109
7.5	Generator Connection	109
7.6	Cavitation and Turbine Setting	110
7.7	Draft Tube Design	111
7.8	Detailed Design Summary	113
8.0	Prototype Construction and Testing	114
8.1	Prototype Construction	114
8.2	Performance Test Apparatus	115
8.3	Performance Test Procedure	117
8.4	Performance Test Results	119
8.5	Cost and Material Discussion	123
8.6	Performance Test Discussion	123
9.0	Conclusions	127
10.0	Recommendations	130
11.0	References	132
	Appendix A: Market Research	138
	Appendix B: Design Drawing Package	140
	Appendix C: Matlab Program Code – Detailed Design	166
	Appendix D: Matlab Program Code – Flat Blade Runner Performance Prediction Model	169
	Appendix E: Uncertainty Analysis	173

List of Tables

Table 1: Power output classification of hydropower scheme (source: Williams & Porter, 2006)	10
Table 2: Initial baseline experiment results	42
Table 3: Follow-up experiment results.....	42
Table 4: Comparison of turbine technology types for preliminary selection	48
Table 5: Generalized sizing of concept cross-flow runner	51
Table 6: Conceptual design parameters of cross-flow turbine runner.....	52
Table 7: Concept design summary	54
Table 8: Field research activity by location.....	56
Table 9: Visited installation sites	67
Table 10: Length and condition of primary road network.....	68
Table 11: Calculated flow angles and stagger angles.....	98
Table 12: Incidence, deviation and final flow angles	103
Table 13: Detailed design summary	113
Table A1: Market research list of materials and associated costs	138
Table E1: Instrumentation uncertainty	173

List of Figures

Figure 1: Consumption of electricity and wood fuel versus income per capita	3
Figure 2: Map of Cameroon	6
Figure 3: Off-grid generation cost.....	11
Figure 4: Off-grid capital cost	12
Figure 5: Pico hydro system components.....	14
Figure 6: Turbine selection chart based on head and flow rate	16
Figure 7: Pelton turbine	18
Figure 8: Tesla turbine	19
Figure 9: Turgo turbine	19
Figure 10: Cross-flow turbine	20
Figure 11: Reaction turbine	22
Figure 12: DTU propeller turbine design - stator (top left), runner (bottom left), and shaft (right)	25
Figure 13: Assembly propeller turbine developed by University of Karlsruhe.....	26
Figure 14: Range of specific speeds for turbine types.....	29
Figure 15: Cordier diagram	30
Figure 16: Turbine stage velocity diagram.....	32
Figure 17: Blade cascade geometry.....	33
Figure 18: Runner assembly	39
Figure 19: Layout of test apparatus	41
Figure 20: Cross-flow concept sizing parameters	50
Figure 21: Runner design parameter	53
Figure 22: Map of field research locations and approximate travel routes	55
Figure 23: Annual income in M'muock	58
Figure 24: Energy expenditure per household per month in M'muock.....	60
Figure 25: Owned electrical appliances.....	61
Figure 26: Most desired electrical appliances – female (above) and male (below)	63
Figure 27: Perceived primary concern – female (above) and male (below).....	65

Figure 28: Urban wind turbines – Bafoussam site	67
Figure 29: Bafou wind turbine	69
Figure 30: GREEN STEP e.V.p wind turbine – fallen rotor (left), failed weldment (right)	70
Figure 31: Inoperable Firefly turbines.....	72
Figure 32: Debris and siltation in reservoirs (top left), filter netting (bottom left), modifications to penstock (right)	72
Figure 33: Permanent magnet generator Firefly.....	73
Figure 34: Turgo turbine at Ndungweh	74
Figure 35: COIC students of metal fabrication/welding program.....	77
Figure 36: Standard metal workshop.....	78
Figure 37: Pelton turbine system (left) and cups (right).....	79
Figure 38: Initial cross-flow sidewall.....	80
Figure 39: Build trial schematic	81
Figure 40: Material preparation.....	82
Figure 41: Blade forming	83
Figure 42: Blade placement.....	85
Figure 43: Welding.....	86
Figure 44: Final assembly	87
Figure 45: Design configuration of system (left) and turbine (right)	91
Figure 46: C_{Round} as a function of head to determine tip diameter.....	92
Figure 47: Cordier diagram – specific speed as a function of specific diameter.....	93
Figure 48: Various turbine efficiencies as a function of specific speed and specific diameter.....	93
Figure 49: Hub-tip diameter ratio as a function of specific speed using de Haller limit.....	95
Figure 50: Radial blade stations for velocity diagrams	97
Figure 51: Velocity diagram.....	98
Figure 52: Blade loading	101
Figure 53: Blade blockage.....	101
Figure 54: Carter's parameter.....	102
Figure 55: Isometric model of runner – camber-twist blade design (left) and flat blade design (right).....	104
Figure 56: Diagram of flow over flat plate.....	106
Figure 57: Flat blade runner predicted performance	107
Figure 58: Stator – plan (left) and cross section (right).....	108
Figure 59: Inlet basin plan dimensions (mm).....	109
Figure 60: Variation of Thoma Cavitation Coefficient with Power Specific Speed	111
Figure 61: Area ratio as a function of non-dimensional length for draft tube design.....	112
Figure 62: Schematic of test rig.....	115
Figure 63: Test version turbine.....	116
Figure 64: Sensitivity testing of I-beam influence on flow	118
Figure 65: Turbine shaft power and head versus rotation speed under constant flow rates (a) 5.6 L/s, (b) 7.3 L/s, (c) 11.1 L/s, (d) 12.9 L/s.....	119
Figure 66: Turbine efficiency versus rotation speed under constant flow rates (a) 5.6 L/s, (b) 7.3 L/s, (c) 11.1 L/s, (d) 12.9 L/s.....	120
Figure 67: Calculated power and flow rate versus rotation speed under constant 2 m head.....	122
Figure 68: Sensitivity testing results of I-beam influence on flow.....	122
Figure 69: Part flow efficiencies	124
Figure 70: Experimental results and prediction model comparison (a) 5.6 L/s, (b) 7.3 L/s, (c) 11.1 L/s, (d) 12.9 L/s	125
Figure E1: Load cell standard error versus applied load	173

Nomenclature

a	blade throat
A	planform area
A_1/A_2	non dimensional area of conical draft tube
b	axial chord length
C	fluid velocity
C_1	stator inlet absolute fluid velocity
C_2	stator exit/runner inlet absolute flow angle
C_{2x}	stator exit/runner inlet absolute flow angle axial component
$C_{2\theta}$	stator exit/runner inlet absolute flow angle circumferential component
C_3	runner exit absolute flow angle
C_{3x}	runner exit absolute flow angle axial component
$C_{3\theta}$	runner exit absolute flow angle circumferential component
C_{Banki}	Banki defined velocity coefficient = 0.98
C_D	drag coefficient
$C_{e\theta}$	absolute tangential fluid velocity at exit
$C_{i\theta}$	absolute tangential fluid velocity at inlet
C_L	lift coefficient
C_{Round}	Round defined coefficient
D	characteristic diameter
$D_{CFrunner}$	cross-flow runner diameter
dH	de Haller limit
D_h	runner hub diameter
D_h/D_t	hub-to-tip diameter ratio
D_s	specific diameter
D_t	runner tip diameter
\dot{E}_t	rate of work
f	electrical frequency
F_1	force LCDA-1
F_2	force LCDA-2
F_D	drag force
F_L	lift force
g	gravity (9.81m/s^2)
H	head
H_E	available head
h_{GV}	height of the guide vanes
H_S	net positive suction head
i	incidence angle
j	camber angle

k_{Banki}	Banki defined geometric parameter, relates blade spacing to diameter = 0.075-0.10
K_{ug}	tip-to-head velocity ratio
L	chord length
$L_{CFrunner}$	cross-flow runner length
m	Carter's parameter
\dot{m}	mass flow rate
n	turbine speed (units revolution per unit time)
N/R_I	non-dimensional length of conical draft tube
$n_{CFblade}$	number of blades
N_{poles}	number of poles
n_q	Simpson and Williams defined specific speed
N_s	specific speed (units revolution per unit time)
N_{sp}	power specific speed (units revolution per unit time)
P	power
P_m	shaft/mechanical power
p_a	atmospheric pressure
p_v	fluid vapour pressure
Q	flow rate
r	blade station radial dimension
r_e	radius of particle at exit
r_{GV}	radius of guide vanes
r_i	radius of particle at inlet
r_{tip}	tip radius
r_{vp}	V-notch pulley radius
s	blade spacing
$t_{CFblade}$	circumferential blade spacing
t_{CFjet}	cross-flow jet thickness
U	blade velocity
U_e	blade velocity at exit
U_i	blade velocity at inlet
V_{CF}	cross-flow fluid velocity
W	relative fluid velocity
W_2	stator exit/runner inlet relative fluid velocity
W_{2x}	stator exit/runner inlet relative fluid velocity axial component
$W_{2\theta}$	stator exit/runner inlet relative fluid velocity circumferential component
W_3	runner exit relative fluid velocity
W_{3x}	runner exit relative fluid velocity axial component
$W_{3\theta}$	runner exit inlet relative fluid velocity circumferential component
Z	Zweifel criterion
z	height difference between runner base and tail water surface
α	flow angle

α'	blade angle
α_1	stator inlet absolute flow angle
α_2	stator exit/runner inlet absolute flow angle
α'_2	runner blade inlet angle
α_3	runner exit absolute flow angle
α'_3	runner blade exit angle
α_{Banki}	Banki defined fluid entry angle = 16°
α_{GV}	angle setting of the guide vanes
β_2	stator exit/runner inlet relative flow angle
β_3	runner exit relative flow angle
β_{3c}	blade exit camber angle
β_a	flow angle at the throat
β_{Banki}	blade angle based on Banki defined fluid entry angle
δ	deviation angle
δ_{3H}	deviation angle defined by Hothersall
δ_{3S}	deviation angle defined by Schobeiri
ΔF_1	force LCDA-1 uncertainty
ΔF_2	force LCDA-2 uncertainty
ΔH	head uncertainty
ΔP	power uncertainty
ΔQ	flow rate uncertainty
Δr_{Vp}	V-notch pulley radius uncertainty
$\Delta \eta$	hydraulic efficiency uncertainty
$\Delta \tau$	torque uncertainty
$\Delta \omega$	turbine speed uncertainty (units radians per unit time)
η	hydraulic efficiency
θ	camber angle
λ	axial distance between the base of the guide vanes and the runner blades mid height
ξ	stagger angle
ρ	density
σ	Thoma coefficient
τ	torque
ϕ	angle of attack
ω	turbine speed (units radians per unit time)
Ω_s	specific speed (units radians per unit time)
Ω_{sp}	power specific speed (units radians per unit time)

Glossary of Terms

AC	alternating current
ADEID	Action pour un Développement Équitable, Intégré et Durable
AER	Agence d'Électricité Rurale
AES SONEL	AES Société Nationale d'Électricité
APRL	Asian Pheonix Resources Ltd.
ARSEL	Agence de Régulation du Secteur de l'Electricité
CDC	Cameroon Development Corporation
CFL	compact fluorescent light
CNC	computer numerically controlled
COIC	Cameroon Opportunities Industrialization Center
CPI	Corruption Perception Index
DFID	UK Department for International Development
DTU	Development Technology Unit
EDC	Electricity Development Agency
ELC	electronic load controller
FAO	Food and Agricultural Organization of the United Nations
GDP	gross domestic product
IEA	International Energy Agency
IEG	Independent Evaluation Group
LCA	life cycle analysis
LED	light emitting diode
LIRE	Lao Institute for Renewable Energy
MDGs	Millenium Development Goals
MIG	metal inert gas
NCIG	Nkong Hilltop Common Initiative Group
NGOs	non-governmental organizations
OIC	Opportunities Industrialization Center
PAT	pump-as-turbine
PVC	polyvinyl chloride
WB	World Bank
WHO	World Health Organization
XAF	Central African CFA franc (100 XAF = € 0.15)

1.0 Project Environment

1.1 Rural Electrification

Rural electrification is the process of providing electrical services to rural areas: generally regions with sparse populations where agriculture is the dominant livelihood. The recipients of rural electrification tend to have higher labour-to-capital ratios and lower household incomes than in urban areas. After rural electrification, load densities are lower than in urban areas, due to fewer connections, lower consumption rates, and lower load factors (ratios of average demand to peak demand). These factors tend to increase monetary costs per connection and per unit of electricity, making it costly to extend electrical grids to rural areas. In addition, operation and maintenance of rural electrical infrastructure is more problematic and adversely affects the quality of electricity (Munasinghe, 1990). However, if these issues can be overcome, studies (Independent Evaluation Group, 2008; Ranganathan, 1992) have shown that rural electrification enhances welfare through increased security, productivity, health, entertainment, information, and education, with the associated costs and benefits of a given rural electrification scheme being context specific.

1.1.1 The Current State of Rural Electrification

In 2008, it was estimated by the International Energy Agency (IEA) that 1.5 billion people, or 22% of the global population, do not have access to electricity (International Energy Agency, 2009); 85% of this population group are situated in rural areas. In Sub-Saharan Africa, only 29% of the population is electrified, and this percentage is decreasing as population growth outstripped electrification since 2001. In South Asia, more than 570 million people are without access to electricity, with 92% of them in rural areas. Latin America and the Middle East have similar average electrification rate of 93% and 89% respectively, with nearly the entire urban populations having access to electricity, while only 70% and 71% of the respective rural populations have access. East Asia and China have made some marked improvements, dropping from 241million

to 195 million without electricity access (International Energy Agency, 2009). However, some countries within this region continue to have low electrification rates, including Myanmar (13%), East Timor (22%), and Cambodia (24%).

1.1.2 Rural Electrification Options

Rural electrification can be achieved through:

- extensions of national or regional distribution systems, or grids, to rural areas,
- isolated generators electrifying mini-grids to supply a community,
- or, isolated generators electrifying a single house or facility (Munasinghe, 1990).

Electricity can be generated using different types of primary energy. These include fossil fuels (such as coal, natural gas, and petroleum fuels), nuclear energy, and renewable energy. Within the renewable energy classification is biomass, solar, hydro, and wind.

1.1.3 Benefits of Rural Electrification

Rural electrification is often financially viable as the willingness to pay has been commonly found to exceed the long run cost of supply. This implies good rates of return and financial stability. However, this is dependent on two major factors: supply costs and system losses must be minimized, and a balance must be struck between financial stability and reaching the poor (Independent Evaluation Group, 2008).

Rural electrification facilitates global development. On September 8, 2000, commitments were made by 189 world leaders to work towards the eight Millennium Development Goals (MDGs). This commitment exemplified the collective acceptance of the need to significantly reduce extreme poverty and its many forms on a global scale. Though rural electrification was not directly defined as one of the MDGs, it has been recognized that access to energy is crucial for the achievement of these goals (Modi et al., 2006). Rural electrification increases productivity through mechanization, communication, and extended lighting hours, thus spurring on enterprise

development. It improves school environments with regards to lighting, sanitation and access to clean water, therefore increasing attendance and reducing drop-out rates. In addition, improvements are made to health through the supply of refrigeration for medicines and the increased willingness of skilled workers to reside in electrified areas (DFID-Department for International Development, 2002).

Rural electrification can benefit the environment. Electricity is a high quality form of energy that can be used for many applications. It is typically generated more efficiently while releasing fewer pollutants compared to the burning of traditional energy sources such as liquid fuels or wood biomass for lighting or heating purposes. As seen in Figure 1, there is a greater dependence on wood fuel in poorer countries than richer countries. There is an increasing trend of electricity consumption per capita as country wealth increases. This trend is also seen within country populations, with the poor heavily relying on less efficient fuels (Independent Evaluation Group, 2008). In addition, the use of electricity leads to the reduced utilization of traditional energy sources by households. The savings from the reduction in traditional energy consumed is often greater than the cost of the new electrical energy used (Cecelski, 1979).

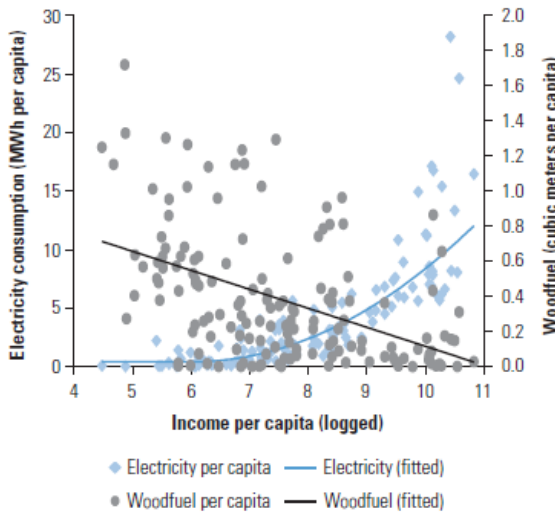


Figure 1: Consumption of electricity and wood fuel versus income per capita
 (source: Independent Evaluation Group, 2008)

Indoor air pollution and smoke inhalation have been identified as a major global public health concern, causing chronic pulmonary disease, adverse fetal development, and infant mortality (Bruce, Perez-Padilla, & Albalak, 2000). Adoption of externally generated electricity for light, heat, and cooking would drastically improve indoor air quality in households currently using indoor biomass combustion. The traditional burning of fuels, specifically for heating and cooking, is strongly linked to social and cultural factors and must therefore be considered.

1.1.4 Applications of Rural Electrification

Rural electrification can be used for residential, public, commercial, industrial, and agricultural connections. To provide some indication of allocation, nearly 95% of the connections to the World Bank's rural electrification projects are residential. The few non-residential connections typically have higher energy demand (Independent Evaluation Group, 2008).

Within households, lighting and television are the dominant uses, making up at least 80% of the total electrical consumption. Rural electrification is rarely used for cooking with the exception of the use of rice cookers in East Asia (Independent Evaluation Group, 2008). With the popularization of mobile phones, battery charging has also become more prevalent.

Rural electrification is often used for lighting in communal facilities such as town halls, which are integral for social gathering, community building, and information exchange. Health centres use electricity for lighting, and if possible, cold storage of medications.

Productive uses of rural electrification include irrigation for agriculture, improved communication for the trading of goods, and the promotion and strengthening of small and medium sized enterprises.

1.1.5 Challenges of Rural Electrification

Many social, financial, and technical challenges must be faced to increase rural electrification.

In most cases, the process of rural electrification is achieved through extending existing power grids outward to non-electrified areas instead of reaching members of the population who already reside in electrified areas but do not have access. The poor benefit less from rural electrification than the non-poor, mainly due to barriers of high connection costs and the lack of information about how to maximize the benefits of rural electrification (Independent Evaluation Group, 2008).

With high supply costs and the dominance of non-productive residential and communal uses, rural electrification is often perceived as cost ineffective. However, the framing of rural electrification must be changed from the stand-alone benefit of electricity and towards the greater long-term social benefit, which builds a stronger case for rural electrification (Ranganathan, 1992).

Improving load factors by levelling out the electricity demand throughout the entire day can increase the financial viability of rural electrification by allowing greater use of transmission and generating infrastructure. Majority residential use typically concentrates the demand in the evenings, whereas, industrial or commercial uses will increase the daytime demand. However, factories in grid-electrified rural settings often continue to use independent generators, typically diesel powered, if the grid supply is unreliable (Independent Evaluation Group, 2008).

1.2 Cameroon

Cameroon is a resource rich country with a relatively stable political situation. Unfortunately, the country remains classified as low-middle income and has been unable to move towards sustained development and decrease reliance on foreign intervention.

1.2.1 Geography

Cameroon is located on the west coast of Central Africa. It shares borders with Nigeria to the northwest, Chad to the northeast, Central African Republic to the east, Congo to the southeast, Gabon to the south, and Equatorial New Guinea to the southwest. Total country area is 475,440 km², with 472,710 km² land area and 2,730 km² water area (FAOSTAT, 2012). As of 2010, the population of Cameroon was 19,600,000 (World Bank Data, 2012).



Figure 2: Map of Cameroon
(adapted: National Geographic & ESRI, 2011)

1.2.2 History

Cameroon has been under outside influence continually during its recent history. In 1884, Germany claimed the coastal region of Cameroon and established direct trading with the African interior. Also during this period, large agricultural estates formed to grow tropical produce for export trade back to Germany (Mbaku, 2005). Following World War I, Germany was forced to

surrender their colonies, and Cameroon came under divided British and French rule under the League of Nations mandates. The western region became British Cameroon. Resentment towards the British was fuelled by neglectful management and the large migration of Nigerians into Cameroon. The eastern region, French Cameroon had an administrative system modeled after nearby French colonies and saw greater agricultural growth and industrial development. During this time, valuable raw resources were extracted for value-added processing in Europe and sold back to Cameroon and other countries, forming a strong dependence on finished goods. After the end of World War II, Cameroon, like many other colonies sought independence. The United Nations oversaw a plebiscite that combined British and French Cameroon. Cameroon became an independent country on January 1, 1960 under the authoritarian rule of Ahmadou Ahidjo, who was supported by the French officials, as the first president (Ndi, n.d.). It was through him that close ties were maintained with France and the Anglophone population was further marginalized. Ahidjo ceded power to Paul Biya in 1982, who introduced democratic reforms (DeLancey, 1986). However, Biya has maintained leadership ever since and as this is written continues to hold firm authority over the political system.

1.2.3 Corruption

Corruption is a significant concern in Cameroon. The country has consistently ranked low in Transparency International's Corruption Perception Index (CPI), a ranking of countries based on the perception of corruption in the public and political sector from country experts and business leaders. Cameroon was the lowest rated country indexed in 1998 and 1999. Accordingly, the government has introduced administrative and judicial reform and increased transparency to combat corruption however significant obstacles remain (African Development Bank, 2009).

Among other public services, the customs department has been cited as one of the most corrupt services in the country. Corrupt practices include the seizure of goods to obligate fees from

customers and the bribing of officials to wrongfully classify goods under “temporary admission” to avoid customs duties (Fonchingong, 2009).

1.2.4 Economics

Cameroon is classified as a lower middle income country with a gross domestic product (GDP) of \$22.39 billion US and a GDP per capita of \$1122 US in 2010 (World Bank Data, 2012). Over the recent past, the country has seen erratic economic growth. Strong growth that occurred during the 1970s and 1980s was mainly attributed to agricultural and oil exports. Due to poor policy decisions and declining exports, Cameroon underwent economic depression from 1986 to 1993. This contraction in the economy turned into a fiscal crisis and translated to significant reductions in public expenditures such as education, health, and infrastructure which adversely affected the poor. In reaction to this, growth strategies were set in place and poverty fell during 1996 to 2001. However, growth did not directly benefit the core poor, and high inequality remained. Since then, the economic structure has remained tied to few export commodities, including oil, leaving Cameroon vulnerable to external trade shocks, impacting government resources, and reducing public spending (Charlier, 2009).

1.2.5 Energy

Cameroon has significant energy resources. It possesses 294 TWh/year of hydro potential, of which 115 TWh/year is considered technically feasible for exploitation. This is the second highest source in Africa (Kenfack et al., 2010; Nfah & Ngundam, 2009). In addition, natural gas and oil reserves have been discovered in the country. The natural gas potential is modest and insufficient for export but can be used for domestic demand (Charlier, 2009). Cameroon is a net energy exporter, trading over 42% of its energy production.

Due to a lack of infrastructure investment, only a fraction of the energy potential is harnessed with total electricity production in 2008 being only 5.55 TWh (World Bank Data, 2012) from

natural gas (7.71%), oil (15.89%) and hydro (76.24%) (World Bank Data, 2012). Electricity production capacity is insufficient at approximately 1000 MW, and there are often service disruptions. The current system is composed of a large grid network serving the two main cities Douala and Yaoundé, a smaller grid system serving the main northern cities, and a number of isolated grids powered by diesel generators for rural centres (Charlier, 2009).

Electricity consumption in 2008 was 5.01 TWh (World Bank Data, 2012). On a per capita basis, consumption is lower than in comparable countries at only 263 kWh which alludes to the low electrification rates. Nearly 14 million people in Cameroon do not have electricity, giving an electrification rate of only 29% (International Energy Agency, 2009). Urban access is 88% and rural access is 23%, with large areas having no service at all. 70% of industrial energy consumption is electricity, largely due to an aluminum smelter in Edea, Littoral that utilizes 300 MW of the national electrical system capacity. Domestically, electricity only accounts for 3.5% of household energy consumption while 86% of household energy consumption is from biomass (Charlier, 2009).

The energy sector has recently undergone significant institutional reform over the recent history. Prior to 1998, the production, transmission, distribution and retail sale of electricity was solely controlled by a public-private company, AES Société Nationale d'Électricité (AES SONEL). Since then, the sector had been liberalized with the objective of increasing private sector investment. Also, a sector regulator (Agence de Régulation du Secteur de l'Electricité-ARSEL), a rural electrification agency (Agence d'Électricité Rurale-AER), and a power sector asset holding company (Electricity Development Agency-EDC) have been formed. However, due to a lack of transparency, experience, and independent authority, these institutions have been ineffective towards improving system interconnection, energy transport, and production cost regulation. (Lejeune, Fogue, Kenfack, & Tamo Tatietse, n.d.).

2.0 Pico Hydro

Hydropower converts the energy in water flows to useful forms such as electricity or mechanical work. The scales of hydropower schemes cover a broad range and are generally classified by power output as in Table 1. Larger schemes generally require damming to create storage capacity and regulate water flow. Given the greater amount of power generation, they are typically grid connected to supply high levels of demand. At the smallest scale are so-called “pico hydro” systems which generate no more than a few kilowatts. Pico hydro systems may require water storage at a non-invasive level, or may be configured as run-of-river and not require any damming.

Table 1: Power output classification of hydropower scheme (source: Williams & Porter, 2006)

Classification	Power Output
Large	> 100 MW
Medium	10 – 100 MW
Small	1 – 10 MW
Mini	100kW – 1 MW
Micro	5 – 100 kW
Pico	< 5 kW

2.1 Pico Hydro for Development

Pico hydro is recognized as a viable option to electrify remote areas, considering economic, environmental, and social perspectives. Recent studies by the World Bank Energy Unit (The World Bank Group Energy Unit, Energy, Transport and Water Department, 2006) found pico hydro yielded the lowest generating costs amongst off-grid energy options (Figure 3). Maher et al. (2003) compared pico hydro systems to solar photovoltaic systems in Kenya and determined that the former was more cost effective on a per-household basis with a 15% lower cost per kWh. With lower material costs and careful consideration of distribution and power management, pico hydro was found to be affordable for most low-income households. These findings were consistent with average annual costs in Vietnam (Energy Sector Management Assistance Programme, 2005) and Laos (Smits & Bush, 2010).

Capital costs for renewable energy systems, including pico hydro, tend to be higher than conventional fuel systems (Figure 4). Khennas and Barnett (2000) reviewed 16 micro hydro projects (micro hydro systems yield comparable per unit capital costs to pico hydro systems) in Sri Lanka, Nepal, Peru, Zimbabwe, and Mozambique and found capital costs per kW capacity of micro hydro electrical generation schemes to be significantly higher than previously predicted in literature due to the incorrect evaluation of non-monetary input costs such as ‘sweat equity’ or community labour. Despite the higher capital costs, Khennas and Barnett still concluded that investment in pico hydro can be recovered and be profitable.

Moreover, the economic success of hydroelectric projects is greatly dependent on a high load factor. Therefore innovative means to better utilize the generation equipment must be incorporated to improve the economic viability (Fulford, 2000; Smith, 1994).

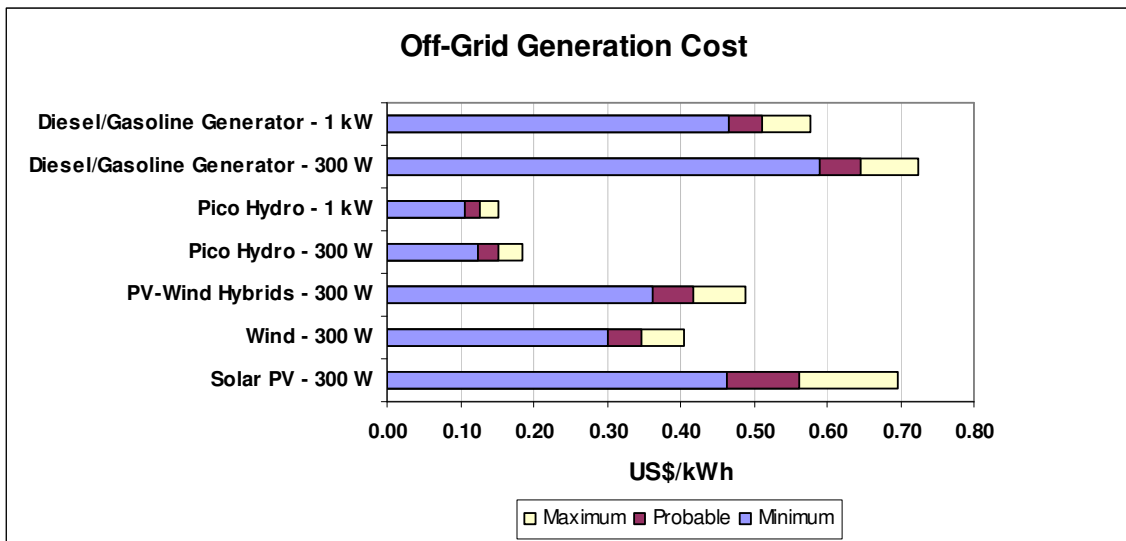


Figure 3: Off-grid generation cost
(adapted: The World Bank Group Energy Unit, Energy, Transport and Water Department, 2006)

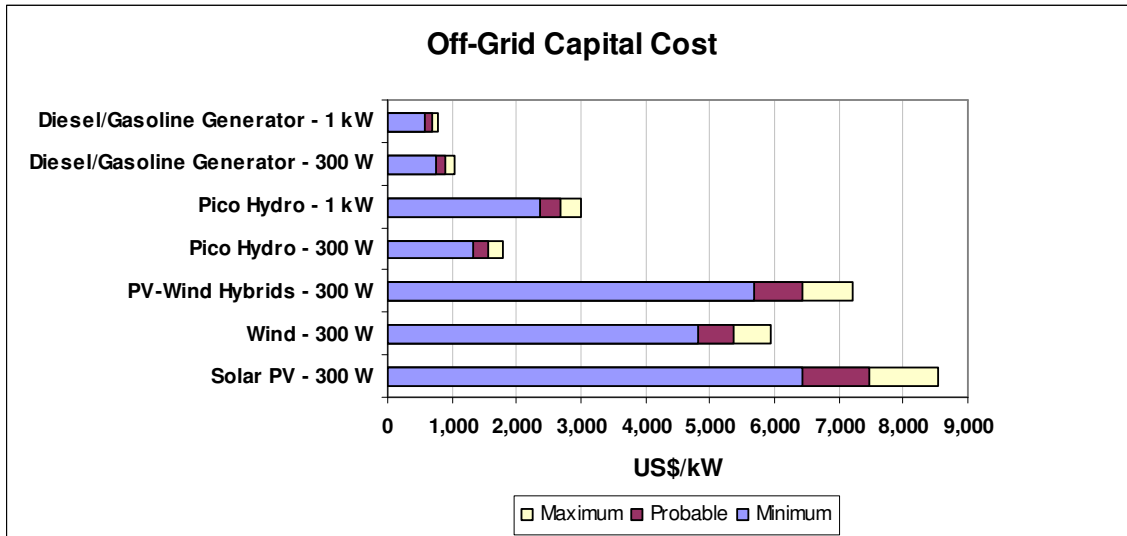


Figure 4: Off-grid capital cost
(adapted: The World Bank Group Energy Unit, Energy, Transport and Water Department, 2006)

Unlike large scale hydropower, there is low environmental impact with pico hydro systems, mainly due to the exclusion of large water containment. Associated large civil works, flooding of habitats, and the modification of downstream flow are not required for the operation of pico hydro systems. In addition, negative impacts of large reservoirs such as siltation, increased mercury levels, and off-gassing of green house gases from submerged decomposing organic material are avoided (Gunkel, 2009).

Pascale et al. (2011) conducted a life cycle analysis (LCA) comparing a 3 kW pico hydro system, a diesel generator, and grid extension and connection for a rural village in Thailand. Measured impact categories included global warming potential, acidification potential, depletion of non-living resources, and energy demand, amongst others. The analysis found that pico hydro had the lowest impact, by a significant margin, in all categories. The largest impact contributors for the pico hydro system were transmission lines, distribution, and the penstock (defined in section 2.3.2).

Pico hydro has positive social impacts. There is a greater potential for active participation of the beneficiaries and the associated social benefits from rural electrification using pico hydro than with other technologies (Chhetri, Pokharel, & Islam, 2009; Williams & Porter, 2006). In addition, since large damming is unnecessary, the displacement of inhabitants and restructuring of livelihoods are avoided.

Disadvantages of pico hydro systems include the site specific nature of installations, high capital costs as barriers for adoption, and little or no support from government institutions (Smits & Bush, 2010). In addition, as with any technology, capacity training and proper management of the systems is required. This has been lacking in numerous incidences and has led to the failure of systems and the wasting of limited resources.

2.2 General Pico Hydro Principles

Hydro energy is the term given to the process of extracting the potential energy from a flow of water over a height difference. The gravitational potential energy associated with the water is converted to mechanical energy that can be used directly or converted again into electrical energy by means of a generator.

The power, P , which can be extracted from a water flow is

$$P = \eta Q H \rho g \quad (2.1)$$

where η is the efficiency of the energy conversion system, Q is total volumetric flow, H is head (the actual height difference between the free surfaces of the reservoirs or channels upstream and downstream of a turbine), ρ is water density, and g is the gravitational constant (9.81 m/s^2).

2.3 System Components

Pico hydro systems are composed of several components. They generally include the forebay, penstock, turbine, and the electrical system (Figure 5).

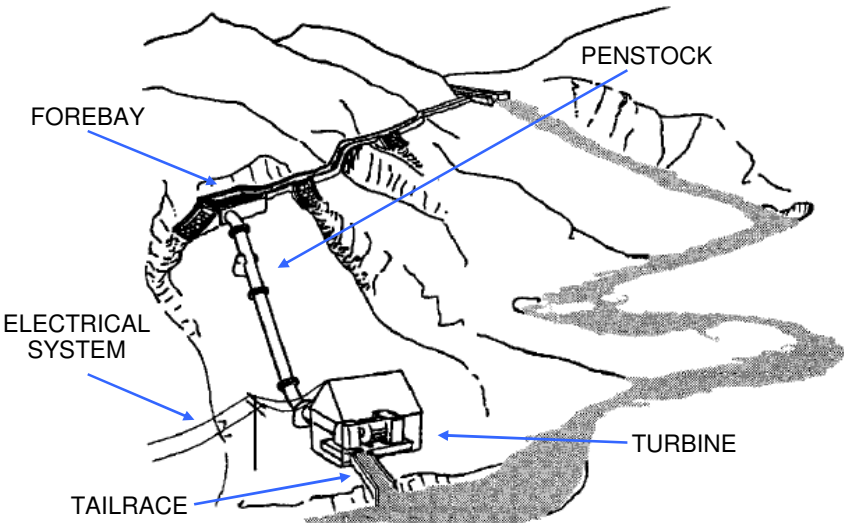


Figure 5: Pico hydro system components
(adapted: Paish, 2002)

2.3.1 Forebay

Small civil works are typically performed to divert a portion of the flow to the forebay tank, which is a reservoir upstream of the turbine. The forebay moderates head and flow to the turbine while also lowering the risk of damage due to flooding.

2.3.2 Penstock

The penstock is a pipe that delivers water from the reservoir or upstream source to the turbine. Care must be taken when determining length, material, inner diameter, and layout as all of these greatly impact cost and performance due to pipe flow losses. In addition, debris, such as leaves and branches, constantly threaten to create blockages in the system. Filters can be employed at the penstock inlet to keep out large foreign objects that could damage the turbine. However, the presence of filters causes a restriction of flow and therefore a loss in pressure head. Fraenkel et al. (1991), Maher and Smith (2001), and Alexander and Giddens (2008) provide in depth

guidance on optimizing the penstock design for pico hydro systems.

2.3.3 Turbine

The turbine is an assembly consisting of a nozzle or stator, runner, and shaft that collectively convert momentum and pressure in a water flow into rotational mechanical work. The nozzle or stator directs the flow to the runner: it may be an orifice that creates a high speed jet, or it may be a set of vanes. The runner is a mechanism that converts the hydraulic energy into mechanical power by redirecting fluid flow. The runner is typically equipped with cups or blades that interact with the moving water and cause the runner to rotate. If electrical generation is the objective, the mechanical work is transferred by the shaft to a generator.

Turbines can be classified as either impulse or reaction.

Impulse turbines – Pressurized water from the penstock is converted to high-speed water jets that transfer the kinetic energy of the jet by impacting the turbine blades or cups causing rotation. The pressure drop in the water flow occurs at the nozzle and the runner operates at atmospheric pressure (Fraenkel et al., 1991). Examples of impulse turbines include the Pelton wheel, Turgo wheel, and cross-flow (Banki-Michell) turbines. Impulse turbines generally operate best with medium or high head (above 10 m).

Reaction turbines – Reaction turbines operate under pressure in an internal flow regime. Water passes the stator, which takes the form of spiral casings or guide vanes, to introduce swirl into the flow. The flow is then redirected by the runner blades. The angular momentum of the water forces rotation in the runner. In contrast to impulse turbines, the water pressure drops at the stator and the runner (Fraenkel et al., 1991). Examples of reaction turbines include propeller, Kaplan, and Francis turbines. Reaction turbines often have complex blade geometries and housings,

which make them more difficult to manufacture at smaller scales in a developing country setting. However, as seen in Figure 6, reaction turbines can perform well even in the low head range (less than 10 m), making them more desirable since low head water sources are more accessible and closer to end-use locations (Paish, 2002).

Different types of turbines can be selected to best suit given head and flow conditions. Figure 6 shows the typical application ranges of various turbines.

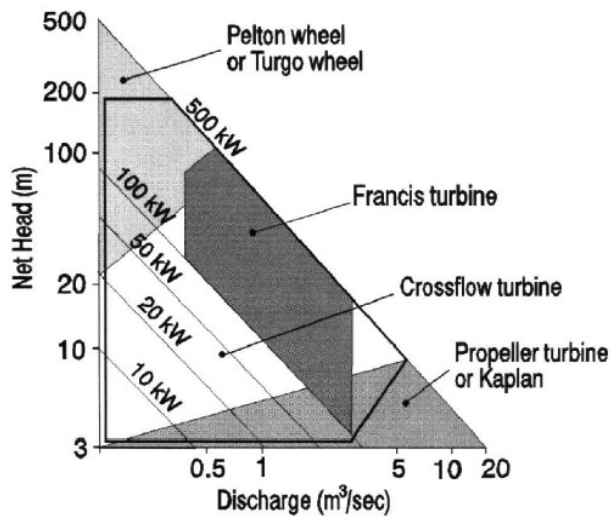


Figure 6: Turbine selection chart based on head and flow rate
(source: Fraenkel et al., 1991)

2.3.4 Draft Tube

A draft tube is an essential component of a reaction turbine, connecting the turbine exit to the tailrace, the reservoir that receives the exhaust water. The draft tube slows the exhaust flow from the runner to recover some of the kinetic energy, and creates a vacuum below the runner resulting in an increased pressure drop across the runner (French River Land Company, 2012; Hothersall, 2004; Paish, 2002).

It is important to consider seasonal variations of downstream water levels when designing a draft tube, because the draft tube outlet must stay submerged. Therefore the draft tube must extend below the minimum level of the tail water surface, while the generator must be positioned higher

than the maximum flood level of the tail water surface (Fraenkel et al., 1991).

2.3.5 Electrical System

The electrical system of a pico hydro generating system consists of a generator, electrical controller, distribution system, and electrical load.

The torque and rotation of the runner and shaft rotate a generator, directly or with a mechanical transmission, and the mechanical power is converted to electrical power. For pico and micro hydro purposes, popular generating devices are vehicle alternators, induction motors, and permanent magnet generators (Howey, 2009; Portegijs, 2003; Smith, 1994; Williams, Simpson, Downes, & Stait, n.d.). The output electricity is single phase alternating current (AC).

Electronic load controllers (ELCs) are used as electrical brakes to regulate the rotational speed of the turbine by diverting power to connected dump loads. Dump loads, which are typically large resistive elements, are used to dissipate excessive electrical power. With the use of ELCs, mechanical flow governing systems are not required, which tended to be the most expensive and unreliable components (Portegijs, 2006). More sophisticated electronic controllers may also conduct further power conditioning to ensure constant voltage and current before use. They may regulate, amplify, convert, and smooth the electrical signal from the generator, reducing the risk of damage to electrical appliances or personal injury. Electricity is delivered to the electrical loads in the households via cables.

2.4 Pico Hydro Turbine Technology

2.4.1 High Head

For high head and low flow applications, Pelton turbines (Figure 7) are typically used due to ease of manufacture and maintenance and the adaptability to some variations in head and flow. Thake (2000) published a comprehensive manual for micro scale Pelton turbines covering theory,

design, manufacture, installation, and maintenance. Maher (2001) in collaboration with Nepalese and Colombian manufacturers extended this work for the pico hydro scale with the “Pico Power Pack” design. The initial bucket design was based on Thake’s design and optimized the thickness of material and the number of buckets using flow analysis and laboratory testing (Williams & Simpson, 2009).

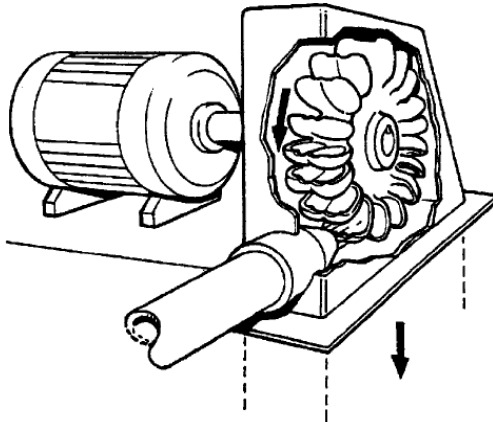


Figure 7: Pelton turbine
(source: Paish, 2002)

Tesla turbines (Figure 8) are often touted as high efficiency turbines that are easy to manufacture and maintain, and also less vulnerable to debris (Rice, 2003). The design consists of several, closely-spaced rigid disks set in parallel on a shaft. The co-rotating disks are centred and locked to the shaft. Located near the centre of the disks are orifices that allow for fluid exhaust in the axial direction. The disk-shaft assembly is set on bearings and enclosed within a cylindrical casing. Water flows through an inlet into the casing and is directed approximately tangentially onto the disks (Tesla, 1913). To date, however, prototype Tesla turbines have not been able to achieve the claimed high efficiencies. Simulations by Ho-Yan (2011) employing Rice’s idealized model (Rice, 1965) have found that the Tesla turbine designs are better suited towards high head applications and yield very low power densities, or output power-to-turbine-volume ratios. Increased volume tends to increase cost (Fraenkel et al., 1991) and also greatly impact portability.

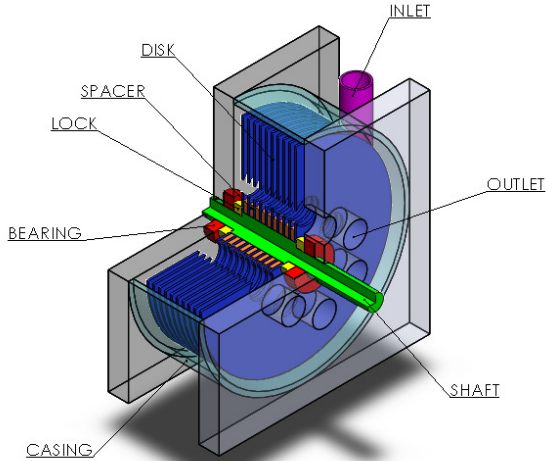


Figure 8: Tesla turbine

2.4.2 Medium Head

Turbines used for pico hydro in the medium head range include Turgo and cross-flow turbines and pump-as-turbine (PAT).

Turgo turbines (Figure 9) are similar to Pelton turbines, however nozzles are angled with respect to the runner directing water flow to enter on one side and to exit the other to avoid interference between flows. This translates to smaller runner diameters and higher rotational speeds when compared to Pelton turbines. The higher speeds make it more feasible to directly connect the turbine shaft to the generator and therefore eliminate the need for transmission systems in medium head environments (Fraenkel et al., 1991).

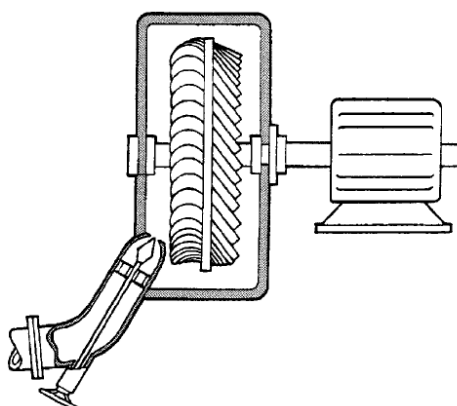


Figure 9: Turgo turbine
(source: Paish, 2002)

Cross-flow (Banki-Michell) turbines (Figure 10) are cylindrical in shape with two end plates connected by a circular array of blades. A rectangular nozzle directs the flow to contact the entire length of the cylindrical runner. The flow contacts the blade array at different locations on entrance and on exit. Efficiencies depend on the sophistication of the design and can reach as high as 85%, however for simpler designs efficiencies typically range from 65% to 80% (Fraenkel et al., 1991). Cross-flow turbines yield relatively high part-flow efficiency which can be achieved by channelling the flow over a portion of the runner. Mockmore and Merryfield (1949) translated Banki's design publication and constructed a turbine in accordance to this design procedure for performance testing which yielded 68% efficiency. Totapally and Aziz (1994) reviewed additional experimental performance tests and determined optimal blade number in the vicinity of 35 blades, optimal blade angles of attack between 22° and 24° , and increases to efficiency when using nozzles narrower than the length of the runner.

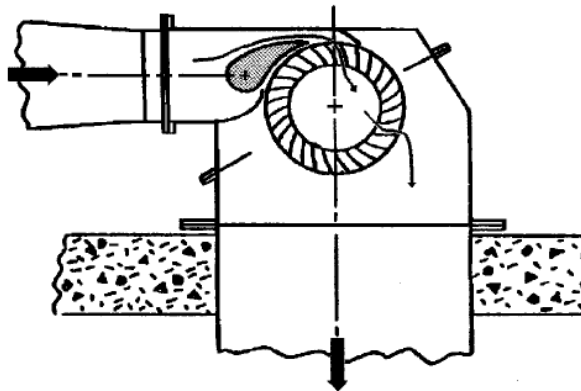


Figure 10: Cross-flow turbine
(source: Paish, 2002)

The “Firefly” turbine was designed by Jan Portegijs (2003) for use in rural Philippines. It consists of a cross-flow turbine directly connected to a car alternator intended for battery charging. This design was also used in rural Cameroon. Further discussion and investigation of the Firefly are in Sections 4.0 and 6.3.

Pump-as-turbine (PAT) involves passing water through pumps in reverse, to turn the pump impellor, which turns an attached generator to generate electricity. The main advantage of this alternative is increased accessibility due to availability of mass produced pumps and widespread distribution networks in some locations. Case studies of applications in developing countries are presented by Maher et al. (2003) and Pascale et al. (2011). Arriaga (2010) provides a review of PAT development while applying selection frameworks for a concept PAT application in Laos. Williams (2004) provides a practical guide to PAT selection.

2.4.3 Low Head

Recent research has moved towards improving low head pico hydro designs, since low head sites are much more common than high head sites. This section documents prior efforts to design, build, and test low head pico hydro turbines.

Date and Akbarzadeh (2009) designed a reaction turbine constructed of a halved polyvinyl chloride (PVC) pipe with the centres offset and joined to a top and bottom PVC plate. The prototype was trialed with a range of operating head pressures (approximately 2 m to 5 m) and flow rates (10 L/s to 28 L/s) were trialed. The resulting output power ranged from approximately 100 W to 500 W with optimal efficiencies of 52% to 56%. Future studies will be conducted on a similar design that replaces the PVC pipe with standardized galvanized pipe fittings in an ‘S’-formation.

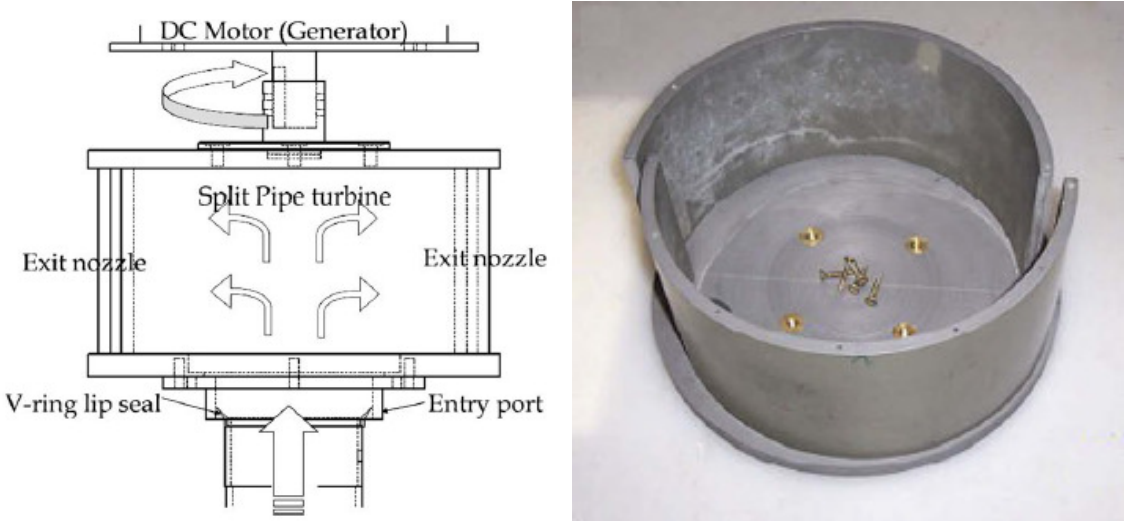


Figure 11: Reaction turbine
 (source: Date & Akbarzadeh, 2009)

Razak et al. (2010) designed, fabricated, and trialed a cross-flow turbine for a low head site at the Universiti Kebangsaan Malaysia. The scheme produced 100 W while operating with a head of 1.2 m and flow rate of 20 L/s. The system incorporated a gear transmission (12:108) to link the turbine and generator. The cylindrical dimensions of the cross-flow turbine were 450 mm diameter and 300 mm length.

Williamson et al. (2011) devised and applied a qualitative and quantitative selection criteria approach and determined that a single jet turgo turbine would be the most suitable technology for 1.3 kW power generation with a 3.5 m operating head, 304 rpm running speed, and 435 mm diameter wheel (Williamson, 2011). A test rig is currently under construction and will be used to optimize the design before field testing and grid connection.

Presently there are numerous pico hydro propeller turbine manufacturers mainly in China, Vietnam, and Indonesia. Costs have been cited to be very low for these systems but they are considered to be unreliable and inefficient (Rijssenbeek, n.d.). That said, the development of these units has helped advance rural electrification in Southeast Asian countries where they have

been extremely popular (Williams, Upadhyay, Demetriades, & Smith, 2000). Smits (2010) estimated nearly 60,000 low-head pico-hydropower units have been installed in Laos, and up to 130,000 units in Vietnam, where there is a relatively higher electrification rate.

Asian Phoenix Resources Ltd. (APRL), situated in Vietnam and Canada, sells a range of pico hydro systems. Their suite of “Powerpal” turbine products includes propeller and turgo turbines for low and high head sites respectively. The nominal generating capacity of the propeller turbines are 200 W, 500 W, and 1 kW with efficiencies ranging from 38.8% to 52.3% (Asian Phoenix Resources Ltd., 2008).

A 5 kW low head propeller turbine with an overall efficiency of 67%, designed to operate at 850 rpm with 5 m head, was developed at the Department of Civil Engineering at the Indian Institute of Science in Bangalore (Rao, 1986; Rao, Prasad, & Kulkarni, 1988; Rao, Prasad, & Rao, 1988). The propeller consisted of 8 helical blades of constant thickness. Disadvantages of this design included low speeds, the difficulty of manufacturing a complex helical blade shape, and non-standard dimensions (Williams et al., 2000).

The Mechanical Engineering Department of the Papua New Guinea University of Technology developed a prototype propeller turbine (Ranatunga & Indrus, 1991). Eight constant thickness blades were machined using computer numerically controlled (CNC) machinery. The turbine power output was 200 W at 200 rpm with 1.5 m head and 0.06 m³/s flow rate. The system coupled the propeller shaft to a generator-gear box assembly (Williams et al., 2000).

The Department of Mechanical Engineering of the University of Canterbury (Parker, Faulkner, & Giddens, 1993) developed a propeller turbine with a 2.8 m operating head, 0.4 m³/s flow rate, and a speed of 612 rpm. The output power was 3.7 kW with an overall efficiency of approximately

37%. The turbine was fabricated using mild steel.

Heitz (1993), with Nottingham Trent University, designed and constructed a unit equipped with 5 guide vanes and 4 runner blades of constant thickness steel plates. The design output was 1 kW at 2100 rpm operating under 2.9 m head and 0.06 m³/s flow rate. This design was adapted (Williams & Holmes, 1995) and installed at a low head site in London, UK. The adapted turbine operated at 650 rpm and employed a belt transmission to drive a 4-pole induction generator. The turbine efficiency was 24%. The runner was redesigned with 6 blades instead of 4 and showed an improvement in performance (Williams et al., 2000).

Development Technology Unit (DTU) (2010) of the University of Warwick developed a “simple-to-make” low head propeller turbine, claimed to produce 200 W with 2.5 m head and 0.04 m³/s flow rate (20% overall efficiency). The stator, shaft, and runner components are illustrated in Figure 12. The stator consists of welded mild steel flat plate and circular tube. The shaft is an assembly of threaded rod, nuts, and circular tube. The runner is fabricated from a series of nuts with welded steel flat plate as blades. The design incorporates standard materials, but relies heavily on welding for the assembly. The trueness of stock material is also relied on, which may lead to misalignment issues and hinder performance. The published reference manual did not include sufficient information for fabrication, lacking key information such as blade angles for the stator and runner.

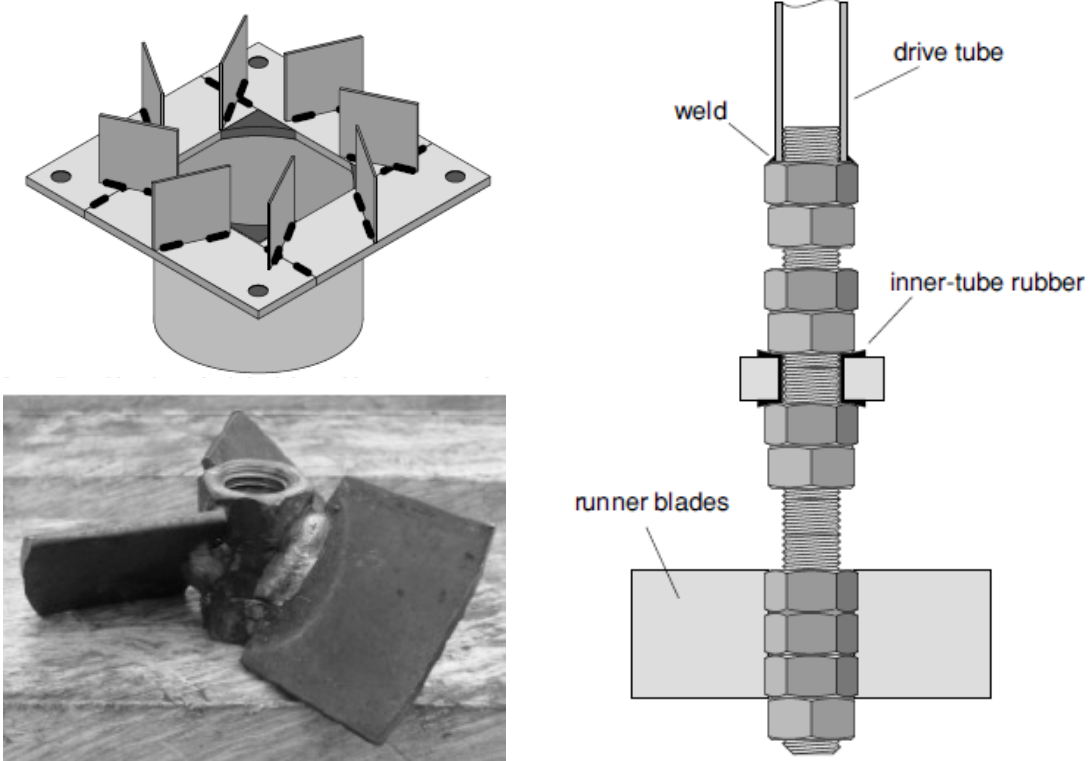


Figure 12: DTU propeller turbine design - stator (top left), runner (bottom left), and shaft (right)
 (source: DTU-Development Technology Unit, 2010)

Alexander et al. (2009a; 2009b) developed low head turbines operating between 4 m and 12 m with efficiencies above 68%. The designs were axial, radial, and mixed flow turbines and incorporated features to simplify manufacture and improve resistance to blockage. Flat blades were used for the axial and mixed flow designs, while blades curved about a single axis were used for the radial flow design.

Singh and Nestmann (2009) designed and tested a five blade propeller turbine that produced 810 W (73.9% hydraulic efficiency) at 900 rpm while operating under a head of 1.75 m and flow rate of 0.064 m³/s. This design was optimized by trialing different inlet and exit blade angles of the runner. Figure 13 displays the turbine schematic and runner. Singh and Nestmann (2011) also investigated the impact of blade height and blade number on performance. Increases to blade height caused an increase in friction, while increasing blade number, the parameter with relatively

greater influence, was found to improve flow guidance but adversely affected performance due to the augmentation of axial flow velocity and the decrease in tangential flow velocity.

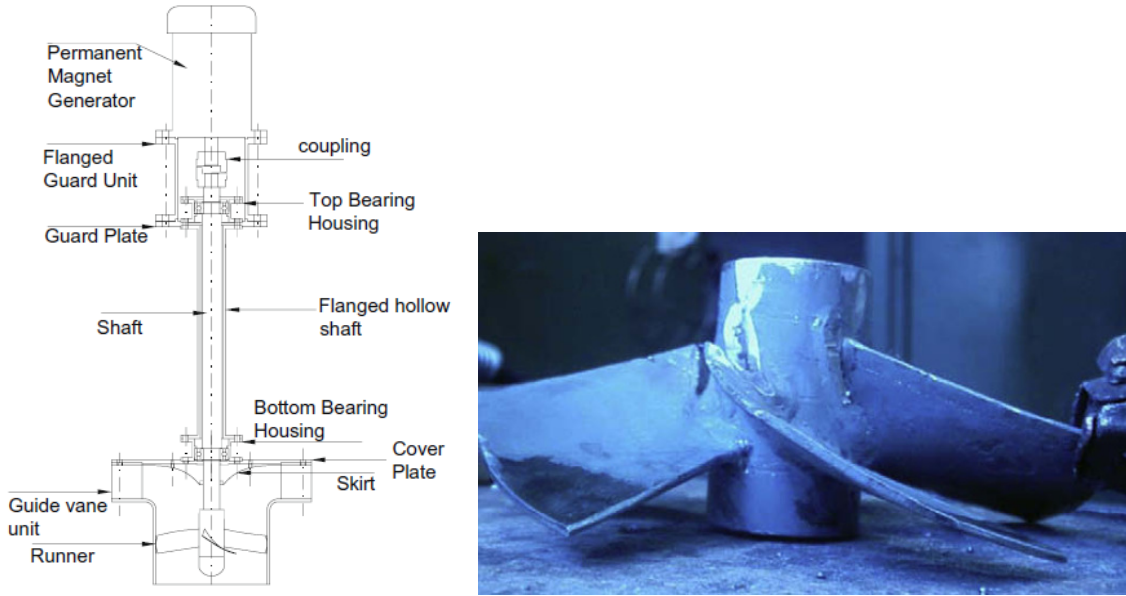


Figure 13: Assembly propeller turbine developed by University of Karlsruhe
(source: Singh & Nestmann, 2009)

At the Nottingham Trent University, Demetriades (1997) developed a propeller turbine with up to 1 kW power output. The turbine consisted of an enclosed spiral casing and guide vanes guiding flow to a propeller runner directly coupled to an overhung generator. The enclosed casing enables a short shaft to directly drive the generator. Optimizations were made to the design based on numerical analysis conducted by Upadhyay (2004). A 5 kW (65% overall efficiency) version (2006) was installed in Peru with tapered rectangular profile spiral casing, 6 guide vanes, and a runner with 4 blades constructed using bent and twisted steel plate. Simpson and Williams extended this work towards an open source propeller turbine design guide (2011).

Williams et al. (2000) conducted a review of low head hydroelectric equipment including novel designs and several conventional propeller designs. It was concluded that propeller turbines match well to low head pico hydro applications mainly due to high rotational speeds allowing for direct driven connections to the generator. This results in compact designs with improved

efficiency and lifespan, and reduced costs and maintenance.

2.5 Pico Hydro in Cameroon

The government of Cameroon has done little to promote adoption of renewable energy (Kenfack, Fogue, Hamandjoda, & Tatielte, 2011). Due to this inaction, non-governmental organizations (NGOs) have played a significant role in the promotion, financing, and installation of small renewable energy systems for rural electrification, including a number of pico hydro systems. Mid to high head turbines have been applied specifically incorporating Turgo, Pelton, and cross-flow type turbines. There is no formal record of the number or functionality of pico hydro sites in Cameroon, however, high failure rates have been known to occur with some of these designs. Pico hydro installation sites were visited during the field research component of this study and are further discussed in Section 6.3.

Nfah (2009) conducted a feasibility study on pico hydro and solar photovoltaic hybrid systems incorporating biogas generation in the Cameroon context. The results of the simulation showed that pico hydro is a key component for the viability of renewable energy systems used for rural electrification in Cameroon at the low power range (10 kW – 50 kW).

2.6 Turbine Theory

This section discusses basic turbine theory, including defining a series of concepts, terms and variables that are used in turbine evaluation and design. This background is relevant to the discussions of turbine design in Chapters 5.0 and 7.0.

2.6.1 Specific Speed and Specific Diameter

The turbine design process often begins with the challenge of selecting the most technically appropriate turbine type for the given design conditions. Previously mentioned was the turbine selection chart based on head and flow rate. This provides some indication, however does not consider the running speed requirements of the generator.

The specific speed of a turbine, N_s , relates the flow rate through the turbine to rotational speed and head, while the power specific speed, N_{sp} (often inaccurately referred to as the specific speed), relates output power of the turbine to rotational speed and head (Fraenkel et al., 1991). Expressed in dimensionless form, it follows:

$$N_s = \frac{nQ^{1/2}}{(gH)^{3/4}} \quad (2.2)$$

$$N_{sp} = \frac{n(P_m/\rho)^{1/2}}{(gH)^{5/4}} \quad (2.3)$$

where n is turbine speed in units of revolutions/unit of time, Q is flow rate, P_m is shaft power, and H is head. Recasting these equations using units of radians:

$$\Omega_s = \frac{\omega Q^{1/2}}{(gH)^{3/4}} \quad (2.4)$$

$$\Omega_{sp} = \frac{\omega(P_m/\rho)^{1/2}}{(gH)^{5/4}} \quad (2.5)$$

where Ω_s is specific speed, Ω_{sp} is power specific speed and ω is turbine speed with units radians/unit time. Note that within the literature the gravity and density variables are often dropped, therefore dimensionalizing the results. Care must be taken for these incidences (Dixon & Hall, 2010).

The specific speed and power specific speed are independent of turbine size. Each turbine technology type has its own characteristic speed range for high efficiency performance as seen in Figure 14. Therefore once power specific speed is calculated, the optimal turbine types with regards to technical performance can be determined.

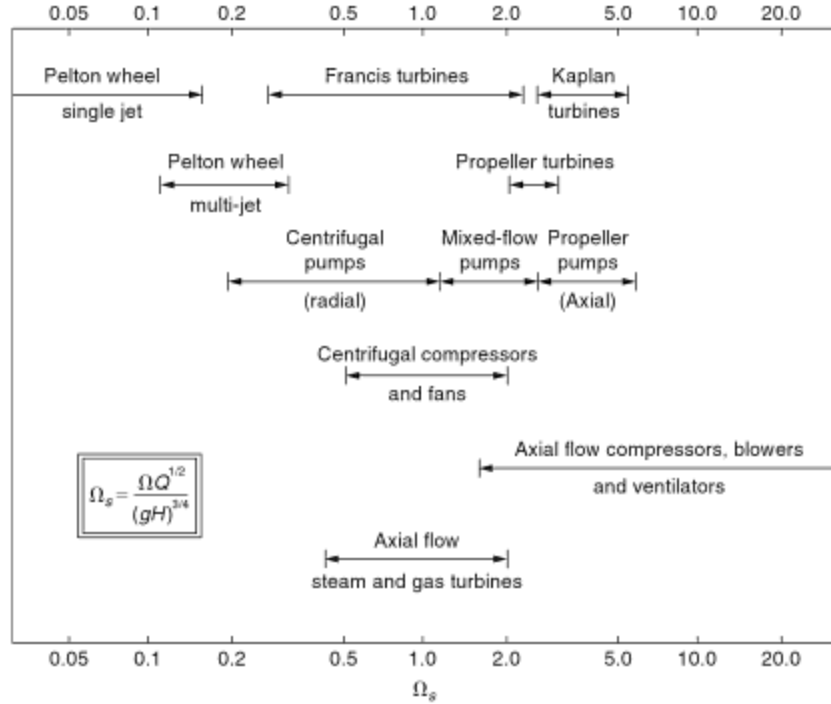


Figure 14: Range of specific speeds for turbine types
(source: Dixon & Hall, 2010)

Figure 14 shows impulse turbines operate with lower specific speeds than reaction turbines. This implies that for a given head and flow rate, the reaction turbines will operate with a higher rotation speed.

Specific diameter, D_s , is similar to the specific speed, but relates performance to the turbine characteristic diameter, D , instead of speed.

$$D_s = \frac{D(gH)^{1/4}}{Q^{1/2}} \quad (2.6)$$

Cordier (1955) found that different types of turbomachines, including compressors, fans, or pumps, could be grouped into different regions when plotted on a specific diameter versus specific speed plot. Balje (1981) and Wright (1999) applied Cordier's analysis to turbines (Figure 15). High head with low flow impulse turbines had high specific diameters with low

specific speeds while low head with high axial flow reaction turbines had low specific diameters with high specific speeds.

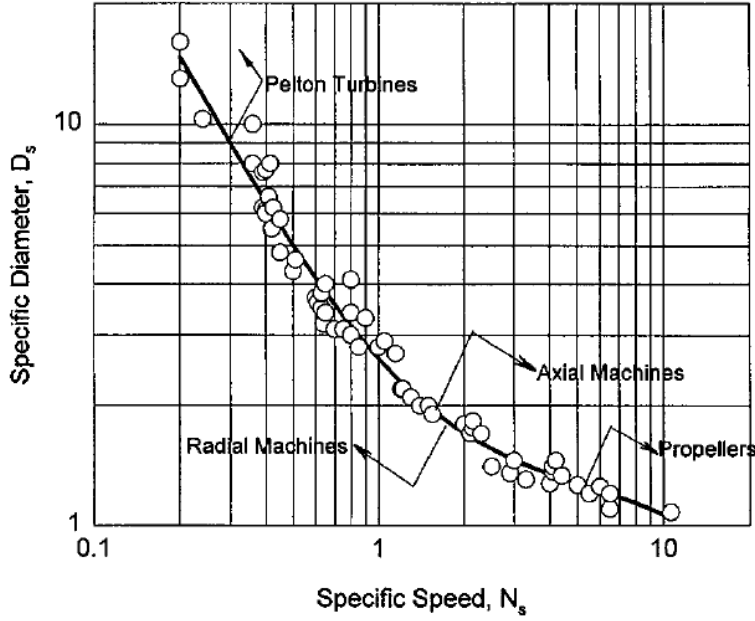


Figure 15: Cordier diagram
(source: Balje, 1981)

2.6.2 Euler Turbomachinery Equation

Torque, τ , developed in a turbine is equal to the rate of change of angular momentum of the fluid passing through the turbine. Torque is given by the product of the mass flow rate, \dot{m} , and the change in the product of radius, r , and circumferential fluid velocity, C_θ , at the inlet and exit positions of the control volume surrounding the blade row. The inlet and exit are denoted by subscripts i and e , respectively. For turbines a steady mass flow rate can be assumed.

$$\tau = \dot{m}(r_i C_{i\theta} - r_e C_{e\theta}) \quad (2.7)$$

The rate of work transferred from the fluid to the runner, \dot{E}_t , is the product of torque and angular velocity, ω .

$$\dot{E}_t = \tau\omega = \omega\dot{m}(r_i C_{i\theta} - r_e C_{e\theta}) \quad (2.8)$$

Since blade velocity, U , is the product of angular velocity and radius, the rate of work per unit mass flow rate therefore becomes

$$\frac{\dot{E}_t}{\dot{m}} = U_i C_{i\theta} - U_e C_{e\theta} \quad (2.9)$$

This is known as the Euler turbomachinery equation and is used for the development of velocity diagrams towards the design of turbomachines such as turbines, pumps, and compressors.

2.6.3 Velocity Diagrams

Velocity diagrams of a turbine stage, as seen in Figure 16, display the relationship between the absolute and relative fluid velocities, denoted C and W respectively, and the blade velocity, U . Absolute fluid and blade velocities are measured with respect to a fixed system. Relative fluid velocity is measured with respect to the rotating system associated with the turning rotor. The vector relation of the velocities is:

$$\vec{C} = \vec{U} + \vec{W} \quad (2.10)$$

Absolute fluid angles are designated α and relative fluid angles are designated β . All angles are measured relative to the axial direction. Numbered subscripts are applied to the angle and velocity terms to denote the turbine station defined as follows:

1 – stator inlet

2 – stator exit and runner inlet

3 – runner exit and draft tube inlet

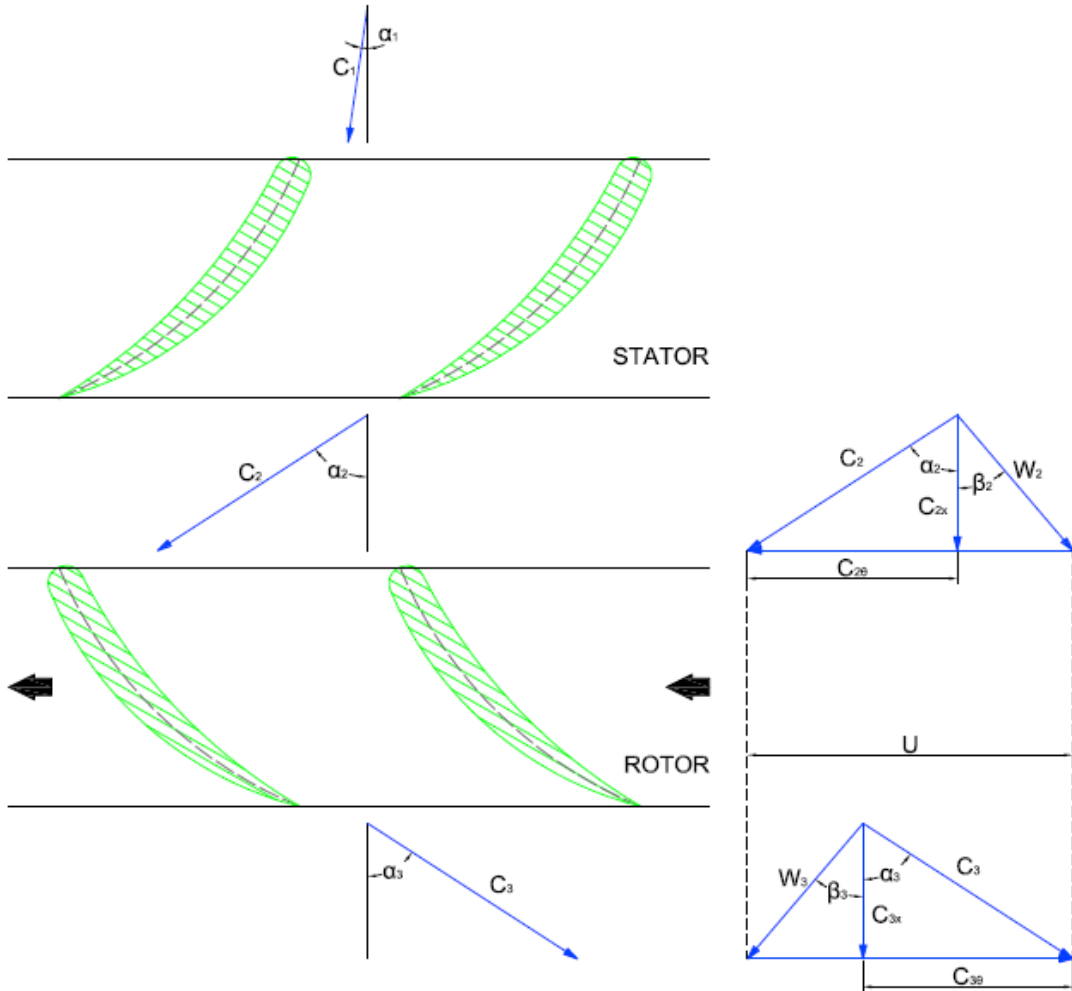
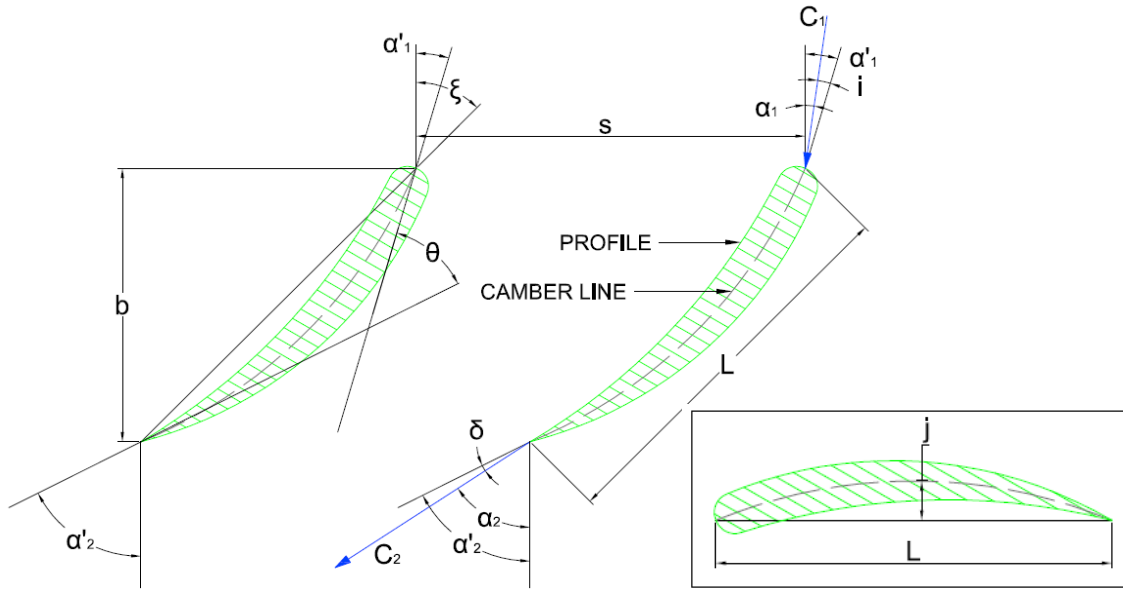


Figure 16: Turbine stage velocity diagram

2.6.4 Blade Cascade Geometry

Figure 17 displays two blade profiles of a row of blades, also known as a blade cascade, and includes the notation used to characterise the blade cascade geometry.



Symbol	Description
L	chord length
j	camber
b	axial chord length
s	blade spacing
α'	blade angle
θ	camber angle
ξ	stagger angle
α	flow angle
i	incidence angle
δ	deviation angle
C	fluid velocity

Figure 17: Blade cascade geometry

3.0 Problem Statement

3.1 *Problem Statement and Significance*

Low electrification rates in Cameroon hinder the fight against poverty and the development of the country. The current government's inaction towards the development of the country's energy sector presents the need for a decentralized approach towards rural electrification. Currently in Cameroon, various pico/micro hydro turbine systems have been introduced at both medium and high head sites. The performance and reliability of most of these projects is unknown. Foreign manufactured low head pico hydro systems exist, but have been noted by Williams et al. (2000) to operate with low efficiency and are observed to be unreliable. In addition, due to corruption in Cameroon's trade sector, it has been difficult to import these designs into the country (Seymour, 2011).

Limited rural electrification and an unreliable electricity supply continues to be a prominent issue in Cameroon despite having significant hydro potential. The development of a locally manufactured low head pico hydro turbine, can provide the Cameroonian rural population situated near potential low head hydro sites with a viable means to electrify their households. To address this need, the thesis designs a robust and reliable turbine for local manufacture in Cameroon. This turbine is a subset of a pico hydro system with the following characteristics structured from field observations (explained further in Sections 3.2 and 6.0):

- Affordability of the pico hydro system at the household level (less than €150)
- suitable for household electricity demand (250 W)
- use domestically sourced materials
- can be manufactured locally at a small industrial scale
- requires low maintenance
- optimally operate under conditions with 2 m head

3.2 *Affiliates*

This project involves several stakeholders including non-governmental organizations (NGOs) and international universities.

GREEN STEP e.V. (<http://www.green-step.org>) is a German NGO with the objective of improving rural livelihoods in Cameroon by providing training and co-financing of renewable energy projects, building environmental awareness through education, and sustainable agriculture extension. They have taken the lead role of the overarching project of constructing a training school in Foumban, Cameroon with the objective of training young people in renewable energy technologies, and specifically in the building and maintaining pico hydro and small wind turbines.

Pico hydro technology has been a primary focus and GREEN STEP e.V. has implemented nine units in rural Cameroon, however, a year after installation, only two turbines remained in operation at a limited capacity. Observations (Hertlein, 2011) made from these implemented systems include:

- Concerns regarding ownership have arisen, especially in situations where multiple stakeholders (i.e. community or multiple household ownership) are involved. The need for smaller systems targeted towards single dwellings has been identified as lines of responsibility are defined more clearly and free-rider issues are mitigated at the household scale.
- Improvements are needed to the current turbine design to reduce the complexity and increase robustness.
- End-users may not be made aware of the importance of maintenance; in addition, distances to workshops are far.
- The previous systems employ relatively expensive car alternators, car batteries and

inverters. These components are also prone to failures, with the wearing down of alternator brushes being the main observed failure mode.

- The willingness-to-pay for a pico hydro system is estimated to be €150.
- Training is required for local construction of pico hydro systems.

This thesis addresses the pico hydro turbine design. The design will be used towards the local manufacture at this school site and for training purposes.

Nkong Hilltop Common Initiative Group (NCIG) (<http://www.nkonghilltop.org/>) is a non-profit non-governmental community-based organization working in the Fako and Liabelem regions of Cameroon. Their objectives are to improve the socio-economic status of the community with focus on rural and urban poor women. Initiatives include capacity building, adult literacy education, and microfinance. With their expertise and experience in community building they have been instrumental in connecting with the rural villages.

Action pour un Développement Équitable, Intégré et Durable (ADEID) is a Cameroon based NGO with objectives of poverty reduction through the promotion of sustainable participatory development. They have successfully implemented solar photovoltaic and micro hydro systems. Recently, GREEN STEP e.V. has connected with ADEID for their renewable energy training school initiative. Given ADEID's experience in developing renewable energy systems and close proximity to the school site, it is planned that ADEID will take on the day-to-day management role of the school once it is built.

Two mechatronics engineering students from Regensburg University of Applied Sciences in Germany, Petra Kürzinger and Johannes Urban, are developing the electronic controller and generator components respectively.

Dr. Ing. Stefan Krebs is a member of Ingenieure ohne Grenzen (Engineers without Borders)-Regensberg, and is the project manager of the pico hydro system development project.

3.3 Scope of Work

The turbine development involved several research components:

- established baseline knowledge of the existing technology employed and evaluated suitability to the system requirements,
- reviewed alternative technologies to determine strongest options,
- developed concept designs based on the selected technologies,
- conducted field research in Cameroon to establish contextual understanding,
- devised detailed design based on technical theory and field research,
- developed performance prediction model,
- constructed prototype and test rig for performance testing,
- analyzed test results, and
- made recommendations towards future turbine development.

4.0 Baseline Investigation

The primary goal of this project was to develop an improved pico hydro turbine design for use in rural Cameroon. Before designing a new turbine, it was necessary to investigate the current technology deployed by GREEN STEP e.V. in Cameroon. This was done in two stages: (1) a prototype turbine of the type used in Cameroon was constructed and tested at the University of Guelph, and (2) field research including visiting the sites of previously installed turbines and interviewing local stakeholders was conducted. This chapter describes the prototype turbine testing. The field research in Cameroon is documented in Chapter 6.0.

All of the pico hydro turbines previously constructed and installed by GREEN STEP e.V. and local stakeholders were based on the Firefly cross flow turbine design (Section 2.4.2). A prototype of this turbine was constructed at the University of Guelph for laboratory testing, based on the instructions of Portegijs (2003). The Firefly is a cross-flow turbine directly connected to a car alternator intended for battery charging. Laboratory testing was conducted with focus on the low head range as the Firefly documentation did not provide performance for heads below 3 m (Portegijs, 2003).

The turbine runner has 27 blades supported by circular side plates with a 75 mm diameter and height of 55 mm (Figure 18). A 51 mm wide nozzle guides the flow to the turbine. The range of operating head is 3 m to 7 m, and 8 m to 25 m with governed flow (Portegijs, 2003).

In the original Firefly design, the field current of the alternator is controlled by 4 incandescent light bulbs (3 x 20 W and 1 x 10 W) and switches connected in parallel. Six different resistance values are possible, which allows for optimization of the field current (Portegijs, 2003).

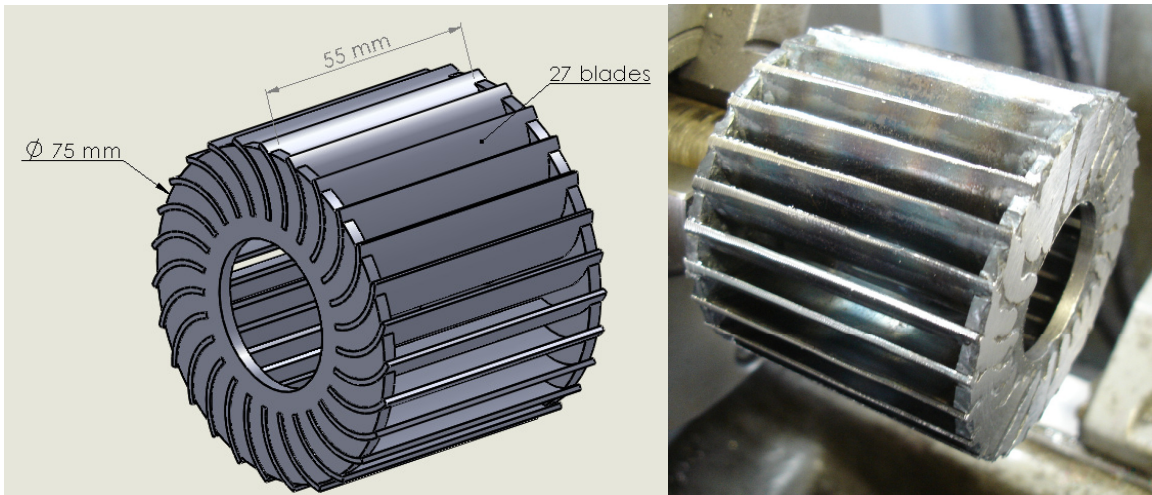


Figure 18: Runner assembly

4.1.1 Baseline Construction - Firefly

Construction of the Firefly for testing at the University of Guelph generally followed the design manual (Portegijs, 2003). The cross-flow sidewalls were laser cut rather than hand cut. The blades were manually sheared and formed as per instructions. The turbine assembly was welded instead of soldered as detailed in the design manual, however this is in agreement with practices used for the Cameroonian units (Hertlein, 2010). The nozzle and frame were also fabricated as per instructions. The casing was excluded as the test unit would not be exposed to a harsh field environment: a ridged plastic cover was placed over the turbine during laboratory testing. A Valeo model AB180128 automobile alternator was used. All construction (except for laser cutting) took place within the engineering machine shop facilities at the University of Guelph.

Several lessons were learned from the build process. Significant skill on the part of the fabricator is required to build these units. Difficulty would be further accentuated by limited resources. The use of jigs, especially for blade cutting and bending, could improve consistency from blade to blade and simplify the turbine assembly. Additional practical advice on fabrication would be a useful addition to an updated construction manual. The turbine sidewall fabrication involves cutting multiple curved slots for the attachment and soldering/welding of the curved blades. Consistently cutting the curved slots in the side walls would be extremely difficult for unskilled

workers, which lead to the laser cutting of these components. It should be noted that skilled workers with metal working experience using appropriate jigs could mitigate much of these concerns.

Variability between individual Firefly units is also introduced if different models of alternators are used. For example, the joining of the turbine to the alternator shaft differs slightly between the Guelph unit and the instruction manual, owing to a different configuration of the alternator shafts. This need to adapt to different alternator models affects the standardization of the build process, complicating construction by forcing builders to veer away from the design manual.

4.1.2 Baseline Test Apparatus

The Guelph laboratory test apparatus (schematic shown in Figure 19) consisted of an 1135 L (0.9 m x 1.9 m plan, 0.6 m height) reservoir elevated on a 3.3 m high platform. A 100 mm (4 in) diameter plastic penstock connected the drainage hole at the base of the reservoir to the Firefly. The total length of the penstock pipe from the reservoir to the Firefly was approximately 4 m. The Firefly was located above a receiving reservoir. An electric pump was used to return water to the supply reservoir between tests. With the Firefly in place, the system had a nominal head of 3 m, however, the head could be varied by changing the height of the Firefly while adjusting the length of the penstock.

The Firefly's alternator field circuit was connected to a high capacity 12 V deep discharge lead acid battery. A resistor was included in the circuit. Changing the resistance of this resistor allowed the field strength to be varied. The power output of the alternator was directly connected to a 2.0 ohm dynamic braking resistor with a 2 kW capacity.

A Medusa Scientific PowerPro power meter capable of measuring voltage, current and power was

connected to the alternator. The PowerPro was connected to a desktop computer, which recorded data at a rate of 4 Hz.

Flow rate was controlled by throttling a needle valve installed at the penstock inlet at the base of the reservoir. Instantaneous reservoir level, and by extension, flow rate out of the reservoir, was measured using a float connected to an ultra-low friction potentiometer (adapted from an anemometer) by a swing arm. The potentiometer was connected to the PowerPro via a voltage divider circuit, so that head and flow rate were recorded simultaneously with voltage, current and power. Before testing, the output of the float sensor was calibrated and a transfer function was derived that outputs reservoir level as a function of the recorded signal.

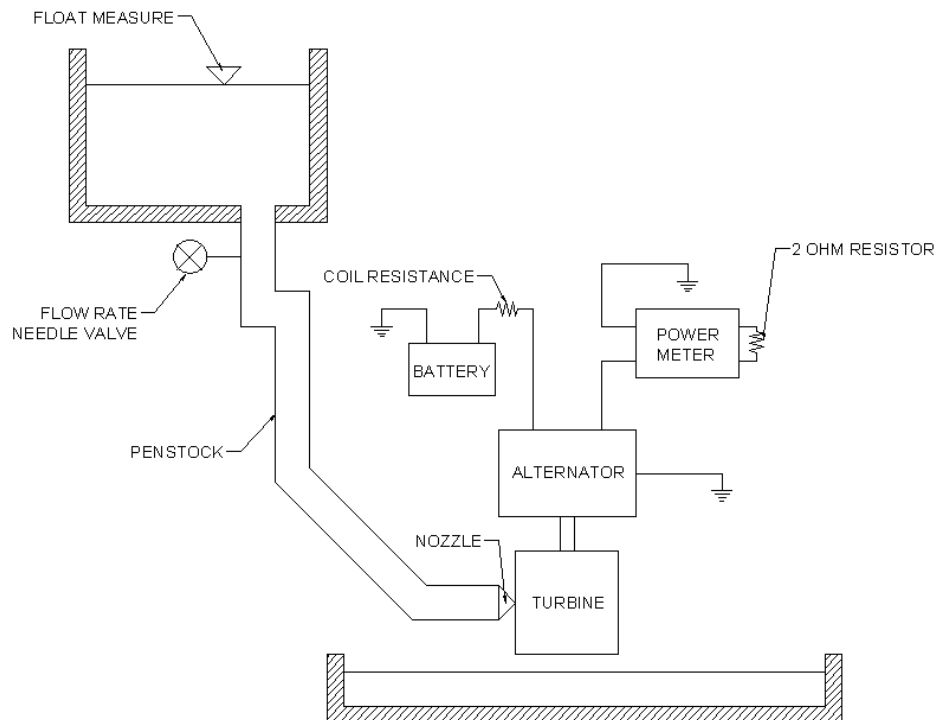


Figure 19: Layout of test apparatus

4.1.3 Baseline Test Method

Tests were conducted with flow rates ranging from 5.37 L/s to 5.81 L/s and average heads of 3.4 m. The field circuit resistance was varied to determine the optimum resistance to include in the field coil circuit. Resistances used were 0 ohm, 5 ohm, 10 ohm, 20 ohm, and 47 ohm.

4.1.4 Baseline Test Results

The results of initial tests are tabulated below in Table 2. Power output from the Firefly under a generally consistent flow rate and head is reported, with varying field resistance.

Table 2: Initial baseline experiment results

Coil Resistance [ohm]	Average Flow Rate [L/s]	Average Head [m]	Average Power Output [W]	Efficiency
0	5.61	3.40	9.39	4.8%
5	5.81	3.39	12.15	5.9%
10	5.52	3.39	11.60	6.0%
20	5.73	3.39	10.70	5.3%
47	5.58	3.39	10.14	5.2%

It was observed that the initial test unit required readjustment due to poor positioning and misalignment of the nozzle with respect to the turbine runner. This was identified as the root cause for the lower than expected performance in Table 2.

The test unit was modified by repositioning the nozzle and further reinforcing the nozzle mount to address the construction quality concern. Follow-up tests were conducted in the same manner as the initial tests and results are shown in Table 3.

Table 3: Follow-up experiment results

Coil Resistance [ohm]	Average Flow Rate [L/s]	Average Head [m]	Average Power Output [W]	Efficiency
0	5.42	3.38	40.53	22.6%
5	5.58	3.38	30.90	16.7%
10	5.57	3.38	30.86	16.7%
20	5.42	3.38	29.27	16.3%
47	5.37	3.39	26.80	15.0%

Significant improvement is seen when comparing the results from the follow-up to the initial test experiment. The 0 ohm field resistance circuit yielded the highest average power of 40.53 W and efficiency of 22.6%. This is more in-line with Portegijs' performance predictions.

Over the entire range of resistances, power output and efficiencies were lower than the predictions of Portegijs (2003). Portegijs predicted, but could not test, that the Firefly would produce 46 W at 3 m head and 5.3 L/s. It should be noted that a typical alternator would be below its normal operating range, and likely to underproduce the predicted value. Portegijs identified this as a concern, and suggested that his calculated values would be high because of this, for the combination of head and flow rates tested here. This is believed to be one reason for the lower than expected performance during testing.

4.1.5 Baseline Test Discussion

Given the lower than expected power outputs and efficiency from the initial tests, it was believed that the test Firefly required modifications to enhance the test results. Construction of the Guelph Firefly was revisited: it appeared that the gap between the nozzle and turbine was higher than other examples of the Firefly. Inspection of the unit after testing showed that realignment was needed of the nozzle with respect to the cross-flow turbine, and that a small amount of nozzle movement was possible. This was considered to be the root cause of the low power output observed in the initial tests. The marked improvements in the follow-up test results, after the nozzle was repositioned and reinforced, demonstrate the criticality of construction training and the need for simplistic designs that are forgiving of low tolerances.

Portegijs (2003) predicted the performance of the Firefly under low head conditions, but could not test it at 3 m head. The experimental results in Table 3 essentially agree with Portegijs' calculations, and can be interpreted as a validation of Portegijs' calculations.

The test results also confirm that for the low head applications intended, the Firefly turbine will not be capable of meeting the design objectives. The tests were conducted at 3 m head, higher than the 2 m head design requirement, and only achieved a fraction of the 250 W goal. In

addition, at the combinations of head and flow rate tested, the direct drive automobile alternator may not be the ideal type of generator to utilize, due to inefficiencies when operating at low rotational speed, and utilization of a large fraction of the power generated to energize the coils that provide the magnetic field. The efficiencies in Table 2 and Table 3 do not account for the power used to energize the alternator coils.

5.0 Technology Selection and Concept Designs

5.1 *Technology Selection*

Given the complexity of designing a new pico hydro turbine for a particular location and application, initial turbine technology selection should be based on not only technical, but also, social, environmental, and economical factors. Conventionally, turbines have been mainly selected based on the specific speed. While this narrows the options down to the most technically applicable turbine types, it does not address the qualitative factors surrounding the successful adoption and long term sustainability of the resulting system.

The rationale used for the preliminary selection of turbine technology type for this project informally followed the multi-criteria analysis proposed by Williamson, Stark & Booker (2011). The formal analysis employs a point system for both quantitative and qualitative factors that are normalized and combined with an applied weighting defined by the stakeholders. A point system was not employed in the selection process for this project, but strengths and weaknesses were identified to eliminate less preferred technologies. The factors used for the technology selection for this system expand on the ones used by Williamson et al. and include:

- *Efficiency* – the efficiency under design and off-design conditions.
- *Constructability* – the degree of complexity to build the components and assemble the system. This involves the required materials, tooling, and labour and the allowable tolerances during manufacture.
- *Cost* – the monetary cost to produce the system.
- *Maintenance and Serviceability* – the level of repair and continuous maintenance required for the system to properly operate and the complexity involved in the maintenance process.
- *Portability* – the volume for manageable construction and transport. The sites will be

situated near water arteries and typically involve steep terrain in rural areas where road infrastructure is, for the majority, non-existent.

- *Scope of Modularity* – the ability to break up the overall system into smaller components to allow for the replacement of parts in the field and for troubleshooting breakdowns.

This is not prescribed by the technology type, but is a function of the design.

It can be seen that the factors are inter-dependent: design choices that directly affect one factor, also have indirect affects on the others. For example, increased volumes generally increase material and cost, complicate transport, and are more cumbersome to construct and maintain.

Impulse turbines, such as Pelton and Turgo wheels are established technologies that operate well under mid to high head environments. They exhibit relatively high design flow efficiencies and are currently manufactured in several developing countries, including Cameroon, albeit at a low production scale. Seals are not required since the runner operates under atmospheric conditions and therefore not subject to cavitation. Another advantage is relatively better partial flow efficiency (Fraenkel et al., 1991). However, when applied to low head environments, these turbines will require large diameters and operate at low rotational speeds, thus introducing the need for transmission systems (Williamson, 2011). This will adversely impact manufacturing, maintenance, and transport.

Cross-flow turbines are relatively easier to build. Moreover, the greatest advantage of this technology is the Cameroonian craftsmen's previous exposure to cross-flow turbine construction. Cross-flow turbines are best suited to low or medium head sites. In addition, very high partial flow efficiencies can be maintained at less than 25% flow (Fraenkel et al., 1991) with minimal adjustment, which caters well to the seasonal variations of flow. That said, the peak efficiency is lower than other turbine technologies. As seen in the Firefly, the cross-flow involves a relatively

high number of blades, resulting in increased potential for variability in blade geometry and positioning during construction. In addition, with low specific speeds the runner will rotate at a slower rate, increasing the sizes when applied to low head applications and potentially require a transmission. This leads to a more cumbersome unit to manufacture, maintain, and transport.

Propeller turbines are high efficiency machines that operate under low head conditions with high specific speeds. This allows for the generators to be directly driven and avoid transmissions. Propeller turbines are manufactured in several developing countries. The runners involve a relatively lower number of fixed blades, therefore simplifying the manufacturing process and reducing the potential for inconsistent blade construction and orientation. There is an associated disadvantage with fixed pitch blades in that the partial flow efficiency drops dramatically and propellers typically perform poorly below 80% flow (Fraenkel et al., 1991). Proper seals are needed to maintain pressure differences which complicate the building process. The complexity of the designs can vary greatly with this technology from employing flat blades to complex cambered blades with twists. As the sophistication increases, the design efficiency increases, as does the manufacturing effort; more sophisticated designs can exceed the capabilities of even most developed workshops.

High efficiencies under medium head can be achieved with Francis turbines, but similar to propeller turbines, performance sharply declines under part-flow conditions. The geometries of the blades are very complicated and require well equipped high tech workshops for manufacture. There is a relatively higher cost associated with Francis turbines.

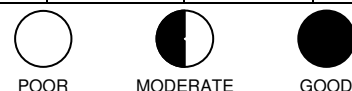
Kaplan turbines are very efficient reaction turbines with good part flow efficiency mainly due to the adjustability of the runner blades. However, the complex nature of the turbine and the high level of maintenance required are considerable barriers.

Pump-as-turbine involves the reconfiguration of manufactured pumps to run in reverse. There is the benefit that the systems and components already exist. However, as there would be considerable variation between pumps, the technology does not cater well in a manufacturing setting. The process of procuring pumps is also vulnerable to economic factors such as supply, import tariffs, and, of course bribes.

Table 4 compares the different turbine types against the above criteria, and demonstrates that no unit is perfect, however among the different types the propeller and cross-flow turbines stand out. They both can function under low head, and the strongest aspect of these two turbine types is the proven record of local manufacture within developing countries. They are highly constructable given that these are fixed blade runners and that less complex blade shapes can be used. With local manufacture, skills will be attained and can be applied towards turbine system maintenance. Also, simpler designs may reduce maintenance issues. In addition costs will be minimized as import costs are avoided. Efficiencies will be lowered if simplifications are to be made to the design to fit within the Cameroon manufacture context.

Table 4: Comparison of turbine technology types for preliminary selection

Characteristic	Turbine Type						
	Pelton	Turgo	Cross-flow	Propeller	Francis	Kaplan	PAT
Efficiency – design	●	○	○	●	●	●	○
Efficiency – off design	●	○	●	○	○	●	○
Constructability	○	○	●	●	○	○	○
Cost	●	○	●	●	○	○	○
Maintenance & Serviceability	●	○	●	●	○	○	○
Portability	●	○	●	●	●	●	●
Scope of Modularity	●	●	●	●	●	○	○



5.2 Concept Design

Focus was directed to the design of the runner for a new turbine, since this is the most complex component, and runner choice impacts design decisions regarding other aspects of the turbine system. Conceptual designs for the cross-flow and the propeller runners were formulated based on a requirement for 250 W power generation at 2 m head. Estimates of generator and electronic controller efficiencies resulted in a required shaft power of 370 W. The intent of the conceptual designs was to determine feasibility of the selected technologies and establish approximate sizing. Moreover, they were to be used as discussion points for other team members to stimulate building process thinking, introduce potential designs to the Cameroonian artisans for their critique and input, and identify comfort levels of familiar and novel aspects. Hand sketch formats were used to represent the preliminary nature of the concept design and to offer the artisans a more approachable format amenable to change, as opposed to rigid mechanical drawings which can be misinterpreted as complete.

For a direct driven system that provides output power useable for general appliances, the system should output alternating current at the Cameroonian standard frequency of 50 Hz. Using the following equation, the required rotational speed in revolutions per minute, n , can be determined based on desired electrical frequency, f , and the number of poles, N_{poles} , in the generator.

$$n = \frac{f}{\frac{N_{poles}}{2}} \times 60 \quad (5.1)$$

A 4, 6, or 8 pole generator, with corresponding rotational speeds of 1500, 1000, and 750 rpm respectively, was considered buildable and therefore defined the target range during the concept designs.

5.2.1 Cross-flow Concept Design

Fraenkel et al. (1991) cited equations from Aarter and Meier (1990) that provide generalized sizing of the cylindrical cross-flow runner, namely diameter, $D_{CFrunner}$, and length, $L_{CFrunner}$ and jet thickness (Figure 20).

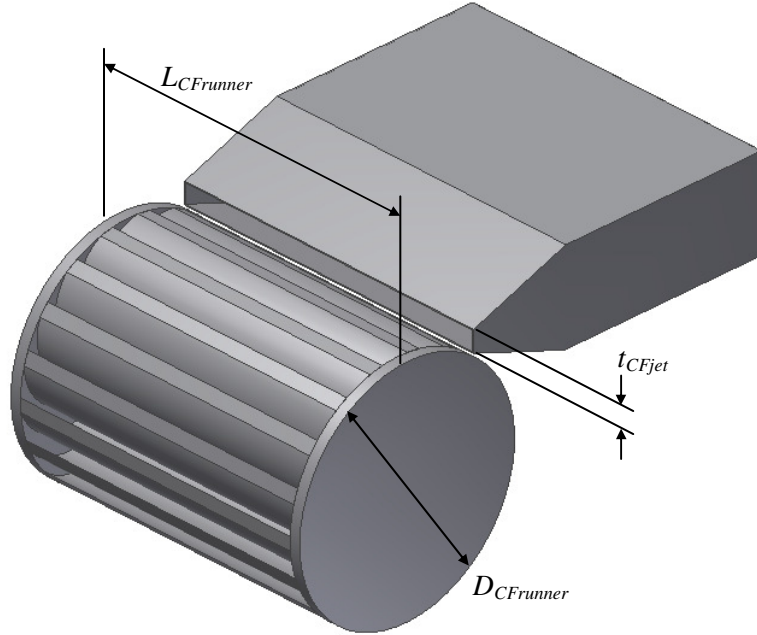


Figure 20: Cross-flow concept sizing parameters

$$D_{CFrunner} = 40 \frac{\sqrt{H}}{n} \quad (5.2)$$

$$t_{CFjet} \approx \frac{D_{CFrunner}}{10} \quad (5.3)$$

$$L_{CFrunner} = \frac{0.23QH}{t_{CFjet}} \quad (5.4)$$

Where Q is the flow rate (m^3/s), H is the head (m), and t_{CFjet} is the thickness of the jet (m).

Generalized sizing as a function of rotational speeds are tabulated below.

Table 5: Generalized sizing of concept cross-flow runner

Speed, <i>n</i> [rpm]	Runner Diameter, <i>D_{CFrunner}</i> [m]	Jet Thickness, <i>t_{CFjet}</i> [m]	Runner Length, <i>L_{CFrunner}</i> [m]
250	0.23	0.02	0.51
500	0.11	0.01	1.02
750	0.08	0.01	1.52
1000	0.06	0.01	2.03
1250	0.05	0.00	2.54
1500	0.04	0.00	3.05

Mockmore and Merryfield (1949), translated Donat Banki's "Neue Wasserturbine" and outlined more detailed equations. Banki defined optimized parameters such as fluid entry angle, $\alpha_{Banki} = 16^\circ$, velocity coefficient, $C_{Banki} = 0.98$, and geometric parameter, $k_{Banki} = 0.075-0.10$, which relates blade spacing to diameter.

Based on the head and power requirements, and Banki's suggested parameters, conceptual designs were determined. A length multiplied by diameter parameter is initially defined:

$$L_{CFrunner} D_{CFrunner} = \frac{Q}{k_{Banki} V_{CF}} = \frac{Q}{k_{Banki} C_{Banki} (2gH)^{1/2}} \quad (5.5)$$

A range of runner lengths considered manageable for construction were inputted to determine runner diameter and associated design characteristics such as:

- angular speed, $n = \frac{1}{2} C_{Banki} (2gH)^{1/2} \frac{\cos \alpha_{Banki}}{\pi D_{CFrunner}} 60$;

(5.6)

- blade angle, $\tan \beta_{Banki} = 2 \tan \alpha_{Banki}$;

(5.7)

- circumferential blade spacing, $t_{CFblade} = \frac{k_{Banki} D_{CFrunner}}{\sin \beta_{Banki}}$;

(5.8)

- number of blades, $n_{CFBlade} = \frac{\pi D_{CFrunner}}{t_{CFblade}}$.

(5.9)

The resulting cross-flow design parameters are tabulated as follows:

Table 6: Conceptual design parameters of cross-flow turbine runner

Runner Length [m]	Runner Diameter [m]	Angular Speed [rpm]	Circumferential Blade Spacing [m]	Number of Blades
0.1	0.65	86	0.11	18
0.2	0.33	173	0.06	18
0.3	0.22	259	0.04	18
0.4	0.16	346	0.03	18
0.5	0.13	432	0.02	18
0.6	0.11	519	0.02	18
0.7	0.09	605	0.02	18
0.8	0.08	692	0.01	18
0.9	0.07	778	0.01	18
1.0	0.07	865	0.01	18

There is agreement between Table 5 and Table 6 that workable geometries, namely runner length and diameter below 1 m, can only be obtained at low rotational speeds. From Table 6, a balance between the length and diameter dimension was selected. The concept design with $L = 0.3$ m was considered the most reasonable in terms of strength and constructability. However, for all the tabulated concepts, the angular speeds will not meet the upper range of angular speeds for a direct driven design. Given an estimate of 55% efficiency, as suggested by Banki (Mockmore & Merryfield, 1949), the above designs are expected to produce approximately 380 W shaft power with an operating head of 2 m and flow rate of 35 L/s.

5.2.2 Propeller Turbine Concept Design

The Simpson and Williams (2011) design manual for propeller turbines was used for the propeller conceptual design. Design conditions of head (H), flow rate (Q), and rotational speed (n) were inputted to calculate a dimensional version of specific speed (n_q).

$$n_q = \frac{n\sqrt{Q}}{H^{0.75}} \quad (5.10)$$

The calculated specific speed, with units $\frac{(\text{rev})(\text{m}^{0.75})}{(\text{s}^{1.5})}$, fell within the acceptable range, defined as

$70 < n_q < 300$. Referring to Figure 21, which is an adapted graph based on efficient Kaplan turbine design from Bohl (1991), the tip-to-head velocity ratio, K_{ug} , hub-to-tip diameter ratio,

D_h/D_t , and the number of blades were determined.

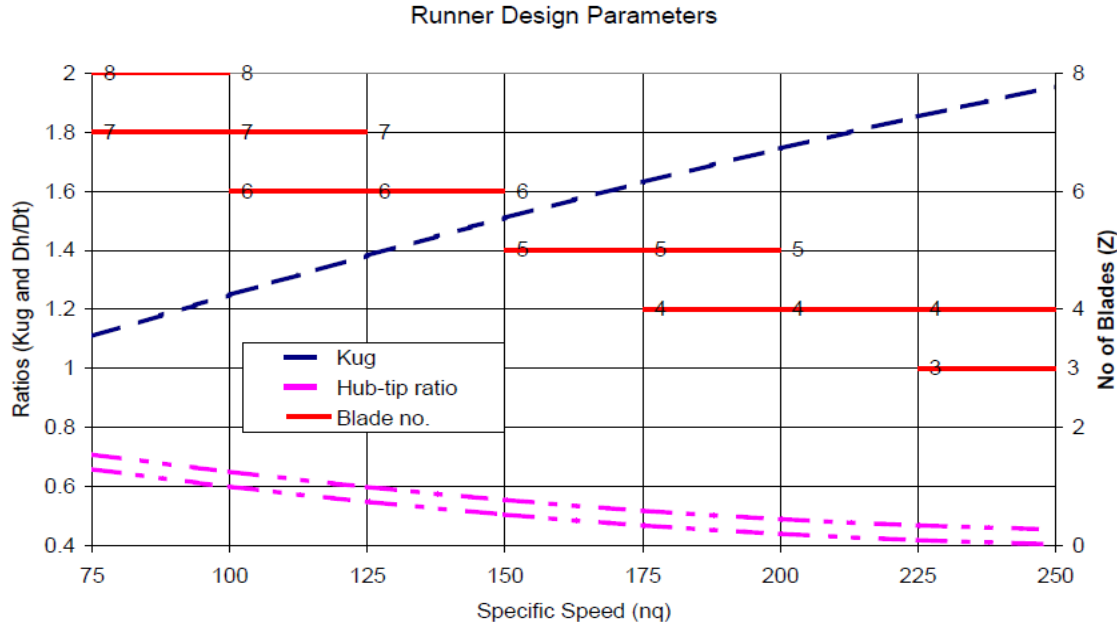


Figure 21: Runner design parameter
(source: Simpson & Williams, 2011)

The tip-to-head velocity ratio can also be calculated as follows, resulting in the determination of tip radius, r_{tip} :

$$K_{ug} = \frac{r_{tip}\omega}{\sqrt{2gH}} \quad (5.11)$$

Two estimates of hydraulic efficiency are calculated based on Anderson's (1980) statistical data of a wide range of turbines. The first estimate is a function of flow rate and the latter is a function of both flow rate and specific speed, which demonstrates the drop in efficiency as specific speed increases (Simpson & Williams, 2011). An average of the two calculated efficiencies were taken and used to calculate the shaft power.

The concept propeller turbine design based on 2 m head and 25 L/s flow rate conditions yielded a 117 mm tip diameter, 64 mm hub diameter, 5 to 6 blades, and was forecasted to produce 363 W at 78% hydraulic efficiency.

5.2.3 Concept Design Summary

Conceptual sizing parameters and performance estimates for the preliminary cross-flow and propeller runners are summarized in Table 7. These conceptual designs were used as part of the communication process during field research in Cameroon.

Table 7: Concept design summary

	Cross-flow	Propeller
Diameter (tip) [mm]	217	117
Axial length [mm]	300	TBD
Number of blades	18	5 or 6
Rotational speed [rpm]	259	1500
Hydraulic efficiency	55%	78%
Required flow rate [L/s]	35	25
Required head [m]	2	2
Power output [W]	377	363

6.0 Cameroon Field Research

In May 2011, field research was conducted in Cameroon with the principal objective of problem contextualization. Focus was placed on the West and Southwest regions. Within these regions, urban, peri-urban, and rural settings were visited. Figure 22 shows a map indicating locations located and approximate routes travelled.



Figure 22: Map of field research locations and approximate travel routes

The field research included:

- Interviews to gain different perspectives through the lens of the end users and artisans. “Artisans” in this case refer to skilled technicians typically, but not restricted to, individuals working as carpenters, welders, metal workers, and electricians. Previous workshops conducted by GREEN STEP e.V. included manual and non-manual labourers. It must also be noted that Cameroonian livelihoods may include several occupational

roles;

- Market research to establish general knowledge of material availability and costs;
- Site visits to hydro and wind turbine installations to identify previous successes and limitations; and
- Collaboration with artisans to gauge capacity, observe the working environment and to develop contextualized design ideas.

Table 8: Field research activity by location

	Interview	Market Research	Installation Site Visit	Artisan Collaboration
Buea		•		•
Dschang		•		
Ndungweh	•		•	
Bafou			•	
M'muock	•		•	
Bafoussam		•		•
Foumban		•		
Lewoh	•		•	

The field research team was composed of Johannes Hertlein and Edwin Njonguo (GREENSTEP e.V.), Stefan Krebs (Ingenieure ohne Grenzen), Johannes Urban and Petra Kuerzinger (Regensburg University), and Bryan Ho-Yan (University of Guelph). All members were involved in the interviews, market research, installation site visits, and artisan collaboration activities. Interviews and site visits in Lewoh were conducted by Johannes Urban, Petra Kuerzinger, and Bryan Ho-Yan. Build trials (further discussed in Section 6.4) were independently led by Bryan Ho-Yan.

6.1 End-user and Artisan Interviews

GREEN STEP e.V., in association with NCIG, conducted a data collection study in the M'muock village in 2008 (Ehlers & Hertlein, 2008) as part of an environmental education project. Collected data included household incomes and energy usage. The study also allowed the

community to identify primary concerns and suggest solutions. Due to the great relevance of this study to the current project, sections of this study have been translated and reiterated in Section 6.1 and supplemented with findings from the May 2011 field trip. Each of the subsections of Section 6.1 begins with the 2008 research findings and is followed by the 2011 findings.

The M'muock village is separated into 27 districts and has a total estimated population of 7,000 residents. Within the 2008 study, 12 districts in the vicinity of potential wind turbine or pico hydro turbine sites were selected. Within these districts, approximately 1,150 households were randomly chosen for interviews. The questionnaires consisted of 17 questions for the owners and 24 questions for the women of each household. The data collection was carried out by local teachers that were trained in a workshop on the handling of the questionnaires (Ehlers & Hertlein, 2008). During the 2011 research trip, informal interviews were held with individuals at the visited locations. Findings from the interviews and empirical observations were documented and sorted into themes. Names of interviewees have not been disclosed to protect privacy.

6.1.1 Household Information

Housing statistics gathered from the surveys showed that 96% of the properties were privately owned and the remaining 4% were either rented, borrowed or family owned. The average number of building units per household was 3.4. An average household had a total of 16 rooms and 7.8 rooms with lighting. The average size of cultivated arable land per household in football fields (approximately 0.5 acres) was 8.3 (Ehlers & Hertlein, 2008).

Land tenure is mainly controlled by the chiefs and is viewed by some as messy and corrupt. An example that was mentioned was the selling of land owned by the Cameroon Development Corporation (CDC), a state-owned organization in the agricultural industry and the second largest employer in Cameroon, to individuals with government connections. Land tenure is bought and

sold, or inherited by males. In addition, the wives and the associated financial responsibility are also inherited. Polygamy is phasing out, however it remains a prevalent phenomena in rural areas. It was explained that the relationship resembles a business relationship between man and woman, where the man owns the land and the woman works to support children and pay rent. In two of the households where the May 2011 research team was housed were structured in this manner, one consisted of the land owner, three wives and at least six children, while the other consisted of the land owner, six wives and fifty children. In some cases, conflict can arise between the multiple wives. In the peri-urban and urban settings, households are smaller in terms of land size and members where six people per household are typical.

6.1.2 Annual Income and Livelihoods

Annual income ranges were documented and displayed in Figure 23.

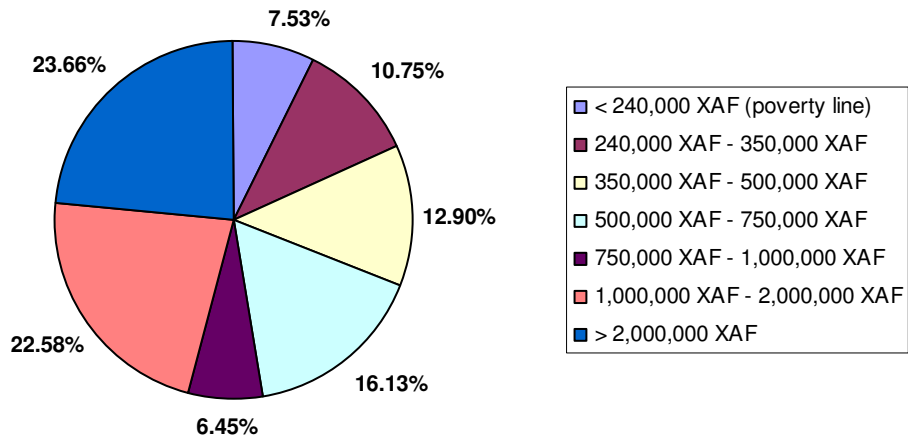


Figure 23: Annual income in M'muock
(source: Ehlers & Hertlein, 2008)

Horticulture is the predominant source of income (83.3%) followed by handcrafts (4.17%) and livestock (2.48%). Most part-time income is generated from retail and animal husbandry (Ehlers & Hertlein, 2008).

Both subsistence and commercial agriculture were observed in the rural areas. Crops included coffee, potatoes, bananas, cocoa, kola nut, pumpkin, cassava, cocoa yams, plantains and peppers and livestock included fish, chicken, pigs and goats. M'muock is the largest potato exporter in Cameroon. Additional livelihoods in Ndungweh were trades such as blacksmithing, tailoring and carpentry. There were no mechanics or electricians. Trades training can be acquired through vocational schooling or apprenticeships. In one of the rural villages there was a metal worker who had worked in the urban city of Bamenda as an apprentice for five years and then independently for one year. Following that he had moved to a rural village to open a shop. After one year in operation, there was not enough work for him and he was intending to leave for a larger town to find more work. Governments pay teachers and health care workers to work in the rural areas, however payments can take up to a year to be transferred. The government funding is insufficient at times as seen in one village where the community supplements teacher salaries. These factors deter professionals from working out in the rural areas. Construction of a health centre in a village was completed five years prior to commencing operations. The delay was partly due to lack of personnel to operate the health centre. This health centre has now been managed by a trained nurse for the past five years and also has a connecting pharmacy run by a community member.

An electrician spoke of his livelihood transforming since working as a small wind turbine and pico hydro system technician. He has become confident in his new craft, providing consulting and training services in addition to maintenance and construction. This was observed during an exchange with the pharmacist in Bafoussam (Section 6.3) as he provided technical advice. In addition, the artisan enrolled himself in a national artisan competition to display his wind turbine.

6.1.3 Energy Expenditure

As seen in Figure 24, the highest overall expenditure found in the 2008 survey was for petrol. 59% of respondents have access to vehicles (25%), motorcycles (5%) or gasoline generators (29%). Other fuel energy costs are attributed to kerosene, which is generally used as lamp fuel for lighting and firewood. Most residents harvest firewood from the surrounding forests (Ehlers & Hertlein, 2008).

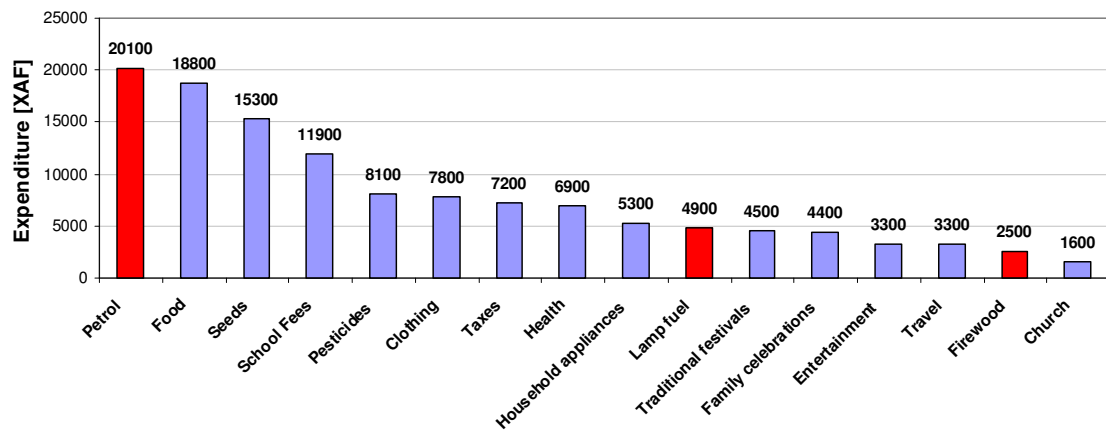


Figure 24: Energy expenditure per household per month in M'muock
(source: Ehlers & Hertlein, 2008)

With regards to lighting applications, 52% of the population use open fires as their primary means of lighting. This is closely followed by 47% of the population using kerosene lamps. Electricity for lighting from gasoline generators or disposable batteries is only a tertiary alternative. During the study, 511 kerosene lamps were counted. The average usage was 10 hours per day per lamp, relating to an average household consumption of approximately 3 L per month of kerosene and resulting in an average household spending of 5,000 XAF per month for the operation of the kerosene lamps (Ehlers & Hertlein, 2008).

Petrol costs were 25% higher for Ndungweh villagers compared to their urban counterparts, with

quoted costs of 600 XAF/L in Dschang and 750 XAF/L in Ndungweh. The price for a gasoline powered generator was in the range of 30,000 XAF to 35,000 XAF. Estimated petrol consumption was 5 L/day, resulting in a cost of 3,750 XAF/day. Diesel generators had a lower running cost of 3,000 XAF/day. Health clinics in the villages have diesel generators but a healthcare worker was quoted saying it was too expensive to operate. In the grid connected urban areas, power outages were common. While in Dschang there were power outages on separate occasions, one event lasting for several hours. During this time, many stores used fuel powered generators. Kerosene costs were also higher for village residents with costs of 600 XAF/L in the village of Ndungweh and 450 XAF/L in Dschang. In the Ndungweh palace, kerosene lamps were used prior to the turbine installations. The lamps provided lower quality light while producing noticeable amounts of smoke.

6.1.4 Electrical applications

An inventory of electrical appliances was formulated based on the interviews with results in Figure 25. Households equipped with gasoline generators have a larger number of electric lamps. Disposable battery-powered flashlights were found in 20% of the households. Approximately a quarter of respondents owned a mobile phone at the time of the study (Ehlers & Hertlein, 2008).

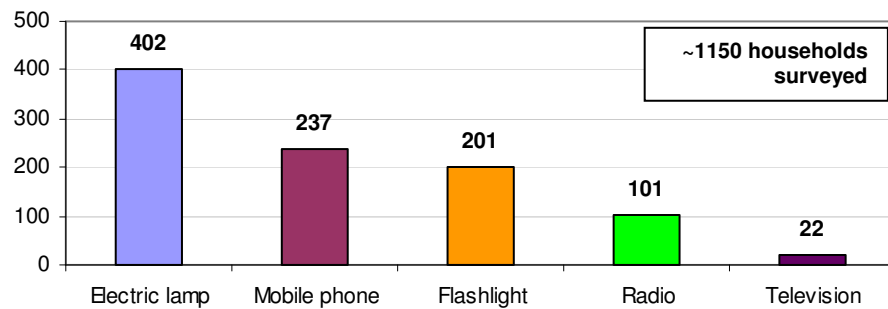


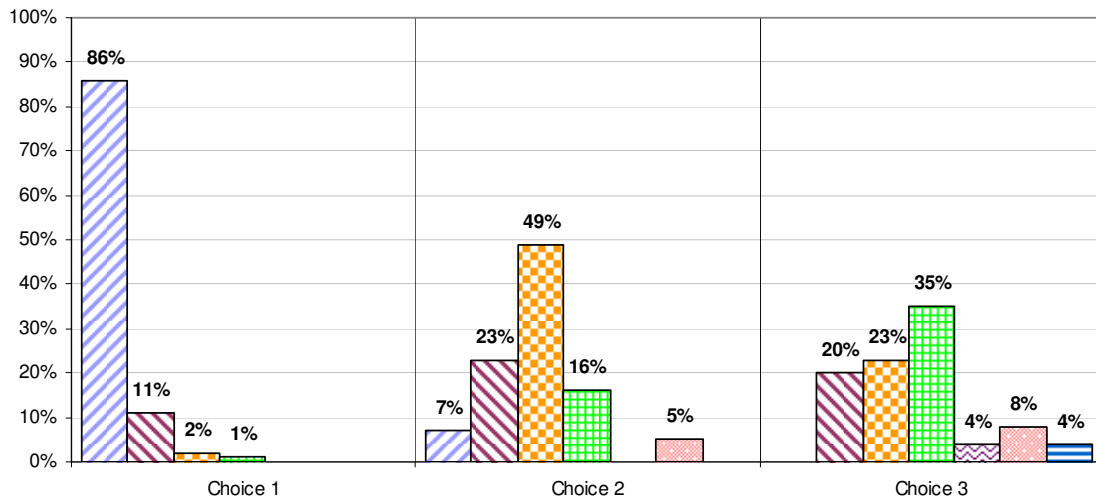
Figure 25: Owned electrical appliances
(source: Ehlers & Hertlein, 2008)

There was relatively less ownership of radios and televisions in the M'muock village. This is partly due to the high cost and the poor reception in the rural areas of Cameroon. Only one

household reported owning an iron (Ehlers & Hertlein, 2008).

Interviewees were provided with a list of seven different electrical appliances (lighting, television, mobile phone, radio, electric grinder, computer and iron) and were asked to choose the top three they would be willing to pay to use. The results were separated by gender to capture the influence of gender on the electrical application preferences (refer to Figure 26) (Ehlers & Hertlein, 2008).

Most desired electrical appliances (female)



Most desired electrical appliances (male)

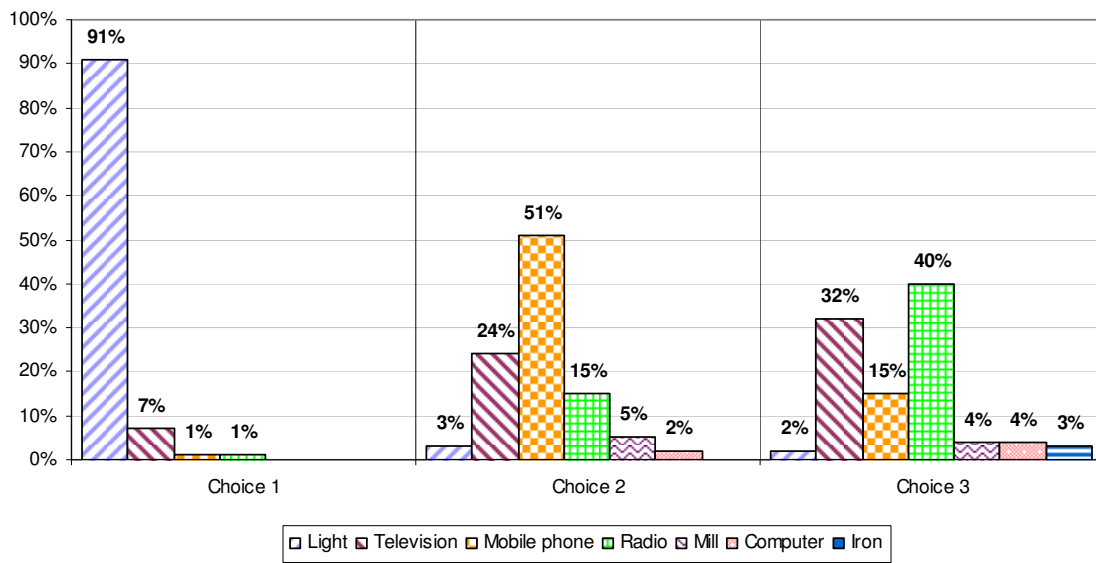


Figure 26: Most desired electrical appliances – female (above) and male (below)
(source: Ehlers & Hertlein, 2008)

For both men and women, the most popular appliances, in order of preference, were lighting, mobile phone and radio. Throughout all three choices, television was generally the second most popular appliance, irrespective of gender. The non-entertainment appliances (mill, computer and iron) are less preferred but are seen to play a relatively more major role as a third choice for the women than the men (Ehlers & Hertlein, 2008).

It was mentioned in Section 6.3 that the chief's palace in Ndungweh was equipped with a Chinese Turgo turbine and powered 10 compact fluorescent lights throughout the compound. Prior to this, light emitting diodes (LEDs) were used for lighting as it was seen to be the least energy intensive option, however, replacement LEDs were difficult to find within a reasonable proximity to the village and the LEDs were therefore replaced with the CFLs.

When asked what the applications would be in the case of greater electrical supply, a village resident responded that the electricity would be used towards refrigeration and additional lighting. In another rural village with partial electrical grid connection, it was observed that despite the more than sufficient electrical supply, refrigeration was not being employed by the residents. A commercially productive application was observed, where a gasoline engine was used in a bakery for dough kneading. In addition, a commercial coffee farmer had expressed his desire for a coffee cracking machine. The existing coffee preparation procedure consisted of harvesting coffee cherries, sun drying and then transporting the shelled coffee beans to neighbouring cities for cracking. It is to be noted that it was unclear if a manual or power-assisted coffee cracking machine was intended.

Community applications include health centres and schools. One health centre worker expressed the need for electricity for lighting, medical refrigeration and the use of microscopes. This was similar to the existing and intended uses of the electricity generated by the pico hydro turbine at the health centre in Lewoh. For the schools, an educator described the desire for electricity to provide students a place to study. In the urban and peri-urban areas, insufficient power supply was observed. At a location in Buea, grid supplied lighting was observed cycling on and off. This was an indication of an insufficient voltage supply, which damages connected electrical appliances. An electrician explained that a significant portion of his work is repairing appliances

due to this issue.

6.1.5 Perceived primary concern

The 2008 interviews included an open question regarding which particular problem was the primary concern for the individual. Responses to the question were once again separated by gender and illustrated in Figure 27. Other problems mentioned included water shortage, problems in the storage of agricultural products, high education costs, less firewood, dirty water, poor roads, poverty, less acreage, high fuel and fertilizer prices and lack of capital for investment (Ehlers & Hertlein, 2008).

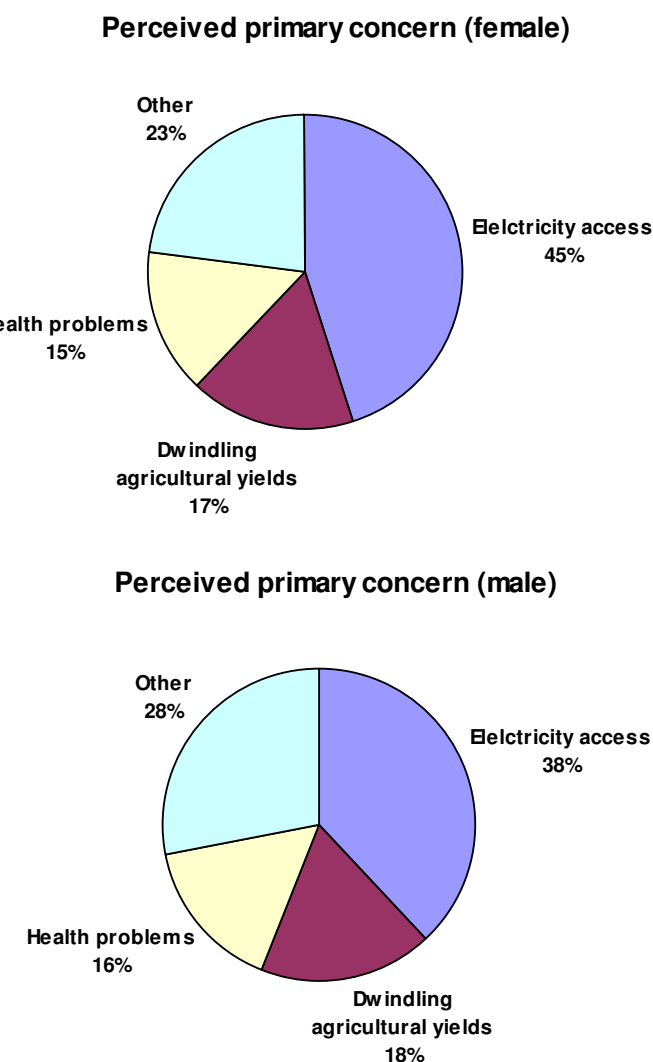


Figure 27: Perceived primary concern – female (above) and male (below)
(source: Ehlers & Hertlein, 2008)

One of the village residents mentioned they had applied for a road and indicated this as the top priority, followed by improved access to electricity.

6.2 Market Research

Approximate bill of materials were formulated for the conceptual designs developed in Chapter 5.0, and broken up into the different facets of the system: turbine, generator, and electronic controller.

It was found that materials useful for the turbine and generator such as steels, plastics, building construction material, motors, compressors, and automotive components were accessible within the peri-urban city of Buea. Electronic components for the controller were readily available in Bafoussam, the main city of the Western region. Obscure material sizes and specialized items were attainable from Cameroon's financial capital, Douala. The vendors of all of the components were generally microenterprises, with the exception of a few large building construction material distributors, such as Ste. Cogeni. A source of permanent magnets could not be found, which would be required if permanent magnet generators are to be employed for electrical production. A list of materials available in Cameroon and the local costs of these materials were formulated by the research team (Appendix A). The listed prices have some uncertainty: for example, some figures may be inflated due to vendors observing the researchers being foreign and consequently adjusting prices.

6.3 Installation Site Visit

Several sites of pre-existing pico hydro and small wind turbine installations were visited to sensitize the research team and identify lessons learned. The sites visited are listed in Table 9 detailing the application and technology.

Table 9: Visited installation sites

Location	Application	Technology	Functioning?
Bafoussam	Hotel	Wind turbine	Yes
Bafou	Health clinic	Wind turbine	No
M'muock	Battery charging station	Wind turbine	Yes
Ndungweh	Palace	Firefly/Turgo	No/Yes
Ndungweh	Household	PMA Firefly	No
M'muock	Palace	Firefly	No
M'muock	Fon's residence	Firefly	No
Lewoh	Health clinic	Turgo	Yes

In Bafoussam, the third largest city in Cameroon, two small wind turbines were located on the street level outside of Hôtel du Centre (Figure 28). The turbines were designed and commissioned by the owner, a relatively affluent pharmacist with interests in wind turbines and renewable energy technology, and built by two employed metal workers. The turbines consisted of 6 straight metal blades, transmission, permanent magnet generator and tail. The older turbine (right side of Figure 28) was approximately 1m in diameter and was observed to rotate at a speed of 30 rpm. The newer turbine (left) was being installed at the time of the visit; it had a larger blade diameter of approximately 1.25 m and a transmission with a 7:1 gear ratio.



Figure 28: Urban wind turbines – Bafoussam site

With the exception of the Bafoussam site, all the installations were in rural communities. A common characteristic was that the sites were fairly isolated and only accessible via a single unpaved road connection. These road connections often became impassable during the rainy season. Table 10 shows the limited extent of paved roads and the impaired conditions of the primary road network for the nation of Cameroon. Poor transport infrastructure greatly impacts the ability of the poor to access basic services, and is a more pronounced problem in rural areas. At the time of the field trip, road improvement construction was observed occurring on portions of some of the ancillary roads connecting the villages to cities, however the extent of the construction was unknown. The lack of reliable roads increases time and cost associated with buying and selling of goods. Dschang is the nearest city to Ndungweh, Bafout, M'muock, and Lewoh (Figure 22) and is where majority of the trading takes place in this region.

**Table 10: Length and condition of primary road network
(adapted: Charlier, 2009)**

Length	Paved	Gravel	Earth	Total
Kilometres	4090	9929	12110	26129
Percentage of network	16%	38%	46%	100%
Condition	Paved	Gravel	Earth	Total
Standard	21%	27%	29%	27%
Mediocre	37%	70%	6%	35%
Bad	42%	3%	65%	38%

In Bafou, a foreign NGO donated approximately €50,000 for the import and installation of a small-medium wind turbine system (see Figure 29) for lighting and water pumping purposes for a health clinic. The wind turbine system utilized two 12-bladed rotors and was equipped with an electronic controller and a 24 unit battery bank. The system functioned for approximately a year and has not been functioning since as early as 2008 as reported by local residents. The primary cause of the malfunction was unknown, but it was observed that a blade and tail of one of the turbines had disconnected, likely due to the high rotational speeds that would occur under no electrical load and high wind conditions. The electronic controller and battery bank were stored

in a concrete shelter. Health clinic personnel have attempted to repair the system, but they cannot access the required parts due to the lack of availability and high costs. They have contacted the foreign NGO to request further funding for the repair. During our visit, the health clinic and pump were connected to the electrical grid.



Figure 29: Bafou wind turbine

GREEN STEP e.V. installed a relatively smaller wind turbine for battery charging in M'muock that has been in operation since 2008. The wind turbine, as seen in Figure 30, is based on the Hugh Piggot design (2010) and was locally built. This design has been adopted by organizations in developed and developing countries including Nicaragua, Madagascar, and Mozambique. The design consists of 3-carved wooden blades mounted on a bearing and shaft assembly and connected to a permanent magnet generator constructed using epoxy, copper coils, and permanent magnets.

This system has experienced failures, but unlike the system in Bafou, the system was promptly repaired. In fact, the day prior to the research team's arrival, a storm had passed through where

high winds led to weld failure and the entire rotor and generator assembly disconnected and fell to the ground (Figure 30). Despite the fall, there was no damage to the rotor and generator assembly. The failed weld connection was a repeat failure and was repaired and further reinforced by a local welder to prevent future recurrence; electrical components were purchased from a local store to replace damaged connections. Both the welder and store owner were not affiliated with GREEN STEP e.V. The turbine was fully functional by the following day. Had the research team not been present, a service person trained by GREEN STEP e.V. would have been sent to investigate and repair the fault. Previous failures were both mechanical and electrical in nature and addressed by GREEN STEP e.V. trained local personnel. As mentioned, weld failures had occurred before, and the tail had disconnected due to insufficient fastening. Electrical related failures included ineffective dump loads in the battery charging circuitry resulting in the overcharging of batteries and also the improper use of batteries by end-users as the batteries were disconnected before being sufficiently charged. Both of these failure modes diminish the life of the batteries.



Figure 30: GREEN STEP e.V.p wind turbine – fallen rotor (left), failed weldment (right)

In 2008, four Firefly turbines were installed in Ndungweh and M'muock and situated along water arteries, near the users of power. The paths to reach the pico hydro turbines were steeply sloped and not maintained. There were signs of a recent landslide at one of the sites in Ndungweh.

None of the Firefly systems operated longer than 7 months (Urban, 2011). The cause of failure was observed to be the wearing of alternator brushes and consequent damage to the batteries and inverters due to the lack of power. Once this was discovered, the Firefly turbines were disconnected from the flow and the systems rusted as they stood stagnant (see Figure 31). Some of the systems were serviced and returned to use, but failed within the following 2 months (Urban, 2011). Prior to the alternator failures there were environmental effects on the turbine systems. Debris and siltation were apparent in the reservoirs and caused blockages at the intake. These issues were addressed by capping the intake of the penstock using a tin can with punched holes in the end and a porous netting to filter large debris from entering the penstock (refer to Figure 32). Caretakers were instructed to clear the accumulated silt and debris regularly. During the rainy season water levels were very high and washed away portions of the penstock. Local residents report the rainy season occurs in March to June with light rain and from June to September with heavy rain. Another failure occurred while maintenance was being conducted on the system. As the water flow through the turbine was shut off at the intake, the weight of the remaining water in the penstock created a vacuum as it exited out of the turbine, causing the penstock to implode. Figure 32 shows the locally improvised penstock modifications of cutting slits into a section of the penstock to avoid large vacuum formation during flow shutoff procedures. The slits would be blocked in succession allowing for a gradual decrease in flow rate through the penstock before complete flow shutoff.



Figure 31: Inoperable Firefly turbines



Figure 32: Debris and siltation in reservoirs (top left), filter netting (bottom left), modifications to penstock (right)

To improve the robustness of the Firefly by specifically addressing the alternator concern, GREEN STEP e.V. trialed a version of the Firefly equipped with a permanent magnet generator

(Figure 33), similar to that used in the Hugh Pigott (2001) wind turbines. When tested, the revised system produced higher voltages than the original Firefly design installed earlier at the same site. The system was only trialed and not connected for battery charging. Unfortunately, output current was not measured. Large vibrations were observed during testing and led to the system failing within 2 weeks. Documented faults contributing to this failure included cracked resin, cut copper cables, melted electrical connections and broken frames.



Figure 33: Permanent magnet generator Firefly

To replace the inoperable Firefly at the Ndungweh palace, another NGO installed an imported Chinese manufactured Turgo turbine system (Figure 34). The system was rated to supply 300 W (230 V, 1.3 A, 50 Hz at a rotation speed of 1500 rpm) under 14m head and 4 L/s flow conditions. It had been in operation for 2 months prior to the visit. It supplied 141 V to the compound and was used for powering 10 compact fluorescent light (CFL) bulbs and for charging lap tops and mobile phones. Limited consultation occurred with the residents of the chief's palace as the wives of the chief (the chief was not present during our visit) did not have much information to

offer regarding the turbine. This is a stark contrast to the process GREEN STEP e.V. had conducted prior to the installation of the Firefly, where local craftspeople were invited to a training session. Only males were invited to participate in the workshop, however, one of the chief's wives assisted with the delivery of the training session and that led to her later successfully troubleshooting an issue involving a break in the penstock. As recalled from her training, she shut the valve to stop the water flow and repaired the penstock with rubber material and restarted the system.



Figure 34: Turgo turbine at Ndungweh

Another imported turbine was installed by a Canadian NGO for a health centre in the remote rural village of Lewoh intended for powering several fluorescent lights and a refrigerator for vaccine storage. The system consisted of an imported Powerpal MHG-500HH (Turgo turbine with a permanent magnet generator of a capacity range of 275 W to 520 W) and a Swiss electronic controller by Brükmann Elektronik. A 24 V 450-600 Ah battery bank was planned for the system but not integrated as the batteries were not procured at the time of installation. After the installation of the turbine it was observed that significant leakage was located at the base of the turbine and was a source of power loss. A breathing pipe for the penstock to avoid damage when shutting the water supply to the turbine was detailed in the operations manual but was not installed.

Members of the research team were sent to the site to install batteries, and modify the turbine base seal and penstock. Due to the lack of funds, only 4 of the 12 batteries had been purchased and delivered to the health clinic and have been connected, tested and charged. The battery charger of the electronic controller was tested and found to be working. Prior to arrival, the lighting load had been wired to bypass the controller and was powered directly off of the turbine. This modification was performed by the health centre doctor, whom had electrical training from college, because he noticed the electronic controller repeatedly shut off. The research team found that the main switch consistently turned off after 15 minutes in both no load and load conditions. The electrical fault was attributed to a malfunctioning potentiometer on a sub-circuit which acted as a safeguard by shutting off the main switch to protect the system and batteries from excessive draining in the event the turbine stopped operating. Due to the fault, the bypass circuit modification wired by the doctor had been kept as is and the batteries were left disconnected from the controller to ensure safekeeping of the batteries and longer life.

It was also observed that the 300 W-480 W refrigerator was too large a load. The turbine's nominal output is 500 W but only achieved approximately 300 W at the time of the visit. This posed a challenge for the system and it was therefore advised to not use the refrigerator and to consider a smaller refrigerator if possible. The seal was replaced and the turbine reset, resulting in reduced leakage and improved performance of the turbine: output voltage increased from 237 V to 260 V. With the lighting load directly connected to the turbine without the electronic controller, the water flow was manually controlled on the turbine to regulate voltage at 230 V to prevent damage to the lighting system.

Some materials for a breathing pipe to be installed near the top of the penstock had been delivered, however had not been installed. This was due to the lack of a female-female fitting

that was needed to ensure a proper seal of the penstock in the event that the penstock was cut for the breathing pipe installation. It was decided to take the precaution of not installing the breathing tube since the caretakers were able to shut off the main valve situated at the top of the penstock as long as it was done very slowly to avoid damage to the penstock. This was emphasized to the caretakers and was understood as they were asked to demonstrate the shut off process. The breathing pipe materials were left with the caretakers and can be installed in the future when a female-female pipe fitting is attained.

6.4 Craftsmen Collaboration

The design process is iterative and benefits from different perspectives. Manufacturing processes and environments are often neglected by designers at the design stages resulting in flawed end-products. To gain an appreciation of the working environments and the capabilities of artisans, training schools and workshops were visited in the regions. In addition, a build trial was conducted with local artisans.

The Cameroon Opportunities Industrialization Center (COIC) is a vocational school established in 1986 by a global non-profit organization OIC International. The COIC is primarily situated in Buea and has expanded to other regions in the country since its establishment. The Buea campus is comprised of approximately ten buildings and a typical graduating class of over 200 students. It offers a two-year vocational/technical training program where a student can specialize in one of the different fields: auto mechanics, information and communication technology, building construction, hotel catering and management, textiles, metal fabrication/welding and wood work. Within the metal fabrication and welding program, the students were trained in automotive body repair, metal forming, industrial welding, and spray painting.

As seen in Figure 35, at the time of the research team visit, the students were building a

decorative steel security gate involving metal forming, cutting and welding processes. The construction consisted of mild steel rod and galvanized steel pipe welded to a mild steel square tube frame. Upon closer inspection, weld spatter, incomplete and porous welds and parent metal burn-through were observed at some weld joint locations. Slight misalignment of components was also observed. In addition, zinc contained in galvanized coatings has a relatively low vaporization temperature and welding galvanized steel produces zinc oxide fumes that are harmful to human health when inhaled. Precautions to minimize exposure were not apparent. The associated risks were acknowledged by the instructors and it was explained that the students are informed to drink a glass of milk following the welding practice, a historic and ineffective remedy.



Figure 35: COIC students of metal fabrication/welding program

The vast majority of workshop facilities in Buea, Bafoussam and M'muock ranged from permanent to semi-permanent open walled structures with compacted soil floor surfaces. Workshops were equipped with few tools. Tool inventory generally included an arc welder (most times home-made), vice, disc metal grinder and assortments of small hand tools (Figure 36). The workshops were connected to the main electrical grid, which was observed to be a generally insufficient supply with varying voltages, not ideal for welding. The workshops were mainly unfurnished and used improvised working surfaces were used such as discarded engine blocks or

structural members. An example of this was the metal workshop where the M'muock wind turbine was repaired (Section 6.3). Despite the constrained working conditions, adequate joint preparation practices were conducted and good quality welding was observed during the wind turbine repair.

Another craftsman in Buea that owned a workshop as described was tasked with disassembling the casing of a refrigerator motor in the least destructive manner. Unequipped with the specified wrenches, the craftsman proposed alternative methods for the disassembly. Initially he attempted to cut a groove into the hex head nuts to fit a flat head screwdriver for unbolting, however this was unsuccessful because the bolts were seized and he could not apply sufficient torque. It was then proposed to tack weld the end of a bent rod to the top of the hex head to apply more torque to unseat the bolt. This was not pursued because the research team did not want to risk damaging the contained circuitry with the weld electrical current.



Figure 36: Standard metal workshop

There were two workshops that were the exceptions to that as described above. In Buea, there was a relatively large commercial workshop focused towards woodworking. It was equipped with automated tools including a planer, cut saw, table saw, belt sander, and band saw. The floor was a poured concrete pad and the workspace was furnished with work tables. In addition, metal

working was performed here as well. A welded assembly of hollow steel tube was underway. Weld quality of the work was similar to that of the COIC. In Bafoussam, there was a metal workshop that belonged to a craftsman associated with ADEID. The tools of the workshop included a lathe, commercially-made arc welder, punch, drill press, tooling for aluminum sand casting, metal grinders and custom tooling for jigs and patterns. Mills for palm oil processing were fabricated and have been a long-standing business for the craftsman. In addition, finished Pelton turbines were seen at the facility and the production quality was observed as very high. Several units had been made in the past and implemented in rural villages. Aluminum sand casting was used for producing Pelton cups for 10 kW and 15 kW systems. Both a finished Pelton turbine system and Pelton cups can be seen in Figure 37.



Figure 37: Pelton turbine system (left) and cups (right)

Interest in producing cross-flow turbines was expressed by ADEID. Prior to the research team visit, recent attempts had been made by the craftsman to fabricate the sidewalls. Figure 38 show an initial trial that was performed by hand-cutting each individual slot and resulted in uneven sidewalls. Through discussions, improvements to the side plate construction were considered and defined: rough cut the disc by hand, turn on the lathe to the finished diameter and locate centre, employ a jig that restricts the translation of the disc but allows the rotation about the centre, rotate

about the centre and mark the blade circular array punch out the slots for the blades.



Figure 38: Initial cross-flow sidewall

In Buea, a build trial focused on the propeller turbine design was conducted with a craftsman identified as the top participant from the GREEN STEP e.V. training. Given the craftsman's familiarity with the cross-flow turbine from past experiences of the Firefly model, the cross-flow concept design was not trialed. A hand-sketched schematic, as seen in Figure 39, was loosely based on the propeller runner concept design (Section 5.2.1) and provided three days prior to the trial to allow the craftsman to analyze the problem and develop independent solutions. It was explained that the unit was to be built with minimal guidance from the design engineer, if any. The schematic detailed a propeller runner with four circular arc curved blades with radial outward increasing chord length. Emphasis was placed on several aspects:

- the blade forming techniques
- accuracy of the blade forming to the design specification
- repeatability of the blade forming
- assembly of the propeller

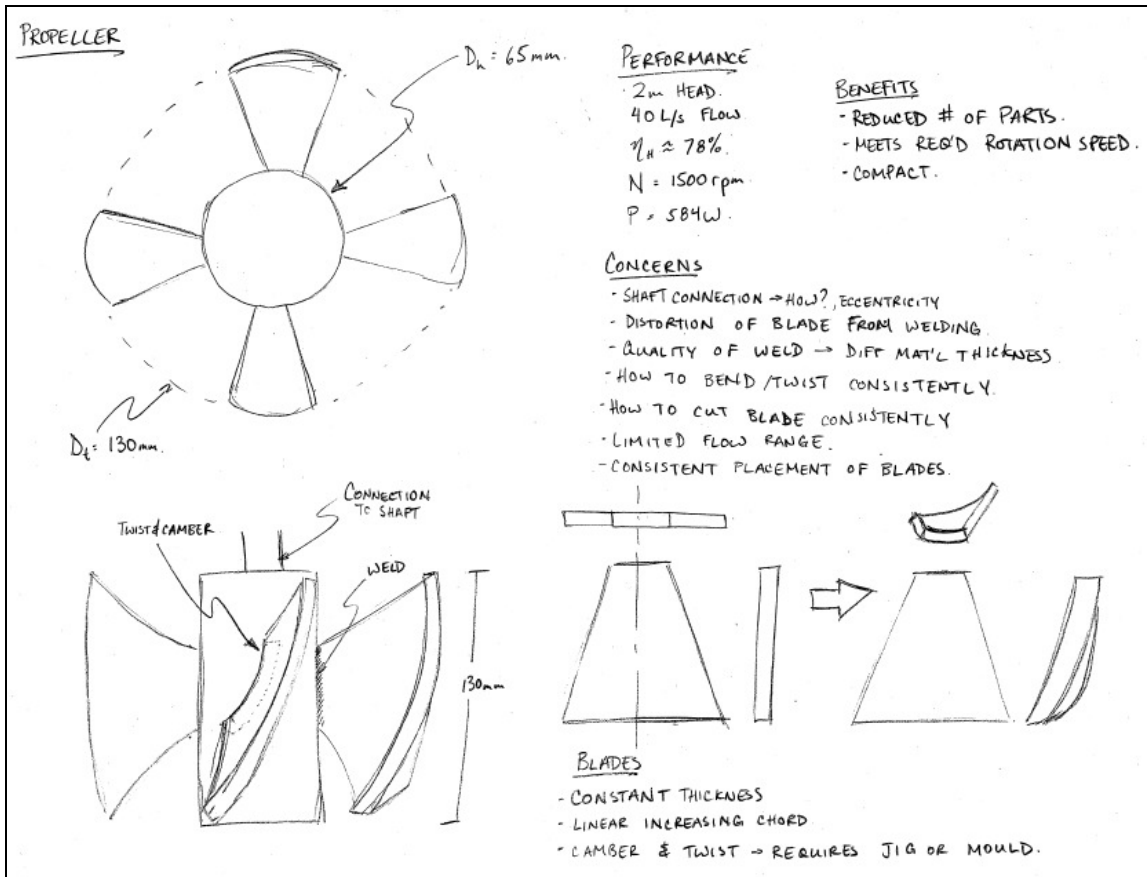


Figure 39: Build trial schematic

The trial was conducted in a rented workspace of a small metal workshop equipped with a commercial grade welder, disc grinder, assorted small hand tools and a stand-mounted vice. The workshop was owned by a welder who employed an apprentice. The craftsman typically rents workspace at a larger more equipped facility but was not accessible at the time of the trial. The craftsman was accompanied with two colleagues that were electricians by trade.

Materials were procured and consisted of a length of mild steel pipe (60 mm diameter and 4 mm wall thickness) and a 1 mm thick mild steel sheet. The materials had noticeable mill scale and surface rust. The pipe was held in a vice and cut with a hacksaw to a length of 135 mm (Figure 40). Straightness or level of cut was not checked. Four rectangles with dimensions $130\text{ mm} \times 65\text{ mm}$ were measured and marked on the metal sheet. The rectangles were cut using hand-shears

(Figure 40). Bending of the sheet occurred during the cutting process. It was initially attempted to flatten the bends with a hammer, using the flange of a small I-beam as a working surface, however the flange was not a large enough surface and insufficiently flat. Instead, the craftsmen alternatively used the compacted dirt floor as the flattening surface (Figure 40). Following this, the rectangles were trimmed to the detailed trapezoid shapes. During the blade forming, it was discovered that one of the trapezoid shapes were inconsistent with the others and subsequently corrected.



Figure 40: Material preparation

Emphasis was placed on the accuracy of the individual blade forming and the consistency from blade to blade. Due to the lack of tooling, it was defined by the design engineer to use the approximately 140 mm diameter grinding disc of the disc grinder as a gauge for the circular arc blade curvature (Figure 41). The GREEN STEP e.V. trained craftsman initially intended to use a cylindrical form, but none could be found. It was proposed by his colleagues to use the

aforementioned small I-beam as a makeshift mould. This involved setting the flat blade parallel to the web while spanning across both flanges. The blade would then be hammered toward the web to form the curve. When the GREEN STEP e.V. trained craftsman was asked if this was sufficient by the design engineer, he expressed his openness to the suggestion. After trialing the I-beam forming method (Figure 41) and comparing to the curvature gauge, it was of the opinion of the craftsmen that the detailed blade form was achieved. The remaining three blades were formed accordingly (Figure 41). When comparing the blades to each other, inconsistencies in the blade forms were observed.



Figure 41: Blade forming

The four blades were to be set equally apart in a circular array surrounding the circumference of the pipe. An arc length of 40 mm parallel to the plane of the circumference was defined for the projected span of the blade. This dictated the blade leading (“start”) and trailing (“stop”) edge

locations on the cylinder, moreover, the blade pitch angle. The axial position of the blades was specified to be centred on the axial dimension of the pipe (Figure 42).

To measure the circumference of the pipe, the craftsmen used, what they termed, a “local” method by wrapping a wire around the pipe one revolution and cutting it to length (Figure 42). The length of wire was then folded and cut into quarter lengths, which was equivalent to the circumferential pitch distance on the pipe between blades. At first, the craftsmen only marked the start positions of the blades and not the stop positions. Only after providing additional clarification by indicating on the pipe the “start-blade” position, “stop-blade” position, “space/skip” length, was the concept understood. In addition, blade positioning was planned based on the flattened hub chord length of 80 mm and the artisan needed reminding that the hub chord length was changed due to the curving of the blade. Consequently, the hub chord length was measured to be approximately 75 mm. Only one blade was measured and assumed to be correct and equivalent to the other blades. Once placing the blades on the pipe, it was realized by the craftsmen that it did not sit flush on the pipe and were therefore modified with a disc grinder in an attempt to achieve a closer fit (Figure 42). Wire cutters were used to remove the burrs from the ground ends.



Figure 42: Blade placement

A particular weld connection was not specified in the schematic. The welding was performed on the compacted soil floor and then subsequently conducted on a provisional stand, a discarded I-beam (Figure 43). Prior to the welding, care was not taken to clean the materials. The blades were initially tack welded for placement (Figure 43). The GREEN STEP e.V. trained craftsman began the welding, and then handed the welding exercise to the apprentice. A few attempts were required before a steady weld arc was achieved. During the tack welding of the four blades, one of the welded blades disconnected and was tack welded back onto the pipe. Once in place, the master welder, who was able to maintain a relatively steadier arc, completed the welding (Figure 43). Varying gap distances existed due to the insufficient grinding of the blade hub ends, forcing the master welder to apply additional filler material to the weld.

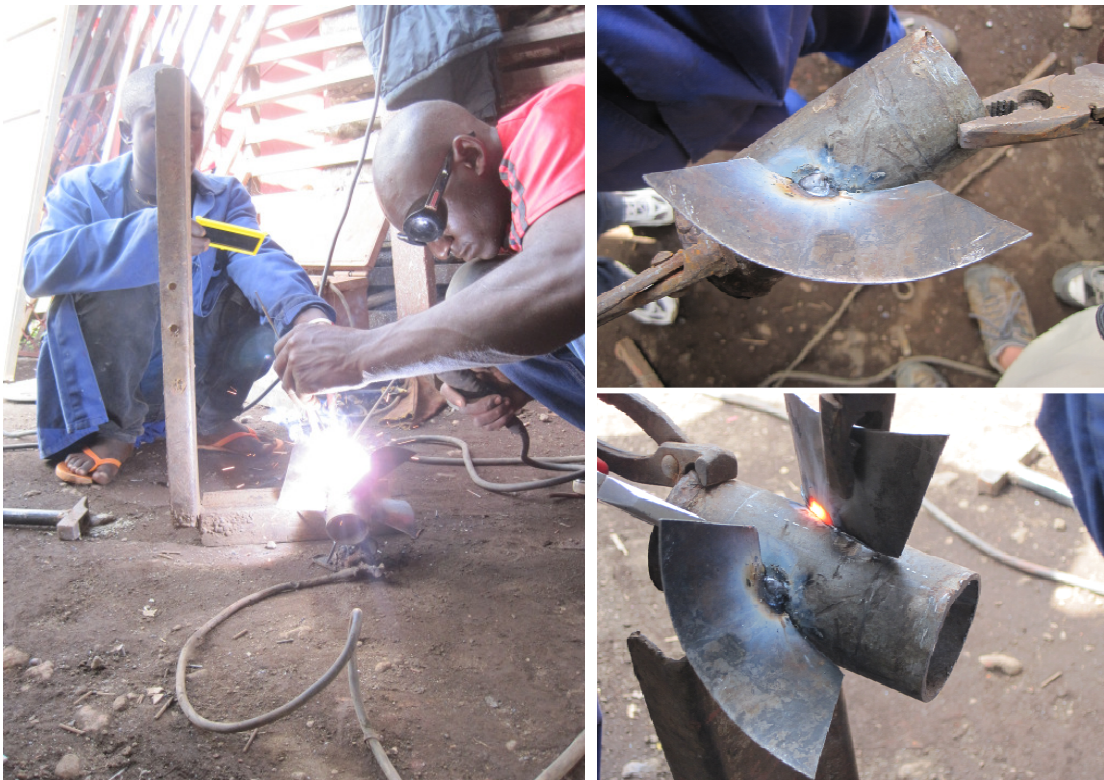


Figure 43: Welding

The build trial time duration was 3.5 hours. The construction quality was poor. The blades were inaccurately formed and imprecisely repeated. The blades were misaligned on the hub (Figure 44). The weld quality was also poor with incomplete penetration at some locations and burn-through in either the blade material or hub (Figure 44). The weldments were inconsistent in length, and discontinuous along the seams. Excessive porosity and weld splatter are seen on some portions of the welds.



Figure 44: Final assembly

In addition to turbine fabrication, proper use and maintenance of pico hydro systems must also be considered. An essential factor for this is caretaker training. ADEID's preferred method is to have the village members primarily identify potential caretaker candidates and collaborate with the village for the final selection. Following the selection, the training is conducted on-site. This was practiced for a 10 kW communal system in Quibeku, a village nearby Ndungweh. Some time after the installation, the system was operational until a bearing failure occurred. This was independently identified by the village caretakers. The caretakers removed the faulty bearing and gave it to ADEID for repair. GREEN STEP e.V. also exercised a similar selection method for their pico hydro installations. The village would initially choose the caretaker and GREEN STEP e.V. would also interview the candidates to evaluate intentions and capability to fulfill the caretaker duties. The evaluation took schedules and other commitments of the candidates into consideration. That said, there have been cases where the caretakers often did not fulfill their responsibilities and GREEN STEP e.V. needed to proactively contact the caretakers for

information regarding the well-being of the systems.

6.5 Field Research Discussion

The field research in Cameroon reaffirmed that electricity is a priority of the rural population. Currently there is great reliance on fossil fuels such as petrol, diesel and kerosene; however, this can be substituted with renewable energy technologies to mitigate the exposure to increasing fuel costs.

Renewable energy systems have been implemented: both imported and locally manufactured technologies have been utilized. Both approaches had advantages and disadvantages. Imported systems tended to be significantly more sophisticated. The imported pico hydro turbines in Ndungweh and Lewoh were operational and able to provide consistent power for lighting. However, this was overshadowed by the inaccessibility of technical support and replacements parts, with the impact more pronounced in the Bafou wind turbine installation. In addition, it is suspected that higher costs were incurred for these imported systems due to comparatively higher capital costs and import costs. The imported pico hydro systems should be monitored to determine the longevity of these systems and the actions taken in the event of a malfunction. The Ndungweh installation demonstrates potential for imported pico hydro systems when combined with the proper training of end users. In contrast, the locally manufactured Firefly models were not operational after several months of use, despite the maintenance and repair work that was performed. This highlights the importance for a more robust design.

All of the visited pico hydro systems utilized turbines operating within the medium-to-high head range. Pico hydro is in its infancy stage however, interest does exist from both the consumer and technician perspective. By establishing a knowledge base through training and learning-by-doing, improved efficiencies can be achieved to the system design and the manufacturing process.

In addition, this may create work opportunities and empower artisans.

It was previously realized that cross-flow technology can be locally constructed; results from a build trial demonstrated that a propeller turbine can also be built. However, the designs must be communicated in a clear manner within the Cameroon context and incorporate the working environment. As seen from the build trial, build quality was poor, mainly with inconsistent blade forming, placement, and weld quality. This would adversely impact strength and power generating performance of the turbine. It is to be noted that the build trial was the craftsmen's first exposure to propeller runners and may not have had adequate time and equipment to prepare. This emphasizes the need for the provision of additional artisan training, sufficient tooling and workspaces to improve production quality.

Training must also extend to the end-users and caretakers of the systems as was evident in several pico hydro installations. Had there not been trained individuals or end-users with prior experience or knowledge, which is often the case, the systems may have remained inoperable and the investment completely lost had the damage increased beyond repair.

7.0 Detailed Design

From the field research, it was concluded that both cross-flow and propeller turbine designs were viable options since both are operational under low head conditions and that material and build capacity for local fabrication is available. However, based on the project technical requirements (Section 3.1) bias towards improved local manufacturability and lower required maintenance, it was determined that the cross-flow turbine was less suitable. This was mainly attributed to the added complexity when introducing a transmission system required by the cross-flow design for high rotational speeds. In contrast, propeller turbines can achieve high rotational speeds without a transmission system, therefore giving the potential for manageable turbine volumes and lowering maintenance concerns associated with additional components and moving parts. The detailed design process moved forward based on the propeller runner concept design, based on these considerations. To summarize, the propeller turbine is to produce approximately 370 W shaft power with 2 m head and 25 L/s flow rate with a rotation speed of 1500 rpm.

The proposed turbine configuration is an open flume vertical axial flow propeller turbine, as seen in Figure 45. This has been adopted by several pico hydro developers (Asian Pheonix Resources Ltd., 2008; DTU-Development Technology Unit, 2010; Singh & Nestmann, 2009) and has proven to be popular in developing countries in Southeast Asia. It is for this reason that this configuration for the propeller turbine design was selected. The major components of the system consist of an inlet basin, stator, runner, and draft tube.

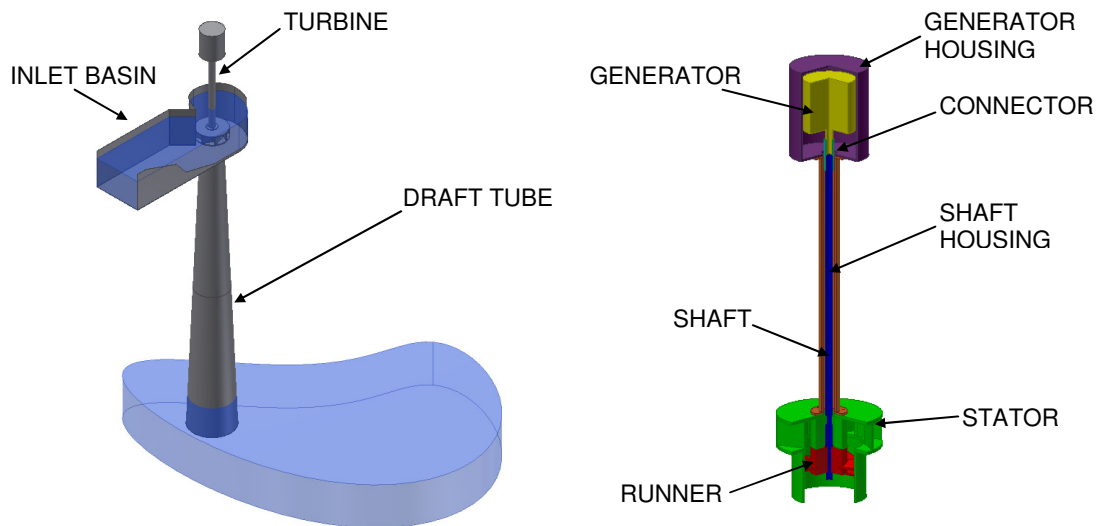


Figure 45: Design configuration of system (left) and turbine (right)

7.1 Runner Design

The runner is the key element of a turbine and impacts design decisions about other aspects of the turbine system. Runner design factors include hub and tip diameter, blade angles, curvature, twist and spacing. Design rationale on these factors is discussed below.

7.1.1 Tip Diameter

Since most aspects of the runner design depend on its size, tip diameter was considered first. The concept propeller turbine design (Section 5.2.2) determined from the Simpson and Williams (2011) method had detailed a tip diameter of 117 mm. This initial diameter was compared to tip diameters calculated using other sizing methods, and the results were used to finalize the runner sizing.

Round (2004) presents coefficient C_{Round} versus head from a wide range of experimental data, as seen in Figure 46.

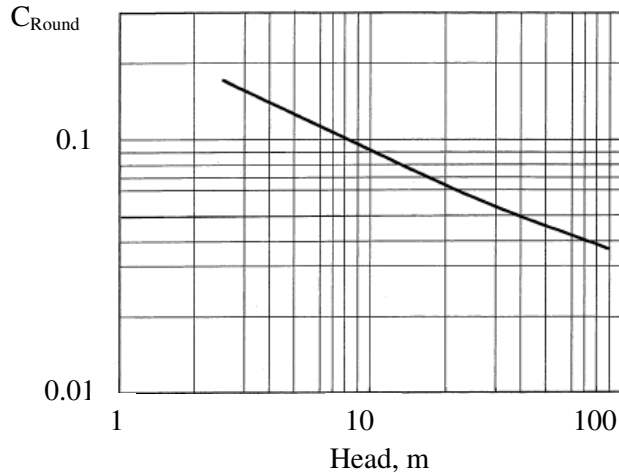


**Figure 46: C_{Round} as a function of head to determine tip diameter
(source: Round, 2004)**

C_{Round} is the ratio of tip diameter to the square root of generated power.

$$C_{Round} = \frac{D_t}{P^{1/2}} \quad (7.1)$$

where D_t is runner tip diameter in units m and P is generated power in units kW. Round states that the plots are taken from operating commercial turbines and that the variation of power specific speed is large in comparison to the much smaller variation amongst the runner tip diameter. From this, Round suggests it is more accurate to base turbine dimensions on a runner correlation rather than a power specific speed correlation. Extrapolating Round's (2004) curve for an operating head of 2 m gives a runner tip diameter of 100 mm for a turbine with generated power output of 250 W.

Wright (1999) suggests referring to the Cordier diagram (reproduced in Figure 47), which correlates specific speed and specific diameter based on empirical data of a range of different turbomachines, and can be used to determine tip diameter. Applying equations (2.2) and (2.6), specific speed and specific diameter were calculated respectively as 2.66 and 1.78 and resulted in a tip diameter of 134 mm. Balje (1981) further adapted the Cordier diagram for turbines operating with liquids (refer to Figure 48). Based on this analysis, greater than 75% efficiency

will be achieved with a tip diameter dimension within the above mentioned range of values.

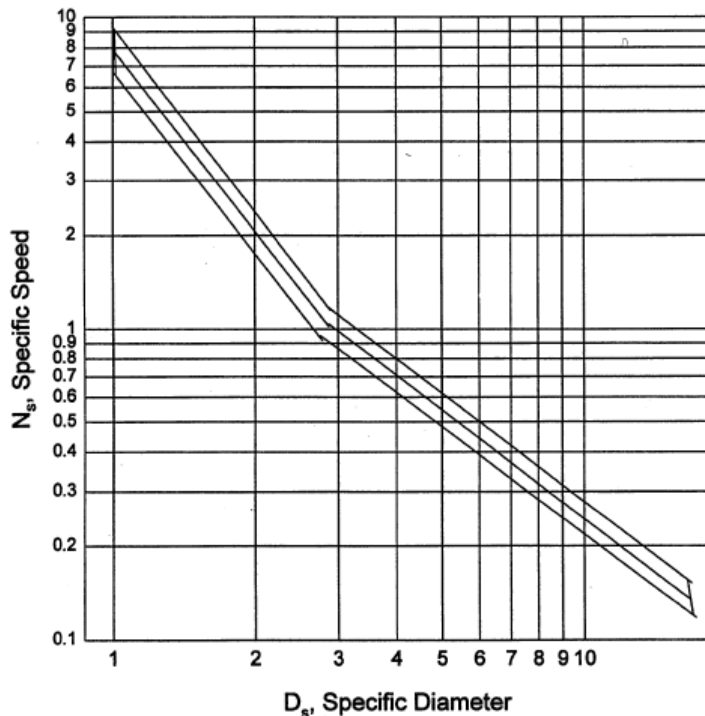


**Figure 47: Cordier diagram – specific speed as a function of specific diameter
(source: Wright, 1999)**

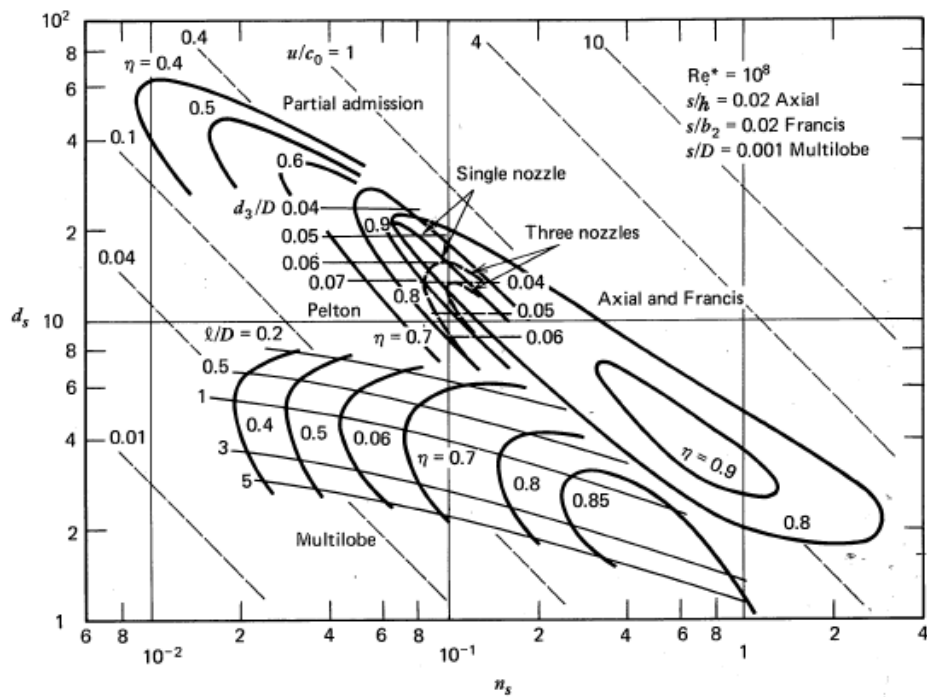


**Figure 48: Various turbine efficiencies as a function of specific speed and specific diameter
(source: Balje, 1968)**

It is planned that steel tubing will be used to house the runner: this sets practical limitations on the tip diameter dimension. Standard steel tube section sizes within the range of these runner tip diameter dimensions were identified. A nominal steel tube section was 141.3 mm × 4.8 mm (5.563 in x 0.188 in) with an actual tube wall thickness of 4.4 mm and an inner diameter of 132.5 mm. Accordingly, the tip diameter was set to 130 mm leaving a 1.25 mm clearance between tips and tube wall.

7.1.2 Hub-Tip Diameter Ratio

The hub-tip diameter ratio, D_h/D_t , defines hub diameter and the annulus flow area for propeller turbines. This also defines the absolute fluid velocity in the axial direction through the annulus, C_x , since flow rate, Q , is the product of the absolute fluid velocity in the axial direction and the annulus area. Recall from the concept design, $D_h/D_t = 0.55$, which with the detailed design tip diameter of 130 mm results in a hub diameter of 70 mm.

Nechleba (1957) makes recommendations for Kaplan turbines based on the sufficient allowance of hub material to anchor the blades. Nechleba provides a table of guidance values, designating a hub-tip diameter ratio of 0.3 for devices with 3 blades, operating in 5 m head (table ranges from 5 m to 70 m head). This is significantly lower than prescribed by Simpson and Williams.

Durali (1976) employs a high hub-tip diameter ratio of 0.8 to incorporate short blades with no twist. This was designated as a major constraint in his design procedure, likely to simplify manufacture. Further rationale was not provided.

Wright (1999) theoretically determined the smallest hub-tip diameter ratios while maintaining the de Haller limit across a range of specific speeds. The de Haller number is typically applied to compressors and is the ratio of the exit relative flow velocity to the inlet relative flow velocity.

Compressor blades decelerate flow to a limit before the flow detaches from the blade surface causing unsteady flow, or blade stall. This can also be applied to turbines (Gunnerson, n.d.) where the de Haller limit, dH , takes the form as follows:

$$dH = \frac{C_3}{C_2} \geq 0.72 \quad (7.2)$$

recalling C_2 is the absolute fluid runner inlet velocity and C_3 is the absolute fluid runner exit velocity. Wright's analysis was in close agreement with guidelines provided by Jorgensen (1983) and past work conducted by Balje (1968). These values were adapted by Wright (1999) and are illustrated in Figure 49.

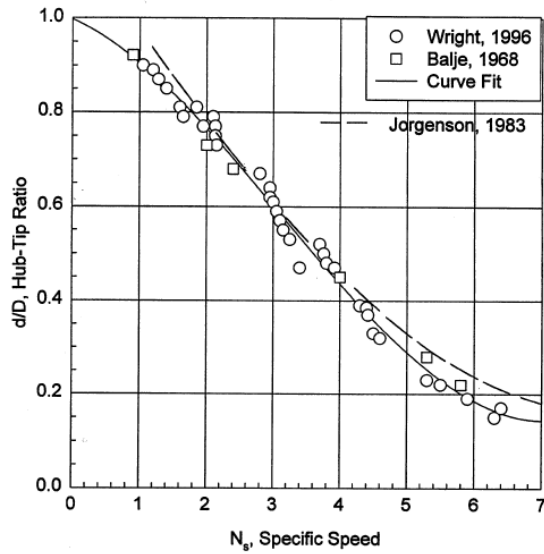


**Figure 49: Hub-tip diameter ratio as a function of specific speed using de Haller limit
(source: Wright, 1999)**

A curve fit applied by Wright (1999) to the data points gives:

$$\frac{D_h}{D_t} \cong \left(\frac{1}{2} \right) \left\{ 1 - \left(\frac{2}{\pi} \right) \tan^{-1} \left[\left(\frac{2}{\pi} \right) (N_s - 3.8) \right] \right\} \quad (7.3)$$

Applying this analysis, a hub-tip diameter ratio of 0.699 was specified.

Singh and Nestmann (2011) concluded that having a larger hub-tip diameter ratio yielded lower runner losses. However, during this study, the impact of blade number (mentioned below) was

also investigated and had greater influence.

Based on the above, there is no clear guidance on hub-tip diameter ratio. Debris in the flow was observed from field research as a significant concern and was therefore decided to set the hub-tip diameter ratio to a larger value to mitigate potential blockages. $D_h/D_t = 0.55$, as determined with the Simpson and Williams method, was incorporated. This resulted in a hub diameter of 70 mm.

It is to be noted that the hub and tip diameter sizing was determined through a review of empirical methods. A universal systematic method to define these sizing parameters was not found from the review of literature.

7.1.3 Design Velocity Diagrams

With the overall blade sizing defined by the tip and hub diameters, the flow can be simulated to determine the formation of the blade.

Radial variation in the flow was characterized at five stations along the radial co-ordinate of the blade using a custom written Matlab program (Appendix C). The stations were equally spaced between the hub and tip locations along the length of the blade (Figure 50). Velocity diagrams (refer to Section 2.6.3) were developed for each station and used to design the blade geometry (refer to 2.6.4 and Figure 17).

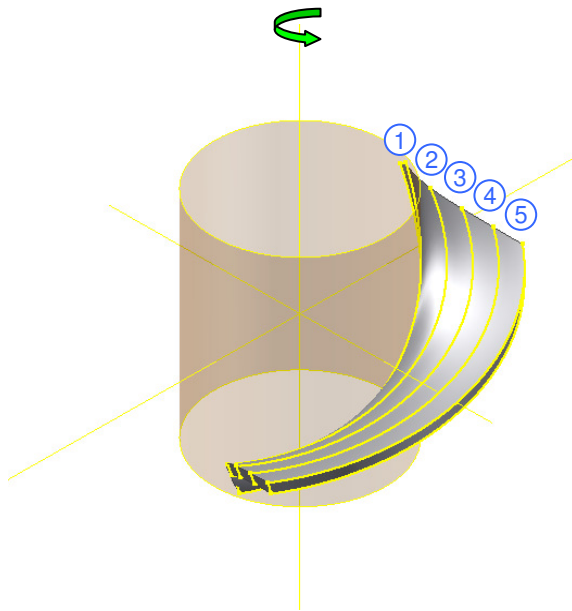


Figure 50: Radial blade stations for velocity diagrams

Many prior runner designs incorporate zero runner exit swirl, $C_{\beta\theta} = 0$. This would theoretically maximize the angular momentum extracted by the runner, but does not necessarily achieve greatest overall system efficiency. Alternatively, Hothersall (2004) suggests maintaining some swirl in the fluid velocity when entering the draft tube to reduce separation and increase efficiency of the draft tube. Having some exit swirl has been supported by Nechleba (1957) and Simpson and Williams (2011) who recommend setting the relative exit velocity to the runner blade velocity, $W_3=U$.

From the velocity diagrams, the mean camber line is developed based on the desired flow angles. The triangles were connected by a camber line using a circular arc to simplify the manufacturing process; however, other problems arise since large arc radii are developed from the shallow angles.

The blade stagger angle, ζ , is the angle between the blade chord line and the reference direction. The reference direction is the axial direction throughout this thesis. For circular arc blades, the

stagger angle is defined as:

$$\xi = \frac{1}{2}(\alpha'_2 - \alpha'_3) \quad (7.4)$$

where α'_2 is the blade inlet angle and α'_3 is the blade exit angle. For the runner blade design, the blade inlet and exit angles are defined by the relative flow inlet and exit angles, β_2 and β_3 , respectively.

Setting $W_3=U$, the velocity diagrams (Section 2.6.3) gave the values shown in Table 11:

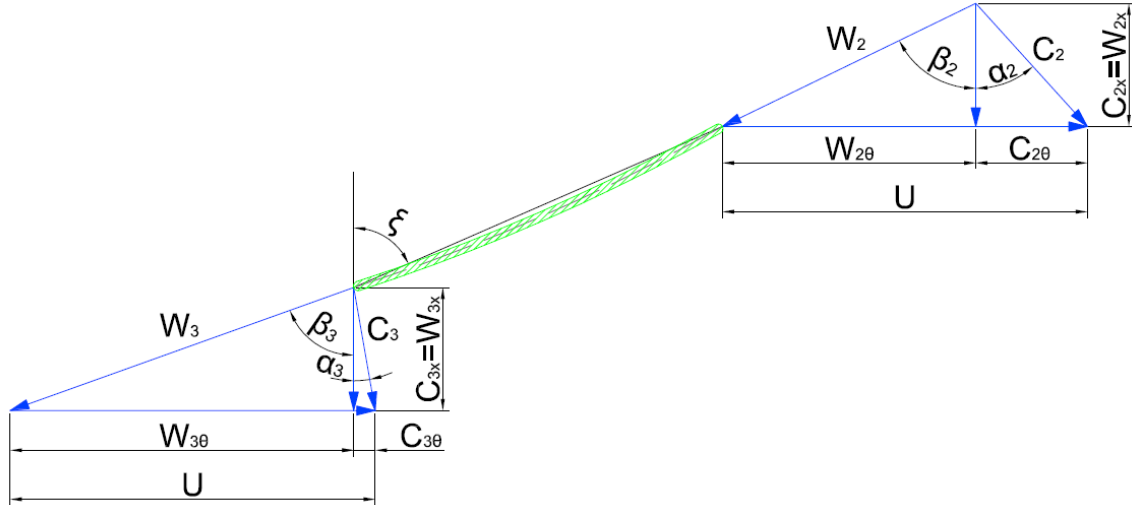


Figure 51: Velocity diagram

Table 11: Calculated flow angles and stagger angles

	Blade Station				
	1-Hub	2	3-Mean	4	5-Tip
Absolute flow angle-inlet (α_2)	52.5°	46.9°	42.2°	38.2°	34.8°
Relative flow angle-inlet (β_2)	37.6°	55.4°	64.1°	69.1°	72.4°
Absolute flow angle-exit (α_3)	14.4°	11.7°	9.9°	8.5°	7.5°
Relative flow angle-exit (β_3)	61.2°	66.6°	70.3°	72.9°	74.9°
Stagger angle, ξ	49.4°	61.0°	67.2°	71.0°	73.7°

7.1.4 Number of Blades and Space-Chord Ratio

The number of blades, blade pitch, and chord length are interconnected. An increase in the number of blades, or a reduction in spacing between blades, improves flow guidance, however

increases losses due to friction. Conversely, with greater blade spacing, lower flow guidance results in increased losses due to flow separation. To optimize this balance, Zweifel established a criterion for the ratio of tangential blade loading comparing the actual to ideal case. The actual loading is the pressure difference across a turbine blade and characterized by the product of the mass flow rate and the inlet and exit tangential velocities. The ideal loading is the product of the incompressible loss-free flow pressure difference across the blade and the span area normal to the tangential direction (Dixon & Hall, 2010; Horlock, 1966). From this, the Zweifel criterion, Z , is defined as follows:

$$Z = 2(s/b)\cos^2 \beta_3 (\tan \beta_2 + \tan \beta_3) \quad (7.5)$$

where s is the blade spacing, b is the axial chord length, β_2 and β_3 are the runner inlet and exit flow angles, respectively. Based on empirical studies, Zweifel had found that a ratio of approximately $Z=0.8$ would achieve minimal losses. Applying this, an optimal space-chord ratio can be determined by the following:

$$s/b = \frac{0.4}{\cos^2 \beta_3 (\tan \beta_2 + \tan \beta_3)} \quad (7.6)$$

Other recommendations on space-chord ratios by Wu, Ytreøy, and Raabe had been cited by Simpson and Williams (2011). It was noted that the values recommended were defined as the ratio of the blade pitch to the aligned chord length as opposed to the axial chord length used in the Zweifel calculation. When compared, the Simpson and Williams recommendations are approximately 3 to 5 times larger than the transformed Zweifel criterion equivalent.

Spacing and axial chord length values were calculated based on the recommendations across a range of number of blade options. Four blades were used for this design. This is lower than the suggested five to six blades from the Simpson and Williams design guide and greater than the three blades in the aforementioned Nechleba table (Section 7.1.2). The four blade design was chosen to simplify manufacture and in following of the Powerpal models. It was decided to apply

the Zweifel criterion for the space-chord ratio.

In addition, Hothersall (2004) suggests a “crude” design simplification of a constant aligned chord length equivalent to the aligned chord length at the hub. This was adopted to simplify the geometry, moreover the manufacture process.

7.1.5 Incidence and Deviation Angle

Ideally the flow will follow the blade geometry, as assumed in the design procedure thus far. However, in reality, the flow diverges and impacts the velocity diagrams, therefore resulting in lowered efficiency of the turbine (Schobeiri, 2005). The difference between the flow angle and blade camber angle at the entrance of the blade is known as the incidence angle, and the difference between the flow angle and blade camber angle at the blade exit is termed the deviation angle. Unlike compressors, turbines are less sensitive to large incidence angles and therefore incidence angle analysis is neglected in some design methods (Dixon & Hall, 2010; Schobeiri, 2005; Simpson & Williams, 2011).

Schobeiri (2005) suggests the Traupel method in determining the deviation angle. The method considers the pressure distribution on the pressure and suction surfaces of a turbine cascade at the throat and exit flow locations to estimate the momentum balance in the circumferential direction. In conjunction with mass continuity and incompressible flow assumptions, a relation is established between the diverging exit flow angle and the throat flow angle. Deviation, δ_{3s} , is calculated (adapted to match the convention used in this thesis) by the following:

$$\delta_{3s} = \beta_{3c} - \beta_3 = \beta_{3c} - \text{acot} \left[\frac{a}{s} \frac{1}{\sin \beta_a} \right] \quad (7.7)$$

where β_{3c} is the blade exit camber angle, β_3 is the flow exit angle, a is the blade throat, s is the blade spacing, and β_a is the flow angle at the throat.

For propeller turbines, Hothersall (2004) analyzes both incidence and deviation angles, where the prior is influenced by blade loading, which is a function of camber angle and stagger angle, and blade blockage. These components of the incidence angles can be determined using Figure 52 and Figure 53 respectively.

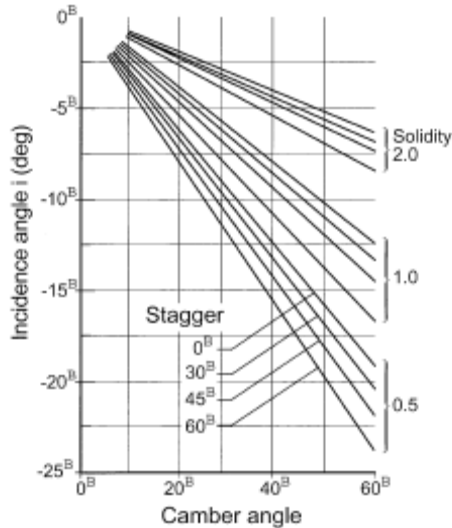


Figure 52: Blade loading
(source: Hothersall, 2004)

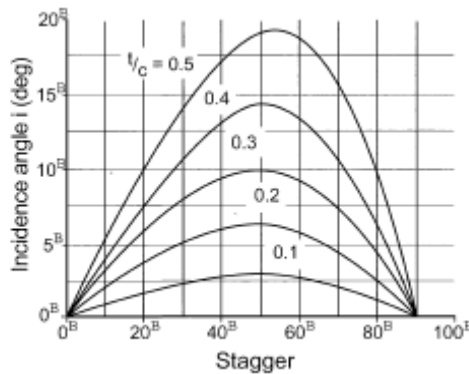


Figure 53: Blade blockage
(source: Hothersall, 2004)

Hothersall (2004) applies a function known as Carter's rule to determine deviation angle, δ_{3H} , and is as follows:

$$\delta_{3H} = m\theta \frac{s}{L} \quad (7.8)$$

where m is Carter's parameter, θ is camber angle, s is blade spacing and L is aligned chord length.

Carter's parameter is a function of stagger angle and differs for circular arc or parabolic arc camber lines and is determined using Figure 54.

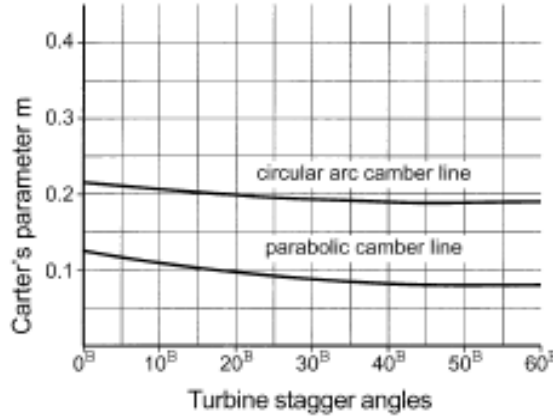


Figure 54: Carter's parameter
(source: Hothersall, 2004)

Calculated deviation angles following Schobeiri and Hothersall were compared and were in general agreement. The hub station showed greatest discrepancy of approximately 4° and diminished moving outward towards the tip to a difference of less than 1° . Incidence and deviation angles determined using Hothersall's method were used for the design and summarized below:

Table 12: Incidence, deviation and final flow angles

	Blade Station				
	1-Hub	2	3-Mean	4	5-Tip
Incidence due to loading	5.0°	1.5°	1.0°	0.5°	0.5°
Incidence due to blockage	1.0°	1.0°	0.8°	0.5°	0.5°
Total incidence	4.0°	0.5°	0.3°	0.0°	0.0°
Final relative flow angle-inlet (β_{2F})	33.6°	54.9°	63.8°	69.1°	72.4°
Deviation	1.9°	1.1°	0.8°	0.5°	0.4°
Final relative flow angle-exit (β_{3F})	63.1°	67.7°	71.0°	73.5°	75.4°

7.1.6 Flat Blade Design

A significant disconnect between theory, design, and manufacture is apparent in the preceding discussion. The above camber-twist blade design is targeted to achieve the technical requirements but does not fit into the present local manufacturing context as it is too complicated to be built in an accurate and precise manner. Therefore, a simplified flat blade design was extracted from the complex geometry design to significantly improve manufacturability at the cost of performance. This is seen as a means to initiate the learning-by-doing process, and as capacity builds, complexities in later revisions can be incorporated to recover the efficiencies.

The exit flow angle from the velocity diagram analysis associated with the mean flow of the camber-twist blade was used to define the flat blade setting angle. This was done to match exit tangential fluid velocity in the mean flow of the flat blade design to the mean flow of the camber-twist blade design. Recalling Euler's turbomachinery equation (Section 2.6.2), generated power is a function of blade speed, and inlet and exit tangential fluid velocity. Therefore, with fixed blade speed and inlet tangential fluid velocity, and by matching the exit tangential fluid velocity of the flat blade design to the camber-twist blade design, the power generated by the flat blade design approaches that of the camber-twist design. With using a flat blade, the Zweifel criterion could no longer be applied. The space-chord ratio was determined by applying the specific speed dependent Quayle ratios recommended in the Simpson and Williams (2011) design procedure. For this design, Quayle suggests a space-chord ratio of 1.18 at the tip and 0.64 at the hub of the

runner blade. This results in a 109 mm tip chord length and a 74 mm hub chord length. This was chosen since it was the balanced approach between solidity and flow guidance amongst the Simpson and Williams recommendations.

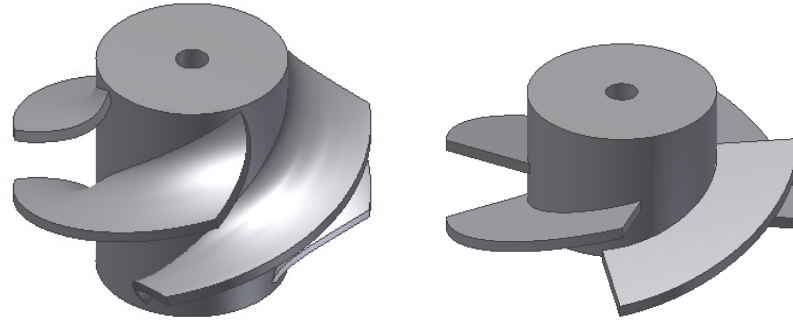


Figure 55: Isometric model of runner – camber-twist blade design (left) and flat blade design (right)

7.2 Flat Blade Runner Performance Prediction

Section 7.1 described the detailed design of the runner. Runner tip, hub diameters, and flow conditions through the turbine were defined based on a single design power, head, and flow rate target. Velocity diagram methods were used to determine runner inlet and exit flow angles, and then to define the curved and twisted formation of the runner blades. This process of defining the design performance goals, and then sizing the runner to meet those requirements, was also the dominant design approach in the literature. However, due to the complexity of the designed curved and twisted runner blade shape, the runner blades were simplified to flat blades to further improve the constructability of the propeller turbine within the current Cameroon local manufacture context.

The dilemma of how to predict the performance of the designed flat blade runner arises because the velocity diagram method is not applicable to flat blades. This is because the method does not consider interactions of the fluid flow with a given blade geometry. The method first assumes fully conforming flow over the blade, then adds corrections to minimize incidence and deviation

of the flow as it enters the blade cascade based on empirical findings (Section 7.1.5). In short, the velocity triangle method is a design tool but cannot be used as a means of predicting performance.

A performance prediction model for the flat blade runner turbine was developed, drawing on the blade element momentum theory as used in wind turbine design. The model was implemented as a Matlab program (Appendix D). As in Section 7.1.3, stations were defined radially along the blade, and the flow at each station was considered two dimensionally. This approach allows relatively straight forward two dimensional flow analysis at each station, while still accounting for variation in flow conditions along the length of the blade. The geometry of the stator and annulus area of the runner being investigated is used to determine velocities and angles of attack of the approaching flow to each runner blade section. It is noted that this approach can be used across a range of blade rotation speeds and flow rates, because these are inputs to the analysis.

Flow over a flat blade section induces lift force, F_L , and drag force, F_D , which are calculated using lift and drag coefficients, C_L and C_D respectively, from flat plate theory (Wright & Wood, 2004).

$$F_L = \frac{1}{2} C_L \rho A W_2^2 \quad (7.9)$$

$$F_D = \frac{1}{2} C_D \rho A W_2^2 \quad (7.10)$$

$$C_L = 2 \sin \phi \cos \phi \quad (7.11)$$

$$C_D = 2 \sin^2 \phi \quad (7.12)$$

where ρ is the density of water, W_2 is the relative fluid velocity, A is the planform area of the blade section, and ϕ is the angle of attack (Figure 56). Flat plate theory is applicable for all angles of attack, including stall angles.

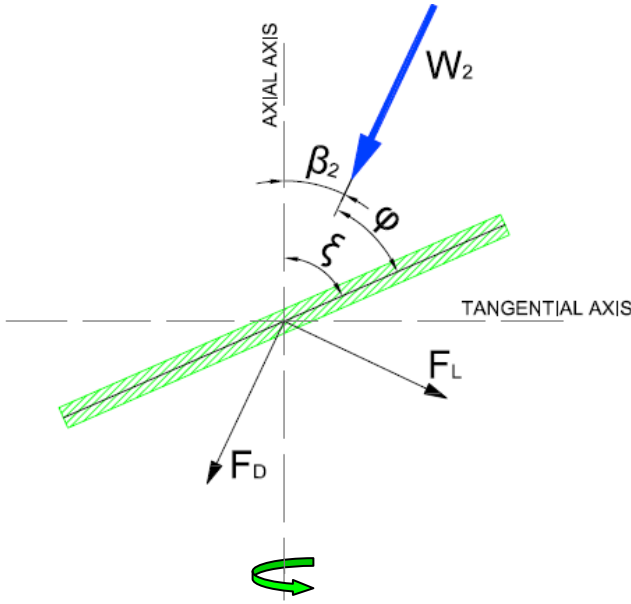


Figure 56: Diagram of flow over flat plate

The lift and drag forces of each section were projected along the runner tangential direction. Torque, τ , was calculated as the product of the sum of projected forces and the blade station radial dimension, r .

$$\tau = \sum (F_L \cos \beta_2 + F_D \sin \beta_2) r \quad (7.13)$$

Predicted power, P , was calculated as the product of torque and rotation speed, ω .

$$P = \tau \omega \quad (7.14)$$

The predicted power for the flat blade runner (specifications in Table 12) is plotted for a range of runner rotation speeds and flow rates (Figure 57). It is to be noted that the performance prediction model does not factor in the required operating head.

Flat Blade Runner Predicted Performance

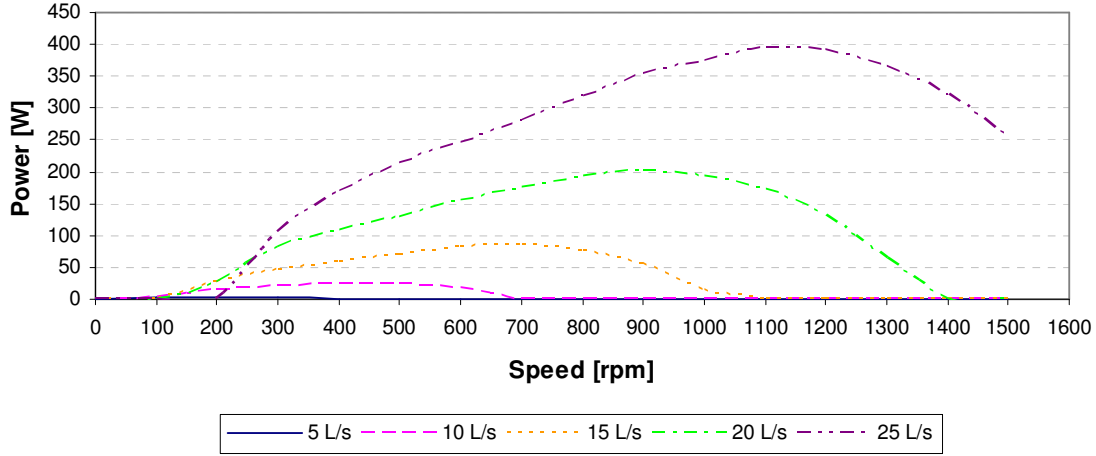


Figure 57: Flat blade runner predicted performance

The performance prediction model indicates the flat blade design will not reach the desired 370 W shaft power and 1500 rpm rotation speed targets with design 25 L/s flow rate. However, along with the performance decrease are improvements to the manufacturability of the design, which cater better to the local manufacture context.

7.3 *Stator Design*

The stator, as seen in Figure 58, was designed to allow radial inflow through a set of guide vanes to further generate swirl in the flow. The guide vanes are eight straight blades set in a circular array around the rotation axis. Straight blades were used to simplify manufacture. After exiting the guide vanes, the flow is directed downward parallel to the axial direction towards the runner, while contained within a cylindrical tube housing.

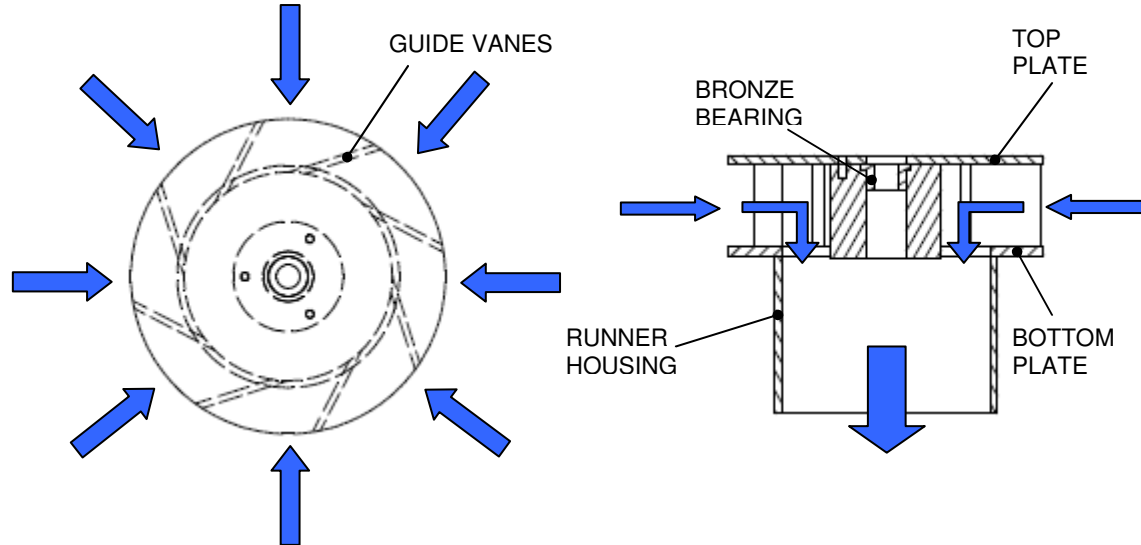


Figure 58: Stator – plan (left) and cross section (right)

The outer radius of the guide vanes, r_{GV} , was set to 100 mm following the Powerpal MHG 200 model. The height of the guide vanes, h_{GV} , and the runner location relative to the guide vanes (axial distance between the base of the guide vanes and the runner blades mid height), λ , was determined as recommended by Nechleba (1957):

$$h_{GV} = 0.4D_t \quad (7.15)$$

$$\lambda = 0.25D_t \quad (7.16)$$

where D_t is the runner tip diameter (Section 7.1.1).

The angle setting of the guide vanes, α_{GV} , was determined with the following equation (Wright, 1999):

$$\alpha_{GV} = \text{atan} \left(\frac{C_{\theta 2}}{\frac{Q}{2\pi r_{GV} h_{GV}}} \right) \quad (7.17)$$

where $C_{\theta 2}$ is the tangential fluid velocity at the runner inlet and Q is the flow rate. The tangential flow corresponding to the mid blade station was used to determine the angle setting.

A bronze bearing is housed within the stator to allow for rotation of the runner and shaft. This bearing is a friction type bearing often used in pumps. The component is low in cost, replaceable, and relatively maintenance free.

7.4 Inlet Basin

The inlet basin was modelled after the Powerpal (Asian Pheonix Resources Ltd., 2008) and Lao Institute for Renewable Energy (LIRE) (2010) designs. It is an open flume volute that generates swirl into the flow prior to entering the stator. Coincidentally, the approach of adopting the Powerpal design, at a larger scale, was also taken by Singh and Nestmann (2009).

The plan area of the inlet basin is illustrated in Figure 59.

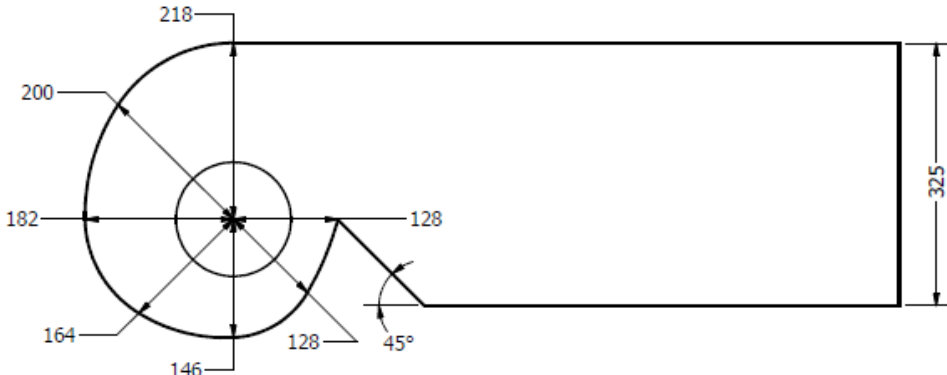


Figure 59: Inlet basin plan dimensions (mm)

7.5 Generator Connection

The generator will be directly driven by the turbine shaft. A connection is needed to ensure concentric alignment to avoid excessive vibrations. A clamped rubber hose connection, as employed in the DTU design, was designed to align the shafts and provided some compliance and damping in the case of eccentricity and vibrations. In addition, the component is cost effective, easily replaceable, and allows for separate maintenance of the generator and turbine.

7.6 Cavitation and Turbine Setting

Cavitation occurs when the local static pressure is lower than the water vapour pressure and begins to boil at normal temperatures. Reaction turbines are prone to cavitation since they operate under pressure, and are more susceptible in low head applications with high fluid velocities and with improper setting of the turbine too high above the tailrace. Cavitation occurs on the suction side of the runner blades or within the draft tube in hydraulic turbines. The blade motion causes a local low pressure region. The phenomenon is aggravated further by dissolved gases within the water which are released when the pressure is reduced (Dixon & Hall, 2010). Bubbles form in the low pressure regions and then migrate with the stream flow to high pressure regions where they collapse. The sudden collapse of the bubbles induces a localized pressure increase. This cycle repeats itself and causes erosion damage to the turbine blades or draft tube walls and generates noise. The erosion leads to pitting, fatigue failure or other failure mechanisms, and reduced performance. If not corrected, mechanical failure of the runner can result. The effect of cavitation can be mitigated through careful hydraulic design that avoids conditions causing cavitation, in manufacturing by employing erosion resistant materials, and by ensuring turbine operation remains within the range of acceptable cavitation conditions. (Kumar & Saini, 2010).

Cavitation can be modelled with the Thoma coefficient (Dixon & Hall, 2010):

$$\sigma = \frac{H_S}{H_E} = \frac{(p_a - p_v)/(\rho g) - z}{H_E} \quad (7.18)$$

where σ is the Thoma coefficient, H_S is net positive suction head, p_a is atmospheric pressure, p_v is fluid vapour pressure, z is height difference between runner base and tail water surface, H_E is available head.

Once determined, the Thoma coefficient can be compared to Figure 60 which displays the

correlation of Thoma coefficient to power specific speed and indicates the safe range of usage.

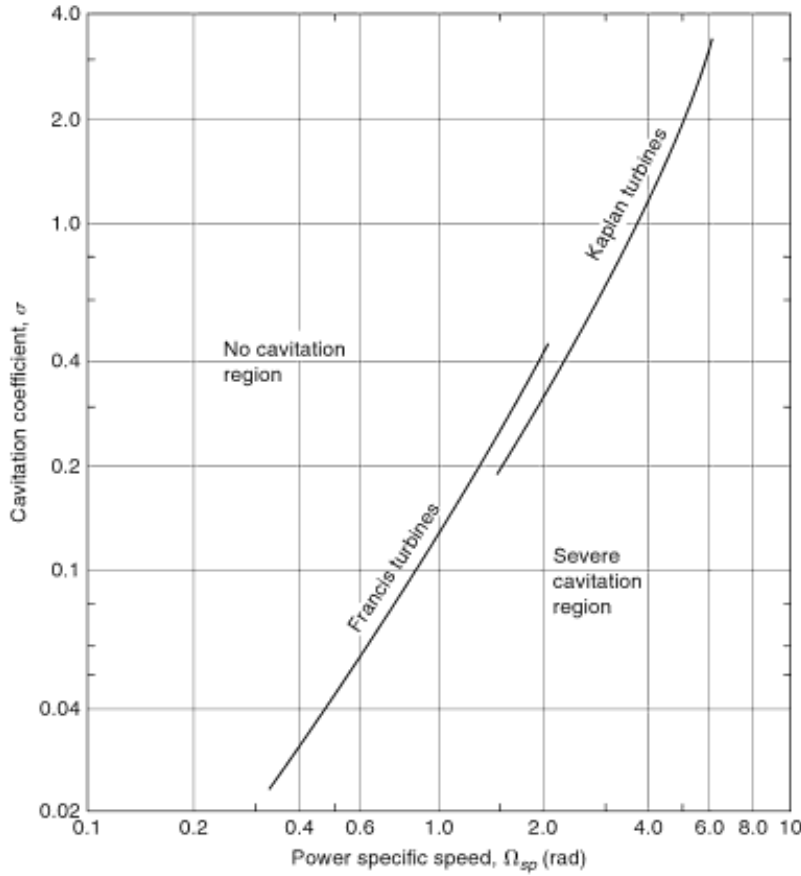


Figure 60: Variation of Thoma Cavitation Coefficient with Power Specific Speed
 (source: Dixon & Hall, 2010)

A check using the above method was applied to determine the turbine setting requirements within the 2 m head range to avoid the potential of cavitation. The peak of Mount Cameroon, the highest point in West Africa, was chosen as the worst case design scenario (4070 m above sea level). It was determined that the turbine could be set anywhere within the 2 m head range without the threat of cavitation occurring. The village of M'muock, 2428 m above sea level, was the highest elevated location amongst the visited sites.

7.7 Draft Tube Design

The draft tube is a hollow thin-walled conical tube positioned immediately downstream from the turbine runner. Several design options were reviewed. Nechleba (1957) and Simpson and

Williams (2011) suggested a flare of 4° from vertical for a height of $10D_t$. LIRE (2010) suggested flaring to correspond with an exit diameter ranging between $1.7D_t$ to $2D_t$. Powerpal had a narrower design for the MHG 200 model (Asian Pheonix Resources Ltd., 2008). Hothersall (2004) designs draft tubes using the relationship shown in Figure 61 which are constant curves of loss coefficients plotted on a graph of non-dimensional length, N/R_1 , versus non-dimensional area ratio, A_2/A_1 . The turbine setting and distance between runner and tail race define N , and R_1 is defined by the outer radius of the propeller tube (Figure 61). The optimal area ratio is then chosen and the degree of flare is determined. The Hothersall method was used. Due to the low head and generated power targets, the optimal design curve was extrapolated for the purposes of this design.

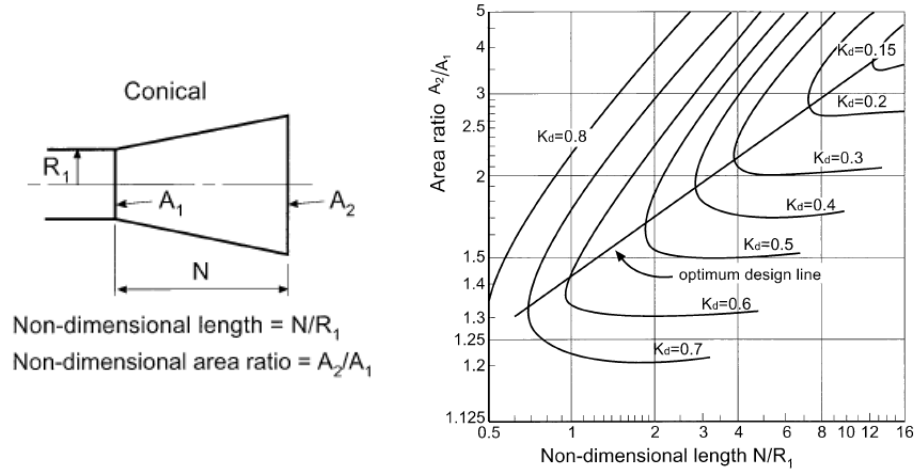


**Figure 61: Area ratio as a function of non-dimensional length for draft tube design
(adapted: Hothersall, 2004)**

The draft tube was designed as three separate components: a collar and two cone segments, each made from sheet steel. The sheet steel is to be rolled and spot welded to close the seam and join the components. The seam and connection points are to be soldered to form an airtight seal. The collar is then welded on to the cone. The draft tube assembly will slide and be clamped over the propeller tube. The maximum length of each component is limited to the throat of the spot welder and therefore dictates the number of components.

7.8 Detailed Design Summary

Detailed design parameters and target operating conditions for the prototype flat blade runner are summarized in Table 13. Mechanical design drawings are included in Appendix B.

Table 13: Detailed design summary

Turbine type	propeller
Blade shape	flat blade
Number of blades	4
Tip diameter, D_t	130 mm
Hub to tip ratio, D_h/D_t	0.55
Operating head, H	2 m
Operating flow rate, Q	25 L/s
Target rotation speed, n	1500 rpm
Forecasted power (1500 rpm, 25 L/s)	255 W
Stagger angle, ξ	71.0°
Tip chord length	109 mm
Hub chord length	74 mm
Outer radius of stator guide vanes, r_{GV}	100 mm
Height of stator guide vanes, h_{GV}	52 mm
Stator guide vane angle, α_{GV}	72.3°
Draft tube inlet radius	71 mm
Draft tube exit radius	150 mm
Draft tube length	1.7 m

8.0 Prototype Construction and Testing

8.1 *Prototype Construction*

A test version of the flat blade runner, stator, and shaft assembly were constructed at the University of Guelph Department of Physics Machine Shop. Construction required the use of hand tools and a lathe. Metal inert gas (MIG) welding was used for the welded joints.

The runner was constructed from hot rolled mild steel flat bar and round stock for the blades and hub respectively. The blades were traced from scaled drawings and saw cut, with excess at the tip edge. The hub was also saw-cut to length and turned down with a lathe to the finished hub diameter. Quadrants of the cylindrical hub were marked and used as a reference position for the blade placement. It was recommended to use an angle jig for accurate blade placement. The blades were initially tack welded in position and checked before the weld seams were finalized. The assembled runner was finally turned on the lathe to the finished tip diameter.

The stator was also constructed out of hot rolled mild steel plate, flat bar, hollow tube, and round stock. The stator blades were milled and the top and bottom plates turned on the lathe. An alternative option to milling is saw-cutting, however sawing is less accurate and would have resulted in more difficult assembly, and was therefore avoided. The runner housing was bored on the lathe to ensure appropriate clearance for the runner. No specialized lathe tooling was required for holding the parts. The recess in the bearing housing was reamed for higher accuracy and a tight fit for the bronze bearing.

For the shaft, cold rolled steel was used for improved accuracy in comparison to hot rolled sections. A further improvement would be to use centreless ground sections, however these are less accessible and higher in cost.

Drills and taps were used for the threaded holes. A die was used for threading the shaft.

8.2 Performance Test Apparatus

The test rig (schematic displayed in Figure 62) consisted of an elevated 1135 L tank connected to the inlet basin via 4 inch (10 cm) plastic pipe. The turbine was set in the inlet basin where flow entered from an open downward oriented pipe from the elevated tank, and exited downward through the turbine and draft tube. The flow was discharged into a 500 L tank. Three gas powered pumps (6.5 hp, 6.5 hp, and 4.8 hp) re-circulated the flow to the elevated 1135 L tank.

Measured maximum flow rates from individual pumps were 5.5 L/s, 5.6 L/s, and 7.3 L/s.

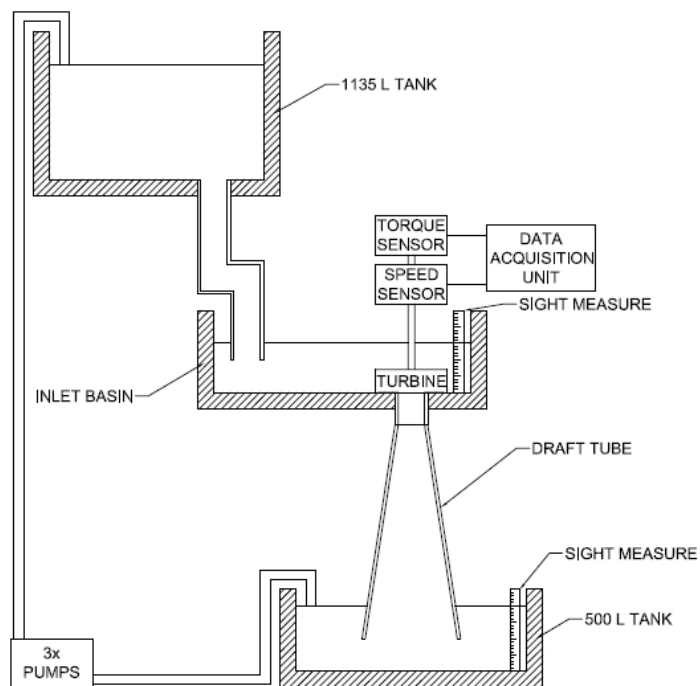


Figure 62: Schematic of test rig

A test version of the turbine was constructed (Figure 63). This test unit included the flat blade runner, lower friction bearing, stator, and shaft. A W5 section type I-beam with an end plate stiffener was used as a rigid mount, connecting to the stator and the upper portion of the shaft with a housed ball bearing assembly.

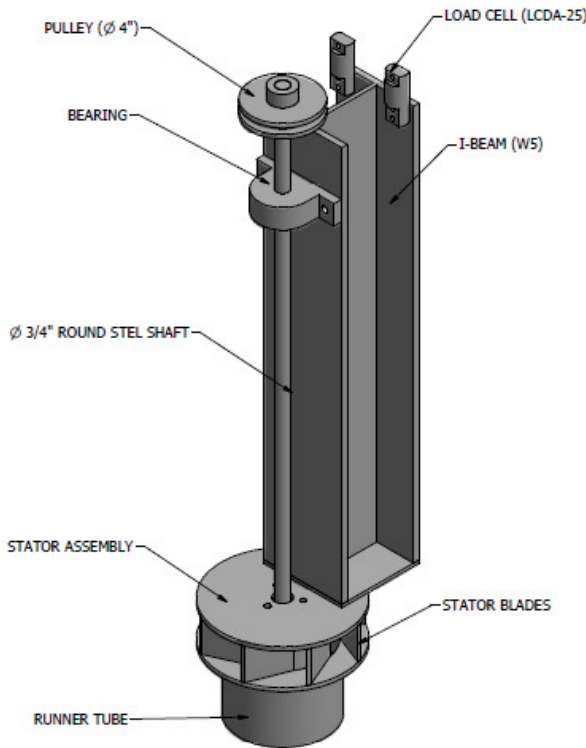


Figure 63: Test version turbine

A rendition of a Prony brake was used to measure torque and angular speed to determine shaft power. The torque was measured by two Omega LCDA-25 bending load cells wired to two Omega DMD-465 BRIDGESENSORS for signal conditioning and mounted on the upper end of the I-beam and a 4 inch (101.6 mm) diameter V-notch pulley at the upper end of the shaft. A nylon string was wrapped around the pulley and tied to eye-bolts fastened to each of the load cells. The load cells measured tension in the string which was adjustable by “tightening” the nut on the eye-bolt. As water turned the runner, shaft, and pulley, the tension in the string on either side of the pulley changed. The tension in the portion of the string opposite to the direction of rotation increased, while the tension in the other portion decreased. This difference in tension was the applied force by the string on the pulley. This applied force occurred at a perpendicular distance equal to the inner radius of the V-notch pulley and therefore created a torque opposing the rotation of the pulley.

The rotational speed of the runner shaft and pulley was measured with a Melexis MLX92211 Hall effect sensor and magnets mounted on the shaft to create a rotating magnetic signal. The magnet swept past the Hall effect sensor as the shaft rotated, causing the sensor to latch and de-latch. The frequency of these events was used to infer rotational speed. The load cells and Hall effect sensor were connected to a National Instruments data acquisition unit (NI USB-6009). Raw voltages, calculated force, and rotational speed were recorded using a Labview 8.6 program.

The load cells were calibrated in-situ by applying a range of calibration weights. The rotational speed measurements were cross-checked using a handheld optical tachometer.

8.3 Performance Test Procedure

Tests were conducted with different flow rates by employing various combinations of pumps. The nominal flow rates were: 5.6 L/s, 7.3 L/s, 11.1 L/s, 12.9 L/s, and 18.4 L/s. Higher flow rates and the design flow rate of 25 L/s could not be achieved due to constrained flow through the turbine (discussed further in Sections 8.4 and 8.6) and with the available pump capacity at the time of testing. At each flow rate level, a series of trials were performed under varied braking torque through tension adjustments to the brake system. Variations to torque directly affected the head across the turbine. The maximum head tested was 2.38 m. Following the torque adjustment, 60 s settling time was given for the system to stabilize before measurements were taken. Inlet head and suction head were sight measured. Tension and angular speed were measured using the Labview program for a 10 s duration with a sampling rate of 500 Hz.

Impacts of blockage due to the I-beam rigid mount were tested by changing the orientation of the test version turbine relative to the water flow in the inlet basin. The test version turbine was rotated approximately 60° clockwise in plan (Figure 64) and tested with 5.6 L/s flow rate.



Figure 64: Sensitivity testing of I-beam influence on flow

8.4 Performance Test Results

Turbine shaft power and head versus rotational speed and efficiency versus speed under constant flow conditions are graphed below in Figure 65 and Figure 66, respectively. Data points from the testing were plotted with trend lines fitted. Error bars indicating calculated uncertainty (Appendix E) were included for the power and efficiency curves.

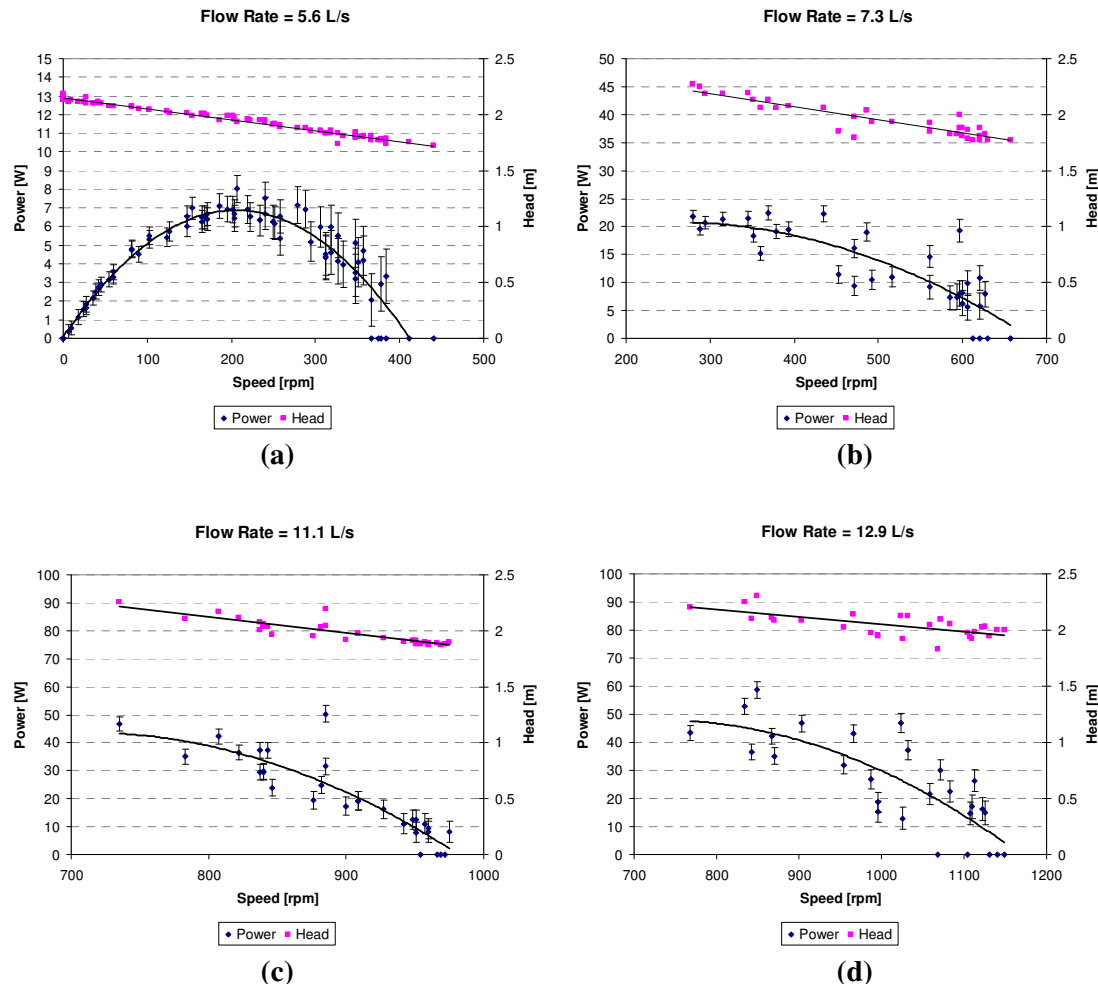


Figure 65: Turbine shaft power and head versus rotation speed under constant flow rates (a) 5.6 L/s, (b) 7.3 L/s, (c) 11.1 L/s, (d) 12.9 L/s

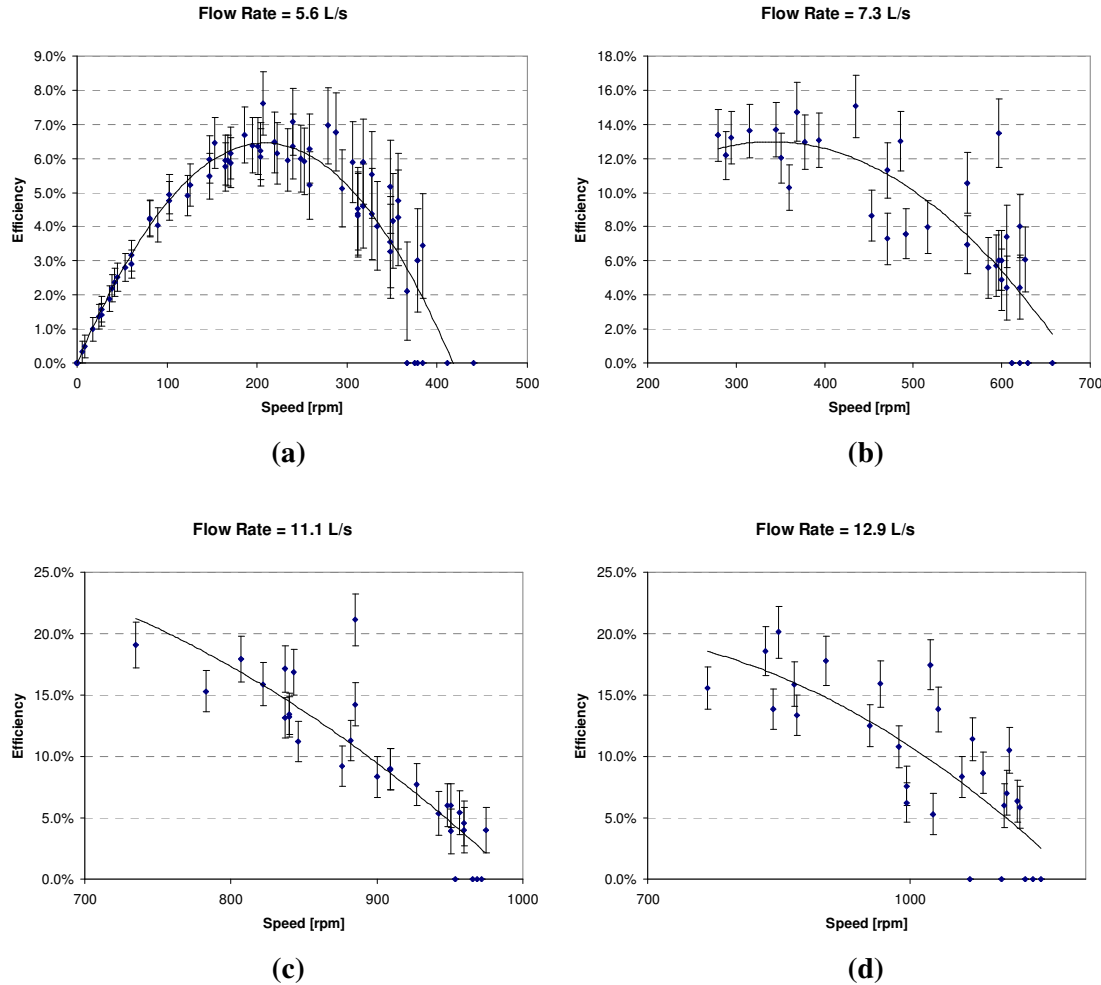


Figure 66: Turbine efficiency versus rotation speed under constant flow rates (a) 5.6 L/s, (b) 7.3 L/s, (c) 11.1 L/s, (d) 12.9 L/s

Tested flow rates with applied torque were limited to below 51.5% of design flow rate. It was observed that greater flow rates through the turbine required head above the maximum capacity of the test rig and overflowed the inlet basin.

From the curve fits of the tests, the highest measured shaft power was 49 W with an efficiency of 19% at 12.9 L/s (51.5% of design flow) flow rate. The highest measured efficiency was 21% with a corresponding shaft power of 43 W at 11.1 L/s (44.3% of design flow) flow rate.

The maximum rotation speed was 1536 rpm with 18.4 L/s (73.6% of design flow) flow rate and

2.2 m head with no applied torque.

Uncertainty analysis of the trial results showed greater error in the measurements with increasing rotation speed. This was mainly due to the error of the load cells being a greater portion of the overall measurement when low loads were applied. Similarly with the efficiency measurements, greater uncertainty was seen in the higher rotation speed regions of the graph. This also was due to the load cell error and was compounded by the greater uncertainty with more pumps being utilized to achieve higher flow rates. Greater scatter of data was also seen at higher flow rates, suggesting more uncertainty than calculated. Missed error may have existed in the calculation of overall flow rate since flow rates of each pump were measured independently and did not account for the affects of interactions between pumps on overall flow rate when working in unison for higher flow rate testing. In addition, higher flow rates may also have been affected by insufficient capacity in the test rig, resulting in lower amounts of water at the pump intakes in the lower reservoir.

Taken from the curve fits of Figure 65, calculated performance of the prototype versus rotation speed with constant 2 m head and varying flow rate is illustrated in Figure 67. Data points corresponding to the tested flow rates were plotted and trend lines were fitted to this data. Under 2 m head conditions, the highest power output is 23 W.

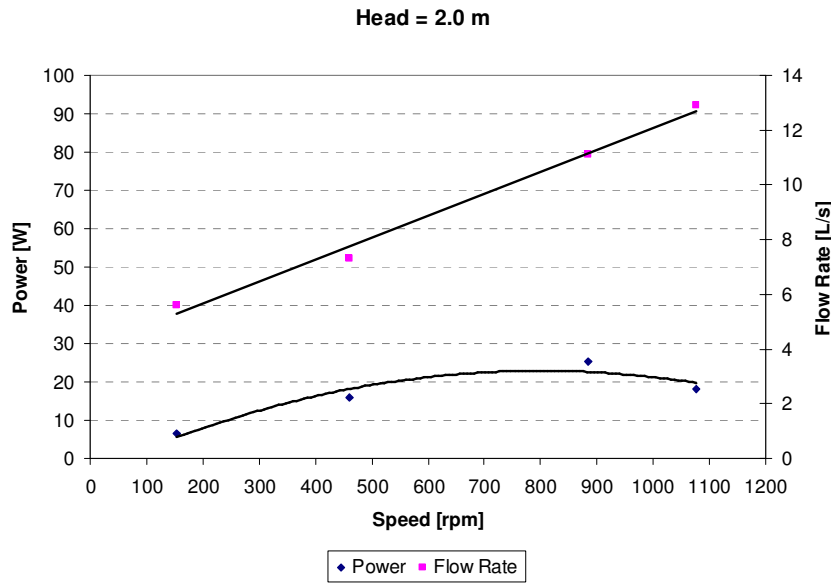


Figure 67: Calculated power and flow rate versus rotation speed under constant 2 m head

Sensitivity test trials with different orientations of the I-beam rigid mount were conducted to test influence of the I-beam on the inlet basin flow. Test result comparisons are plotted in Figure 68.

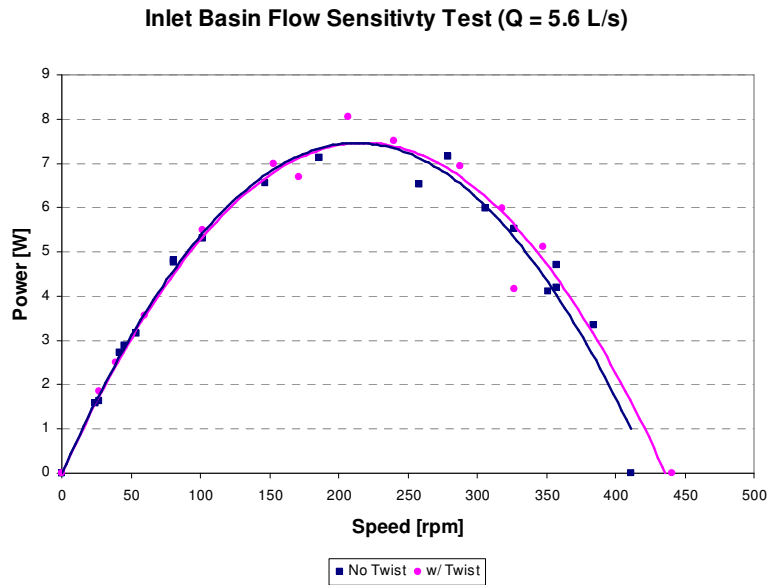


Figure 68: Sensitivity testing results of I-beam influence on flow

Good agreement is seen between the two test configuration results indicating minor influence of I-beam rigid mount orientation on the inlet basin flow.

8.5 Cost and Material Discussion

Mild steel is used for the entire turbine construction. Mass of the production turbine calculated from 3-D solid models is estimated to be approximately 11 kg.

Material costs of the production scale turbine are calculated based on the bill of materials of the test version turbine and estimated to be under €50. Total labour for fabrication of the test version was approximately 14 man-hours and is indicative of the required time for the production version.

Efficiencies in both cost and material are expected in future design revisions and due to economies of scale.

8.6 Performance Test Discussion

Design flow rate conditions were not tested but limited to partial flow test conditions ranging from 22.4% to 51.5% of design flow with applied torque and 73.6% of design flow without applied torque. Figure 69 compares experimental efficiency results with propeller turbine part flow efficiency trends published by Paish (2002), which illustrate lower operating efficiencies of propeller turbines at off-design flow rates. The test results showed higher part flow efficiencies at lower flow rates. The test result efficiencies increased a slower rate as flow rate increased, indicating low efficiencies at higher flow rates and at the design flow rate.

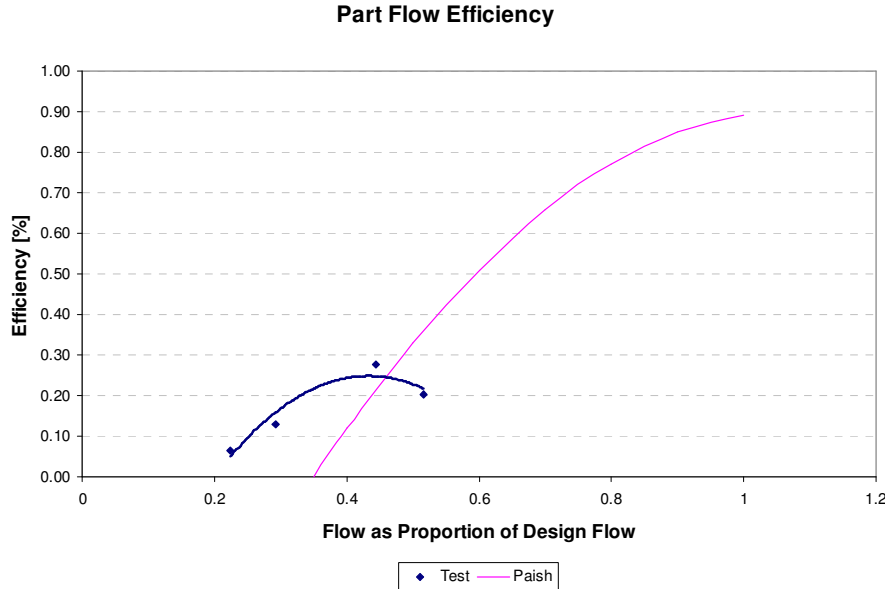


**Figure 69: Part flow efficiencies
(adapted: Paish, 2002)**

Water flow was constrained by the turbine and resulted in an increase in upstream head within the inlet basin beyond the 2 m design head. In addition, due to limited water containment capacity of the test rig, testing with heads greater than 2.3 m could not be conducted. These factors limited the ability to further characterize the performance of the turbine and more importantly, determine the maximum shaft power and best efficiency points for the different test conditions.

The prototype did not meet the power output requirement (Section 3.1), with the highest measured shaft power of 49 W (less than 20% of target electrical generation). The low power output and efficiency was mainly attributed to the design simplification to the flat blade runner. Recall, the runner blade design originally incorporated camber, twist, and changing chord length allowing for improved flow guidance, and was simplified to a flat blade design to better suit the present resources for local manufacture in rural Cameroon. Losses are also generated at the flat blade stator guide vanes and due to the sharp turn of the flow from horizontal to vertical at the exit of the stator to the entrance of the runner. Fabrication accuracy may have also affected

performance. Accuracy of the blade placement and orientation were not measured against the design specifications.

Fair agreement is observed when comparing performance test results with flat blade runner performance model predictions (Figure 70). The performance model predicts comparatively modest power output with lower running speeds at lower flow rates. However, power output predictions and test results converge as flow rate is increased to 12.9 L/s and indicate over prediction of the model at higher flow rates.

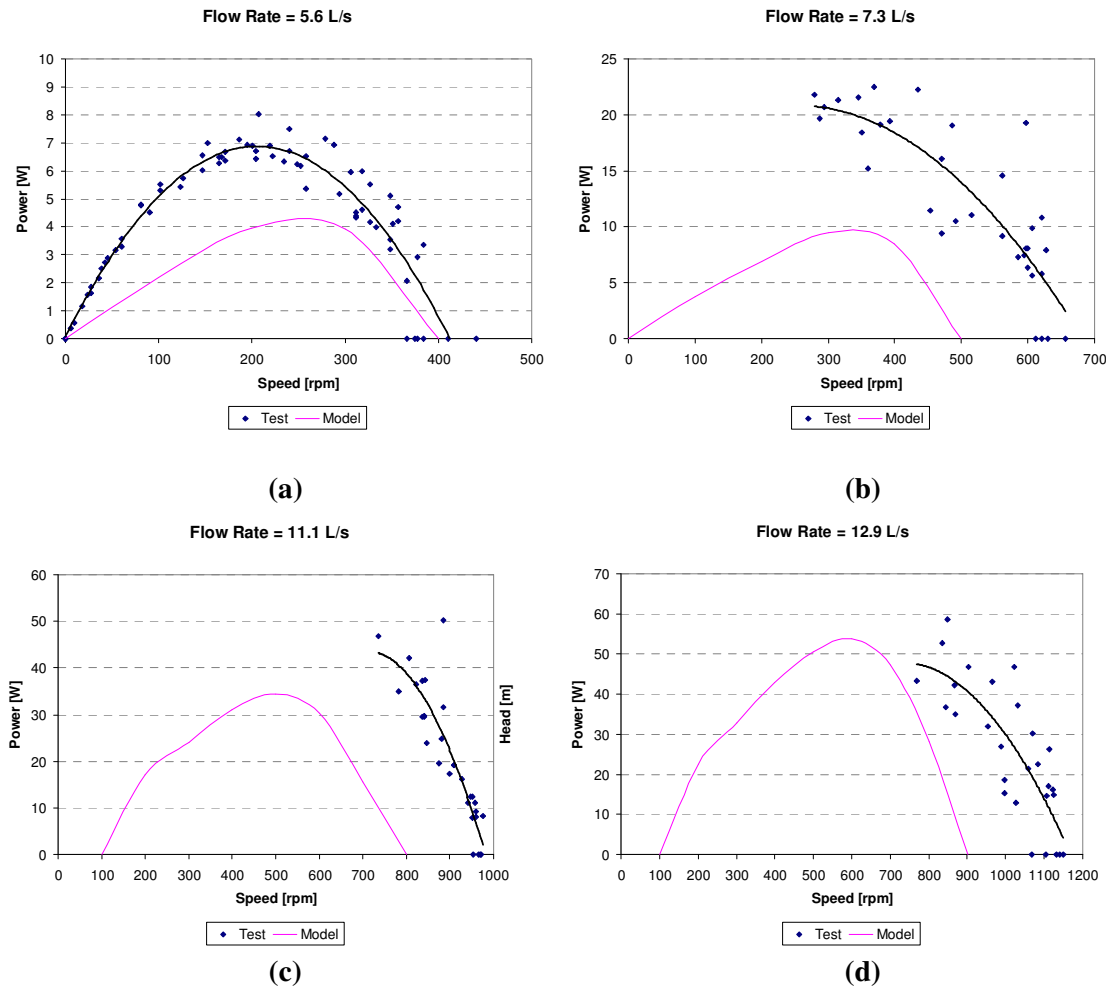


Figure 70: Experimental results and prediction model comparison (a) 5.6 L/s, (b) 7.3 L/s, (c) 11.1 L/s, (d) 12.9 L/s

Based on the test results, the flat blade turbine will not be able to deliver 370 W shaft power to

achieve the system 250 W power generation target with 2 m head and 25 L/s flow rate. Losses occurring at the flat blade runner are suspected, requiring greater head to allow the design flow rate through the turbine. Technical modifications can be implemented to improve flow guidance and include:

- Increasing the blade height and the number of blades
- Introducing camber and twist in the runner blade geometry – changing the runner blade geometry can be staged by separately incorporating camber and twist
- Stator guide vanes can be curved – forming of the stator guide vanes would be relatively less complicated than runner blade forming since blade twisting is not required
- Employing a curved surface between the stator blades and the runner
- Airfoil geometries for the stator and the runner

The above mentioned modifications will improve turbine performance but some may significantly complicate fabrication beyond the current capabilities of well-equipped workshops in developed countries as well as for local manufacture in Cameroon.

Further testing of the flat blade prototype later this year is planned at the University of Regensburg. A test facility with higher pumping capacity is currently under construction at Regensburg for this purpose.

9.0 Conclusions

Low rural electrification rates currently exist in Cameroon despite great energy resources within the country. Pico hydro is recognized as a suitable solution to improving rural electrification and has been applied only in a few instances for medium to high head applications in Cameroon.

Field research surveys and interviews identified rural electrification as one of the top priorities for poverty alleviation of Cameroon's rural population. High costs are incurred due to the current dependence on fossil fuel energy and aggravated by price volatility and premiums paid by inhabitants of remote locations.

Local manufacture and proper training are critical for strengthening the success of small scale electricity generation systems. Sophisticated systems have been imported and implemented and in some cases have faulted or become inoperable due to lack of knowledge transfer, high cost, and poor availability of parts. Local manufacture of pico hydro turbines has proven to be successful in other developing countries and may have led to the wide adoption of the technology. Build trials and past experience demonstrated this as a viable solution for Cameroon. However, previous locally built systems have also failed and illustrate the need for more robust designs. Additional training and improved working facilities will increase the capacity of local artisans, who currently possess a high level of ability and interest in pico hydro technology.

Low head propeller turbine technology was determined to be the most suitable option based on several merits including improved access, ease of manufacture, portability, low cost, and reduced system complexity. A propeller turbine with a runner with constant thickness, curved, twisted, and variable chord length blades was designed to enable 250 W electrical generation with an operating head of 2 m and 25 L/s. Given the current resources for local manufacture in

Cameroon, the runner was simplified to a flat blade runner to improve constructability of the turbine and allow for learning-by-doing training at the initial stages. A prototype version of the turbine runner was constructed at the University of Guelph for testing purposes. The construction process was considered straightforward by the technician and design engineer. Only standard tooling and materials accessible within Cameroon were utilized, therefore fulfilling the domestically sourced material and local manufacture requirements. The materials cost was calculated to be approximately €50, a third of the defined household affordability criteria for the whole system, and expected to decrease as the system is optimized. The turbine design was highly portable with an estimated mass of approximately 11 kg.

Testing of the flat blade runner was conducted and the prototype turbine was functional, however, the prototype did not meet the power output requirement, with the highest measured shaft power of 49 W (less than 20% of target electrical generation). Due to the flat blade runner constraining the water flow, the turbine was not operable with 2 m head and 25 L/s flow rate. The test rig was limited to a maximum head of 2.3 m, therefore only partial flow rate conditions were tested. Consequently, low power outputs and efficiencies resulted as expected since propeller turbine performance steeply declines during off-design operation. Although only partial flow rate conditions were tested, it is believed the flat blade propeller design will not achieve target performance under design conditions.

It is strongly suspected that the main contributor to the low performance of the prototype was the flat blade runner simplification and the associated adverse affect on the flow guidance. With the setting of the flat blades to the mean exit flow angle of the camber-twist blade design, the flow will enter and exit at suboptimal angles and therefore ineffectively transfer energy to the runner. It is also suspected that losses are generated at the flat blade stator guide vanes and due to the sharp turn of the flow from horizontal to vertical at the exit of the stator to the entrance of the

runner. These factors constrained the flow through the turbine therefore requiring greater than 2 m head to achieve the design flow rate. It was observed that the flat blade runner achieved greater than 1500 rpm rotational speed with no applied torque and only 73.6% of design flow rate.

Despite the lower than desired performance test results, the simplified flat blade design is a tangible first step towards fully meeting the design criteria. With further design optimization and testing, in addition to improved local manufacturing capabilities, increased performance through designs with added complexity can be achieved.

10.0 Recommendations

Following are recommendations for further research and development relating to the local manufacture of pico hydro turbines in Cameroon and specifically to the design of a propeller turbine for low head applications:

- *Improve technical design within the local manufacture context* – Primary design improvements must be made to the runner. Experimental investigation can be continued on the flat blade design to determine the impact on performance when varying several factors such as blade angles, chord length, number of blades, etc. This would be costly and time consuming and it is expected that performance improvements will be limited. Therefore, it is recommended to fabricate and test the camber-twist blade runner for future development. In addition, improvements to the stator design can be implemented by using curved blades or curved airfoil profiles. Forming of the stator blades would be relatively less complicated than runner blade forming since blade twisting is not required. Also, a curved surface can be introduced to improve flow guidance between the stator blades and the runner. The current design did not incorporate this to simplify the manufacturing process and reduce material waste. Care must be taken to ensure that these design optimizations fit within an appropriate fabrication process for local manufacture.
- *Apply sand casting techniques* – From the field investigations, sand-casting has been used for Pelton turbine manufacture in Cameroon and may be transferrable to propeller turbine fabrication. Potential applications can be for the runner manufacture (as a single unit or on a per blade basis) and for the stator. There is potential to achieve complex shapes, improve repeatability, and lower production costs. Further investigation must be done to determine the benefits and disadvantages if sand casting is applied to this design.
- *Design critique by local artisans* – Design reviews should be conducted by artisans to

include their perspectives to evaluate appropriateness of the design, identify cost savings measures, and enhance manufacturing process flows. Through this, greater ownership will be taken by the artisans.

- *Collaborate with end-users* – Incorporate viewpoints of end-users to determine effective training methods on topics of proper use, safety, and maintenance. Devise methods for training through demonstrations, workshops, user manuals (considerate of literacy levels and languages), etc.
- *Comprehensive design manual* – once the design is finalized a design manual, written in a comprehensive manner and catered to particular audiences, should be made to communicate the design process.

11.0 References

- Aarter, A., & Meier, U. (1990). *Harnessing power on a small scale*. St Gallen: SKAT.
- African Development Bank. (2009). *COUNTRY STRATEGY PAPER 2010-2014 CAMEROON*. African Development Bank.
- Alexander, K. V., & Giddens, E. P. (2008). Optimum penstocks for low head microhydro schemes. *Renewable Energy*, 33(3), 507-519.
- Alexander, K. V., Giddens, E. P., & Fuller, A. M. (2009a). Axial-flow turbines for low head microhydro systems. *Renewable Energy*, 34(1), 35-47.
- Alexander, K. V., Giddens, E. P., & Fuller, A. M. (2009b). Radial- and mixed-flow turbines for low head microhydro systems. *Renewable Energy*, 34(7), 1885-1894.
- Anderson, H. H. (1980). *Centrifugal pumps*. Morden: Trade and Technical Press.
- Arriaga, M. (2010). Pump as turbine – A pico-hydro alternative in lao people's democratic republic. *Renewable Energy*, 35(5), 1109-1115.
- Asian Phoenix Resources Ltd. (2008). *Use and care instructions for your new powerpal low head micro-hydroelectric generator*. Victoria, Canada: Asian Phoenix Resources Ltd.
- Balje, O. E. (1968). Axial cascade technology and application to flow path designs. *ASME Journal Engineering for Power*, 81(1), 83.
- Balje, O. E. (1981). *Turbomachines : A guide to design selection and theory*. New York ; Toronto: Wiley.
- Bohl, W. (1991). *Strömungsmaschinen 2: Berechnung und kalkulation*. Vogel Business Media.
- Bruce, N., Perez-Padilla, R., & Albalak, R. (2000). *Indoor air pollution in developing countries: A major environmental and public health challenge*. World Health Organization.
- Cecelski, E. (1979). In Dunkerley J., Ramsey W. (Eds.), *Household energy and the poor in the third world*. Washington, DC: Resources for the Future.
- Charlier, F. (2009). In N'cho-Oguie C. (Ed.), *Sustaining reforms for inclusive growth in cameroon : A development policy review*. Washington, DC: World Bank.
- Chhetri, A., Pokharel, G. R., & Islam, M. R. (2009). SUSTAINABILITY OF MICRO-HYDROSYSTEMS - A CASE STUDY. *Energy & Environment*, 20(4), 567-585.
- Coleman, H. W., & Steele, W. G. (1989). *Experimentation and uncertainty analysis for engineers*. New York: Wiley-Interscience
- Cordier, O. (1955). *Similarity considerations in turbomachines*. VDI Reports.
- Date, A., & Akbarzadeh, A. (2009). Design and cost analysis of low head simple reaction hydro turbine for remote area power supply. *Renewable Energy*, 34(2), 409-415.
- DeLancey, M. (1986). In Schraeder P. J. (Ed.), *Cameroon*. Oxford: Clio.
- Demetriades, G. M. (1997). Design of low-cost propeller turbines for standalone micro-hydroelectric generation units. (Ph.D., University of Nottingham).
- DFID-Department for International Development. (2002). *Energy for the poor-underpinning the millennium development goals*. DFID-Department for International Development.

- Dixon, S. L., & Hall, C. A. (2010). *Fluid mechanics and thermodynamics of turbomachinery* (6th ed.). Amsterdam ; Boston: Butterworth-Heinemann.
- DTU-Development Technology Unit. (2010). *SIMPLE LOW-HEAD MICRO-HYDRO TURBINE*. Coventry, UK: University of Warwick.
- Durali, M. (1976). *Design of small water turbines for farms and small communities*. Cambridge, USA: Technology Adaptation Program Massachusetts Institute of Technology.
- Ehlers, C., & Hertlein, J. (2008). *PROJEKT ZWISCHENBERICHT WINDKRAFT-KLEINUNTERNHEMER FÜR KAMERUN*. GREEN STEP e.V.
- Energy Sector Management Assistance Programme. (2005). *Stimulating the pico hydropower market for low-income households in ecuador*. Washington DC, USA: The World Bank Group.
- FAOSTAT. (2012). FAOSTAT. Retrieved January 11, 2012, from <http://faostat.fao.org/default.aspx>
- Fonchingong, T. N. (2009). Corruption, governance and development in cameroon. In T. N. Fonchingong, & J. B. Gemandze (Eds.), *Cameroon : The stakes and challenges of governance and development* (pp. 37-54). Mankon, Bamenda : East Lansing, Mich.: Langaa RPCIG ; Distributed in N. America by Michigan State University Press.
- Fraenkel, P., Paish, O., Bokalders, V., Harvey, A., Brown, A., & Edwards, R. (1991). In Fraenkel P., Stockholm Environment Institute. (Eds.), *Micro-hydro power : A guide for development workers*. London: Immediate Technology Publications in association with the Stockholm Environment Institute.
- French River Land Company (2012). *GREEN AND CLEAN POWER-french river land company's website!* Retrieved December 9, 2011, from <http://www.frenchriverland.com/>
- Fulford, D. J. (2000). Recommendations on the use of micro-hydro power in rural development. *Journal of International Development*, 12(7), 975-983.
- Gunkel, G. (2009). Hydropower - A green energy? tropical reservoirs and greenhouse gas emissions. *CLEAN - Soil, Air, Water*, 37(9), 726-734.
- Gunnerson, F. (n.d.). *AXIAL_FLOW_MACHINES.pdf*. Retrieved February 14, 2012, from http://www.if.uidaho.edu/~gunner/Turbomachinery/LectureNotes/AXIAL_FLOW_MACHINES.pdf
- Heitz, M. (1993). *Design and construction of a small axial flow water turbine*. Unpublished B.A.Sc., The Nottingham Trent University, Nottingham, UK.
- Hertlein, J. (2010). *Prototype manual*. Personal communication.
- Hertlein, J. (2011). *SMALL SCALE WATERTURBINE FOR CAMEROON: Project start document*. Internal report, GREEN STEP e.V.
- Horlock, J. H. (1966). *Axial flow turbines : Fluid mechanics and thermodynamics*. London: Butterworths.
- Hothersall, R. (2004). In Anestis G., Gurkok C. (Eds.), *Hydrodynamic design guide for small francis and propeller turbines*. Vienna, Austria: United Nations Industrial Development Organization.
- Howey, D. A. (2009). AXIAL FLUX PERMANENT MAGNET GENERATORS FOR PICO-HYDROPOWER. *EWB-UK Research Conference 2009*, The Royal Academy of Engineering.

- Ho-Yan, B. (2011). Tesla turbine for pico hydro applications. *Guelph Engineering Journal*, (4), 1-8.
- Independent Evaluation Group. (2008). *The welfare impact of rural electrification: A reassessment of the costs and benefits*. World Bank.
- International Energy Agency. (2009). *World energy outlook 2009*. Paris, France: Organisation for Economic Co-operation and Development.
- Jorgenson, R. (Ed.). (1983). *Fan engineering - an engineer's handbook on fans and their applications*. New York: Buffalo Forge Co.
- Kenfack, J., Hamandjoda, O., Fogue, M., Demenou Tapamo, H., Ghonnang Zekeyo, J. P., & Lejeune, A. G. H. (2010). Public and private hydro initiatives in cameroon. *Hydropower & Dams*, 17(6), 74-78.
- Kenfack, J., Fogue, M., Hamandjoda, O., & Tatielte, T. T. (2011). Promoting renewable energy and energy efficiency in central africa: Cameroon case study. *World Renewable Energy Congress 2011-Sweden*, Linkoping, Sweden.
- Khennas, S., & Barnett, A. (2000). *Best practices for sustainable development of micr hydro power in developing countries*. Warwick, UK: Intermediate Technology Development Group Ltd.
- Kumar, P., & Saini, R. P. (2010). Study of cavitation in hydro turbines-A review. *Renewable and Sustainable Energy Reviews*, 14(1), 374-383.
- Lao Institute for Renewable Energy (LIRE) (Producer), & Lao Institute for Renewable Energy (LIRE) (Director). (2010). *Pico hydropower training guide - 02 making the draft channel* [Video/DVD]
- Lejeune, A. G. H., Fogue, M., Kenfack, J., & Tamo Tatielte, T. (n.d.). *Overview of institutional structure reform of the cameroon power sector and assessments*
- Maher, P. (2001). *The pico power pack*
- Maher, P., & Smith, N. (2001). *Pico hydro for village power*.
- Maher, P., Smith, N. P. A., & Williams, A. A. (2003). Assessment of pico hydro as an option for off-grid electrification in kenya. *Renewable Energy*, 28(9), 1357-1369.
- Mbaku, J. M., 1950-. (2005). *Culture and customs of cameroon*. Westport, Conn.: Greenwood Press.
- Mockmore, C. A., & Merryfield, F. (1949). *The banki water turbine*. Corvallis, Engineering, Experiment Station, Oregon State System of Higher Education, Oregon State College, 1949:
- Modi, V., McDade, S., Lallement, D., & Saghir, J. (2006). *Energy and the millennium development goals*. New York: Energy Sector Management Assistance Programme, United Nations Development Programme, UN Millennium Project, and World Bank.
- Munasinghe, M. (1990). Rural electrification in the third world. *Power Engineering Journal*, 4(4), 189-202.
- Ndi, R. (n.d.). *The history of Cameroon*. Retrieved November 5, 2011, from <http://www.sfu.ca/archaeology/museum/ndi/History.html#Early> history
- National Geographic & ESRI (2011). *National Geographic World Map*. ESRI.
- Nechleba, M. (1957). *Hydraulic turbines : Their design and equipment* (C. Mayer, A. G. Evans Trans.). Prague: Artia.

- Nfah, E. M., & Ngundam, J. M. (2009). Feasibility of pico-hydro and photovoltaic hybrid power systems for remote villages in cameroon. *Renewable Energy*, 34(6), 1445-1450.
- Paish, O. (2002). Micro- hydropower: Status and prospects. *PROCEEDINGS OF THE INSTITUTION OF MECHANICAL ENGINEERS PART A-JOURNAL OF PO*, 216, 31-40.
- Parker, G. J., Faulkner, S. A., & Giddens, E. P. (1993). A low head turbine for micro hydropower. *RERIC Internation Engery Journal*, 15(2), 137-146.
- Pascale, A., Urmee, T., & Moore, A. (2011). Life cycle assessment of a community hydroelectric power system in rural thailand. *Renewable Energy*, 36(11), 2799-2808.
- Piggot, H. (2001). *PMG construction manual*. Scoraig Wind Electric.
- Piggot, H. (2010). *A wind turbine recipe book*. Scoraig Wind Electric.
- Portegijs, J. (2003). *The firefly micro hydro system*. Retrieved January 11, 2011, from http://www.microhydropower.net/mhp_group/portegijs/firefly_bm/ffbm_index.html
- Portegijs, J. (2006). *Microhydro eGroup: Jan portegijs' humbird electronic load controller*. Retrieved February 15, 2012, from http://microhydropower.net/mhp_group/portegijs/humbird/humb_main.html
- Ranatunga, S., & Indrus, N. (1991). Innovative micro plant for electricity generation in remote areas. *International Mechanical Engineering Congress*, Australia. pp. 117-121.
- Ranganathan, V. (1992). Policy recommendations and conclusions. In V. Ranganathan (Ed.), *Rural electrification in africa* (). London; London ; Atlantic Highlands, N.J., USA: Zed Books in association with African Energy Policy Research Network-AFREPREN, Gaborone; Zed Books in association with African Energy Policy Research Network--AFREPREN, Gaborone.
- Rao, G. J. (1986). Investigation on a hydraulic turbine with helical bladed runner for micro power development. (M.Sc., Indian Institute of Science).
- Rao, G. J., Prasad, R., & Kulkarni, B. S. (1988). Simplified turbine runner shows good cavitation resistance. *Water Power and Dam Construction*, , 20-22.
- Rao, G. J., Prasad, R., & Rao, J. K. S. (1988). Investigations of an axial flow runner for micro hydro power development. *8th Fuid Machinery Conference*, Budapest, Hungary. pp. 616-23.
- Razak, J. A., Alghoul, M. A., Zainol, M. S., Zaharim, A., & Sopian, K. (2010). Application of crossflow turbine in off-grid pico hydro renewable energy system. Paper presented at the *Recent Advances in Applied Mathematics. American Conference on Applied Mathematics (AMERICAN-MATH 2010)*, Cambridge, MA, USA.
- Rice, W. (1965). An analytical and experimental investigation of multiple-disk turbines. *ASME Transactions: Journal of Engineering for Power*, 87(1), 29–36.
- Rice, W. (2003). Tesla turbomachinery. In E. Logan, & R. Roy (Eds.), *Handbook of turbomachinery* (2nd ed., pp. 861–874). New York, USA: Marcel Dekker.
- Rijssenbeek, W. (n.d.). *Pico hydro systems in Vietnam*. RR Energy Consulting.
- Round, G. F. (2004). *Incompressible flow turbomachines: Design, selection, applications, and theory*. Amsterdam ; Boston: Elsevier.
- Schobeiri, M. (2005). *Turbomachinery flow physics and dynamic performance*. Berlin: Springer.
- Seymour, D. L. (2011). *Powerpal discussions*

- Simpson, R., & Williams, A. (2011). *Design of propeller turbines for pico hydro*. University of Nottingham.
- Singh, P., & Nestmann, F. (2009). Experimental optimization of a free vortex propeller runner for micro hydro application. *Experimental Thermal and Fluid Science*, 33(6), 991-1002.
- Singh, P., & Nestmann, F. (2011). Experimental investigation of the influence of blade height and blade number on the performance of low head axial flow turbines. *Renewable Energy*, 36(1), 272-281.
- Smith, N. P. A. (1994). Key factors for the success of village hydro-electric programmes. *Renewable Energy*, 5(5-8), 1453-1460.
- Smith, N. (1994). *Motors as generators for micro-hydro power*. London, UK: ITDG Publishing.
- Smits, M., & Bush, S. R. (2010). A light left in the dark: The practice and politics of pico-hydropower in the lao PDR. *Energy Policy*, 38(1), 116-127.
- Tesla, N. (1913). *Turbine* (1061206th ed.). USA:
- Thake, J. (2000). *The micro-hydro pelton turbine manual : Design, manufacture and installation for small-scale hydropower*. London: ITDG Publishing.
- The World Bank Group Energy Unit, Energy, Transport and Water Department. (2006). *Technical and economic assessment of off-grid, mini-grid and grid electrification technologies*. World Bank Group.
- Totapally, H. G. S., & Aziz, N. M. (1994). Refinement of cross-flow turbine design parameters. *Journal of Energy Engineering*, 120(3), 133.
- Upadhyay, D. (2004). Low head turbine development using computational fluid dynamics. (Ph.D., University of Nottingham).
- Urban, J. (2011). Modification of a lundell alternator for the use in a pico hydro generator. (M.A.Sc., Regensberg University of Applied Sciences).
- Williams, A. A., & Holmes, P. G. (1995). A novel low head hydro shceme using an induciton generator. *30th Universities Power Engineering Conference, UPEC 95*, pp. 545-549.
- Williams, A. (2004). *Pumps as turbines: A user's guide*. London, UK: Practical Action.
- Williams, A., & Porter, S. (2006). Comparison of hydropower options for developing countries with regard to the environmental, social and economic aspects. *International Conference on Renewable Energy for Developing Countries*, Washington DC, USA.
- Williams, A. A., & Simpson, R. (2009). Pico hydro – reducing technical risks for rural electrification. *Renewable Energy*, 34(8), 1986-1991.
- Williams, A. A., & Simpson, R. G. (2006). Application of computational fluid dynamics to the design of pico propeller turbines. *International Conference on Renewable Energy for Developing Countries - 2006*,
- Williams, A. A., Simpson, R. G., Downes, D., & Stait, T. (n.d.). Technology options for low-head pico-hydropower.
- Williams, A. A., Upadhyay, R., Demetriades, G. M., & Smith, N. P. A. (2000). Low head pico hydropower: A review of available turbine technologies. Brighton, UK.
- Williamson, S. J. (2011). Low head pico hydro off-grid networks. *EWB-UK National Research & Education Conference 2011*, London, UK.

- Williamson, S. J., Stark, B. H., & Booker, J. D. (2011). Low head pico hydro turbine selection using a multi-criteria analysis. *World Renewable Energy Congress*, Linkoping, Sweden.
- World Bank Data. (2012). World bank data. Retrieved January 11, 2012, from <http://data.worldbank.org/>
- Wright, A. K., & Wood, D.H.. (2004). The starting and low wind speed behaviour of a small horizontal axis wind turbine. *Journal of Wind Engineering & Industrial Aerodynamics*, 92(14), 1265-1279.
- Wright, T. (1999). *Fluid machinery : Performance, analysis, and design*. Boca Raton, Fla. ; London: CRC Press.

Appendix A: Market Research

Tabulated results from the market research of potential materials for the fabrication of the turbine design are tabulated below. The data was taken in various locations in Cameroon.

Table A1: Market research list of materials and associated costs

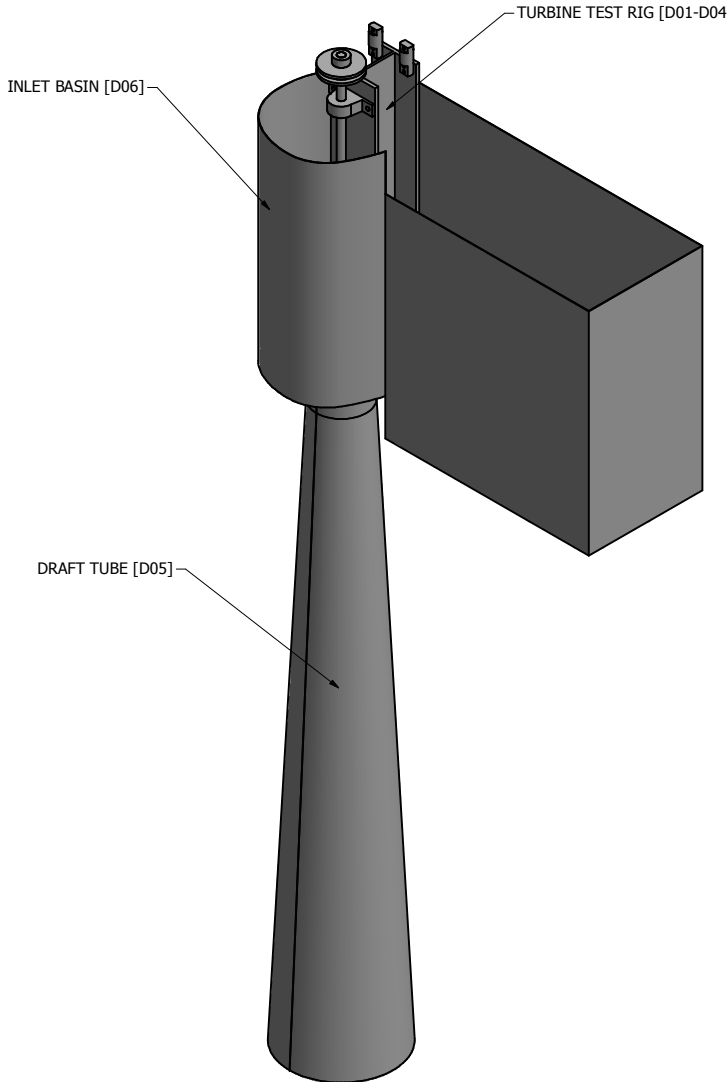
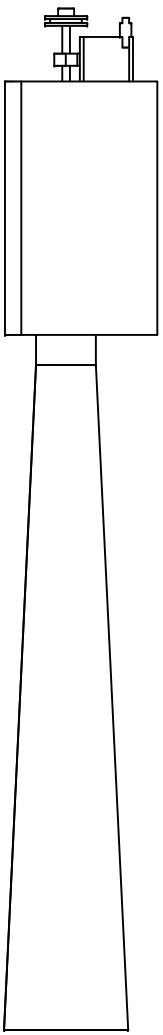
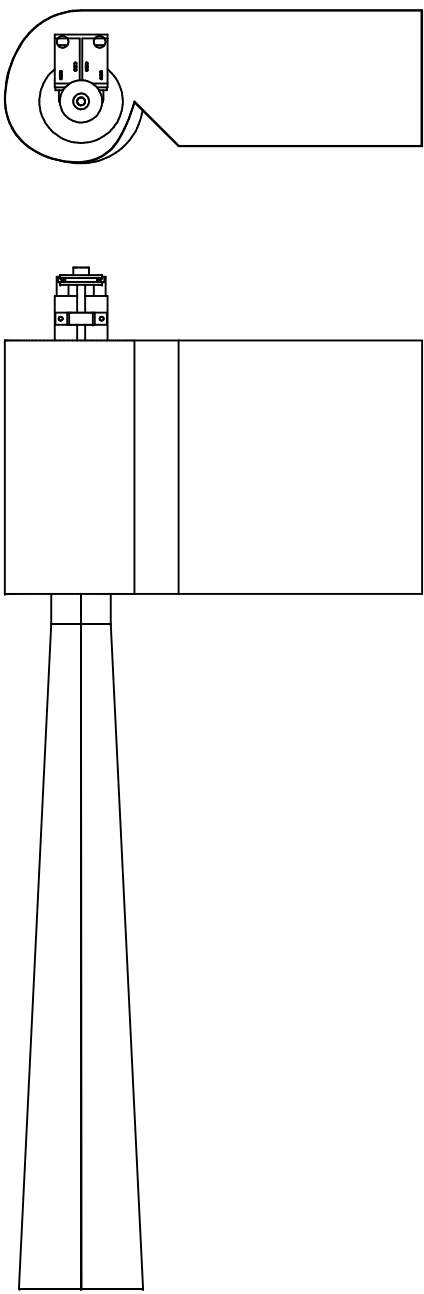
Type	Description	Length [m] or Area [m^2]	Material	Comments	Cost [XAF]	Cost/Unit Length or Area [XAF/m or XAF/m^2]	Cost [€]	Cost/Unit Length or Area [€/m or €/m^2]
Pipe Fittings and Valves	pipe fittings (various types)		brass	Cogeni (fixed price)	325		0.50	
	1/2" valve		brass	Cogeni (fixed price)	2350		3.58	
	1" valve		brass	Cogeni (fixed price)	3750		5.72	
	1-1/2" valve		brass	Cogeni (fixed price)	5400		8.23	
Square Tube (length = 5.8 m)	40 mm x 1 mm wall thickness	5.8	carbon steel	Cogeni (fixed price)	5700	983	8.69	1.50
	60 mm x 1.2 mm wall thickness	5.8	carbon steel	Cogeni (fixed price)	12300	2121	18.75	3.23
	35 mm x 0.7 mm wall thickness	5.8	carbon steel	Cogeni (fixed price)	3400	586	5.18	0.89
Circular Tube (length = 5.8 m)	22 mm	5.8	carbon steel	-Cogeni (fixed price) -unknown wall thickness	3100	534	4.73	0.81
	30 mm	5.8	carbon steel	-Cogeni (fixed price) -unknown wall thickness	4100	707	6.25	1.08
	50/60 (50 mm inner diameter, 60 mm outer diameter)	5.8	carbon steel	-Cogeni (fixed price) -confirm dimensions	16700	2879	25.46	4.39
	66/76 (66 mm inner diameter, 76 mm outer diameter)	5.8	carbon steel	-Cogeni (fixed price) -confirm dimensions	22300	3845	33.99	5.86
Pipe	1/2"		galvanized steel	-advertized price -unknown length	5500		8.38	
	3/4"		galvanized steel	-advertized price -unknown length	8000		12.20	
Rod	14 mm		carbon steel	-advertized price -price seems high	14000		21.34	
	12 mm		carbon steel	advertized price	5500		8.38	
	10 mm		carbon steel	advertized price	3700		5.64	

Table A1 continued...

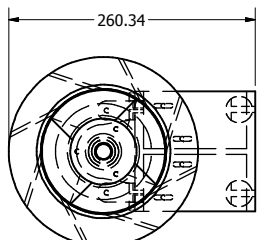
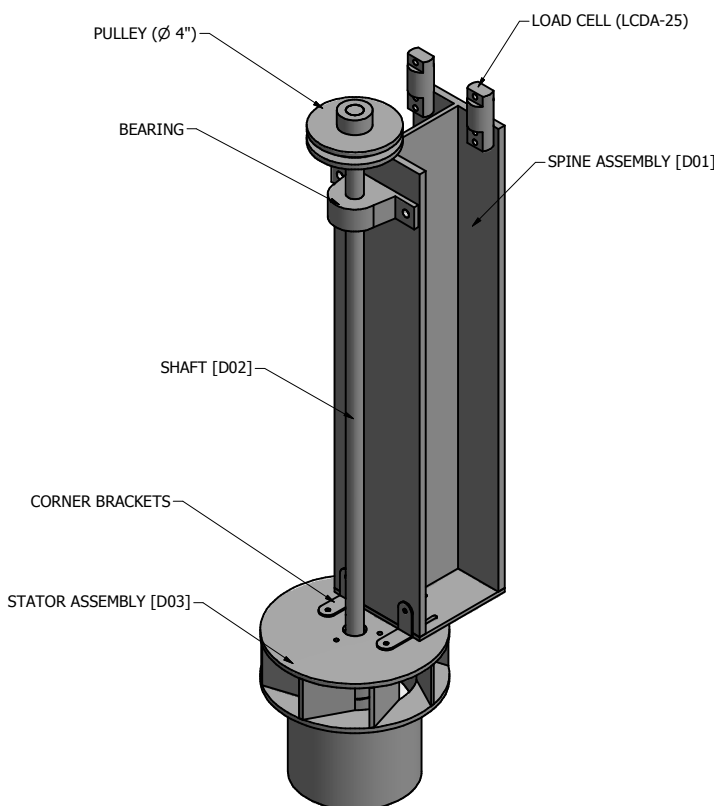
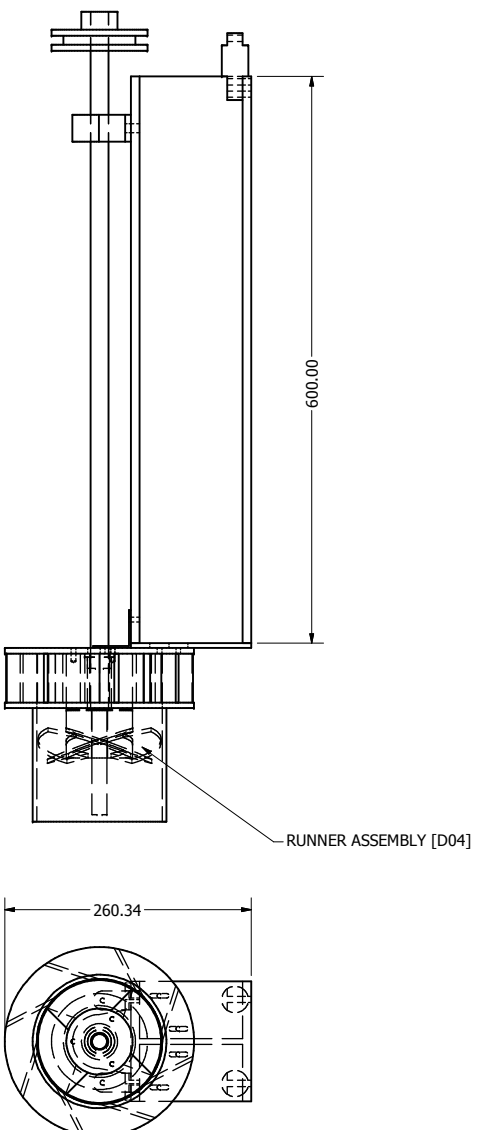
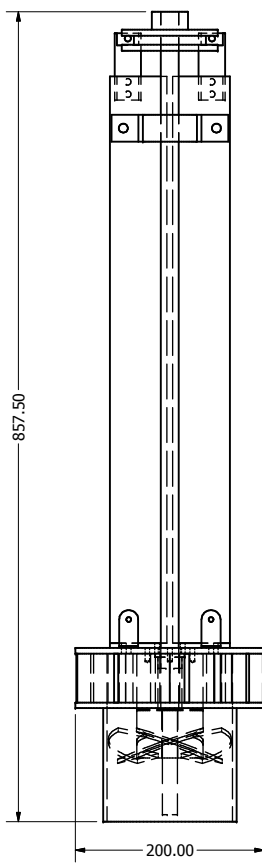
Type	Description	Length [m] or Area [m^2]	Material	Comments	Cost [XAF]	Cost/Unit Length or Area [XAF/m or XAF/m^2]	Cost [€]	Cost/Unit Length or Area [€/m or €/m^2]
	8 mm		carbon steel	advertized price	2400		3.66	
	6 mm		carbon steel	advertized price	1200		1.83	
Angle Iron (length = 5.8 m)	40 mm x 4 mm thickness	5.8	carbon steel	Cogeni (fixed price)	1250	216	1.91	0.33
	20 mm x 2.2 mm thickness	5.8	carbon steel	Cogeni (fixed price)	2500	431	3.81	0.66
Flat Bar (length = 5.8 m)	60 mm x 8 mm thickness	5.8	carbon steel	Cogeni (fixed price)	13300	2293	20.27	3.50
	30mm x 8mm thickness	5.8	carbon steel	Cogeni (fixed price)	8100	1397	12.35	2.13
	20mm x 4mm thickness	5.8	carbon steel	Cogeni (fixed price)	2400	414	3.66	0.63
Sheet Metal (2m length x 1m wide)	15/10 (1.5mm thick)	2	galvanized steel	Cogeni (fixed price)	20300	10150	30.95	15.47
	10/10 (1mm thick)	2	carbon steel	Cogeni (fixed price)	11700	5850	17.84	8.92
	8/10 (8mm thick)	2	carbon steel	Cogeni (fixed price)	8700	4350	13.26	6.63
	12/10 (1.2mm thick)	2	galvanized steel	Cogeni (fixed price)	16200	8100	24.70	12.35
PVC rain gutter				Cogeni (fixed price)	6400		9.76	
Cement	50kg		cement	advertized price	4900		7.47	
PVC pipe	100mm		PVC	advertized price	3500		5.34	
	63mm		PVC	advertized price	2200		3.35	
	50mm		PVC	advertized price	2000		3.05	
	40mm		PVC	advertized price	1800		2.74	
	32mm		PVC	advertized price	1500		2.29	
Pressure pipe	32mm			-advertized price -unknown material -unknown length	2700		4.12	
	25mm			-advertized price -unknown material -unknown length	1500		2.29	
Auto Wheel Bearing	front wheel bearing and hub			private price (too high)	20000		30.49	
	drive shaft			private price (too high)	15000		22.87	
	bearing (bare)			private price (too high)	12000		18.29	
	back wheel (bearing and hub)			private price (too high)	12000		18.29	

Appendix B: Design Drawing Package

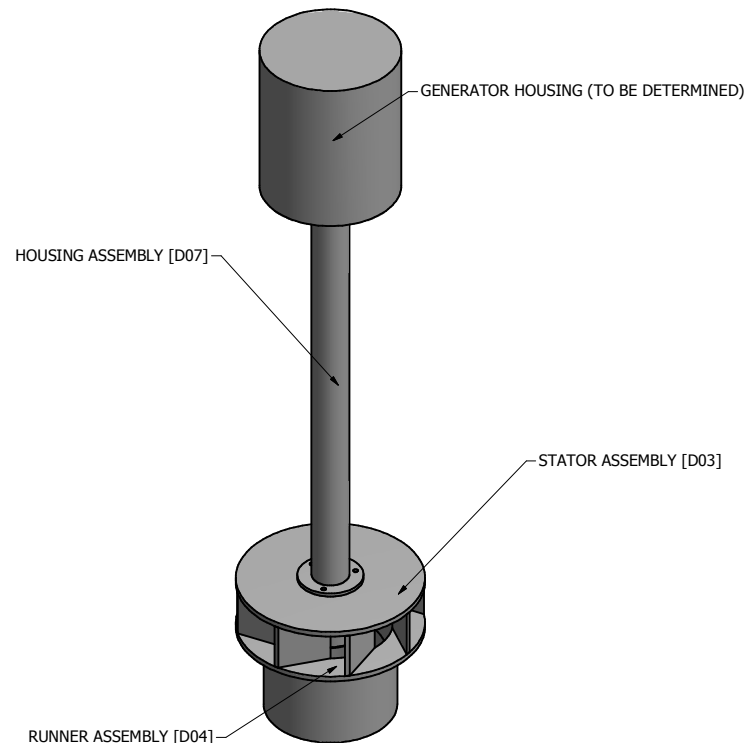
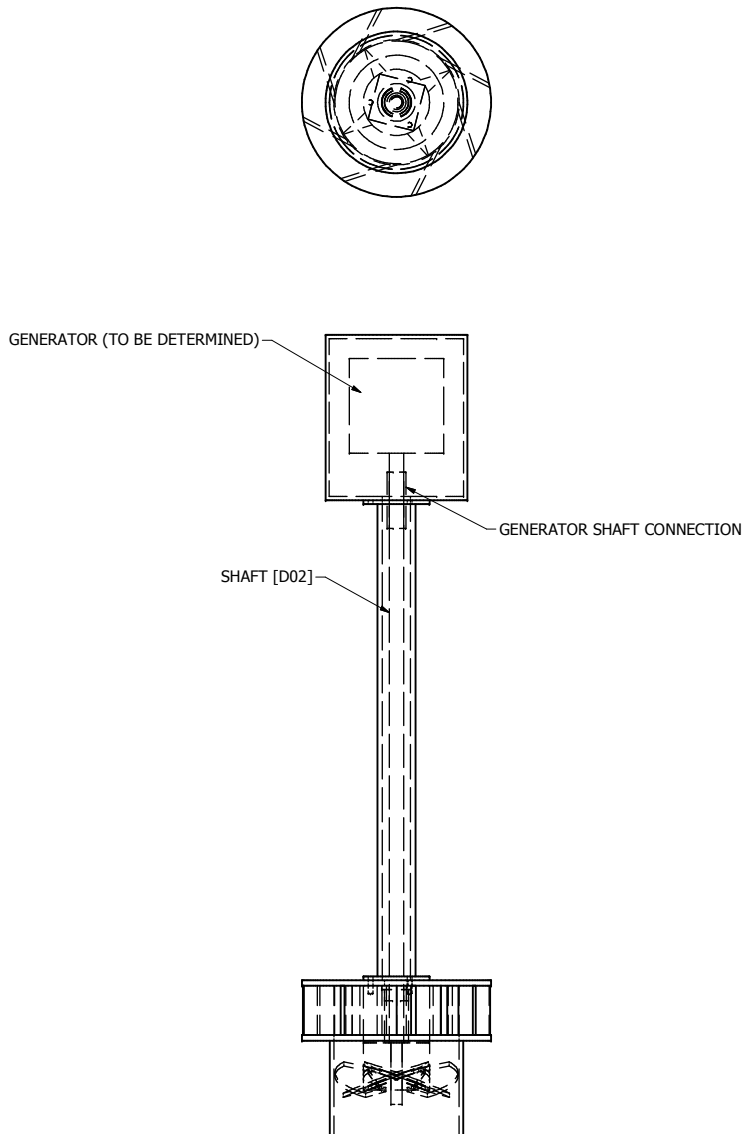
This appendix includes the mechanical design drawing package of the prototype flat blade propeller turbine, inlet basin, and draft tube. These drawings were used for the construction of the prototype turbine for the purpose of performance testing. Also included are drawings of the production version of the turbine.



DRAWN BYH	30/08/2011	UNIVERSITY OF GUELPH		
CHECKED		TITLE		
QA		TEST SYSTEM ASSEMBLY		
MFG				
APPROVED		SIZE C	DWG NO D00-00	REV -
		SCALE		SHEET 1 OF 1

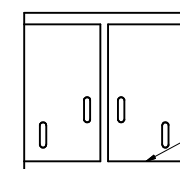


DRAWN BY	04/08/2011	UNIVERSITY OF GUELPH		
CHECKED		TITLE		
QA		TEST RIG ASSEMBLY		
MFG				
APPROVED		SIZE C	DWG NO D00-01	REV B
		SCALE MM		SHEET 1 OF 1



DRAWN BHY	30/08/2011	UNIVERSITY OF GUELPH		
CHECKED QA		TITLE		
MFG		PRODUCTION ASSEMBLY		
APPROVED		SIZE C	DWG NO D00-02	REV A
		SCALE MM		SHEET 1 OF 1

4

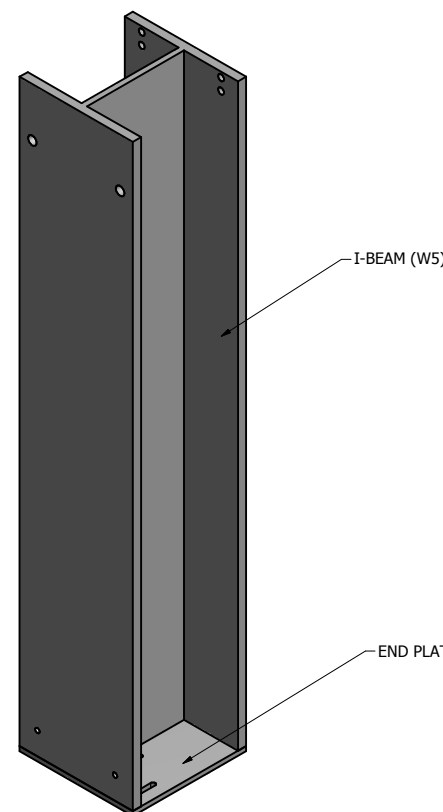
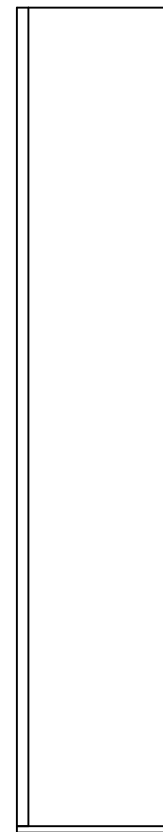


3

3

2

1



DRAWN BHY	04/08/2011	UNIVERSITY OF GUELPH		
CHECKED QA		TITLE		
MFG		SPINE ASSEMBLY		
APPROVED		SIZE C	DWG NO D01-00	REV -
		SCALE MM		SHEET 1 OF 1

4

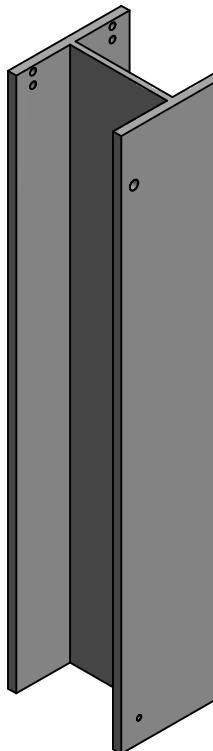
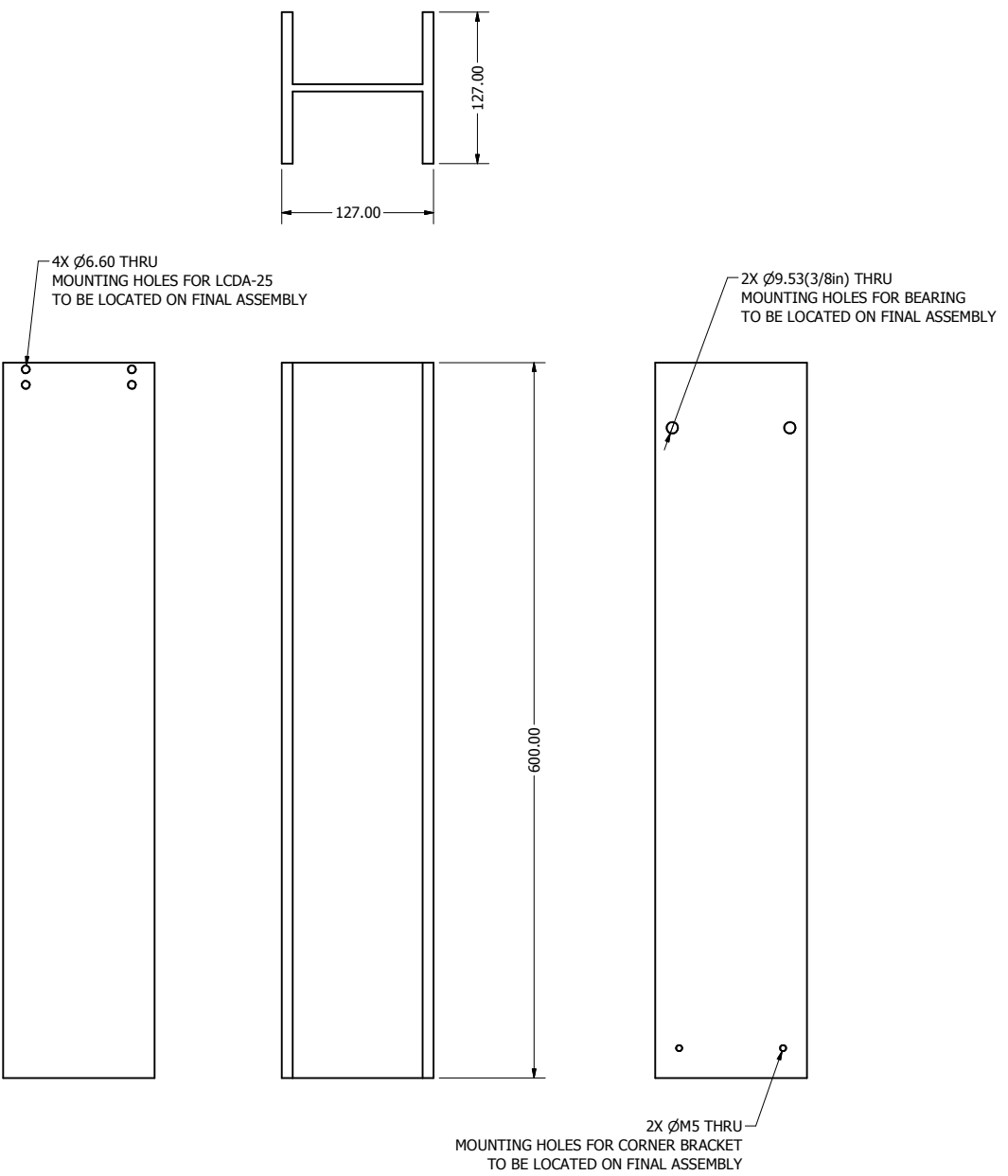
1

3

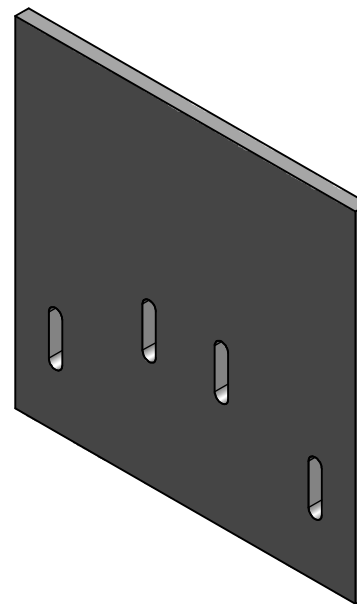
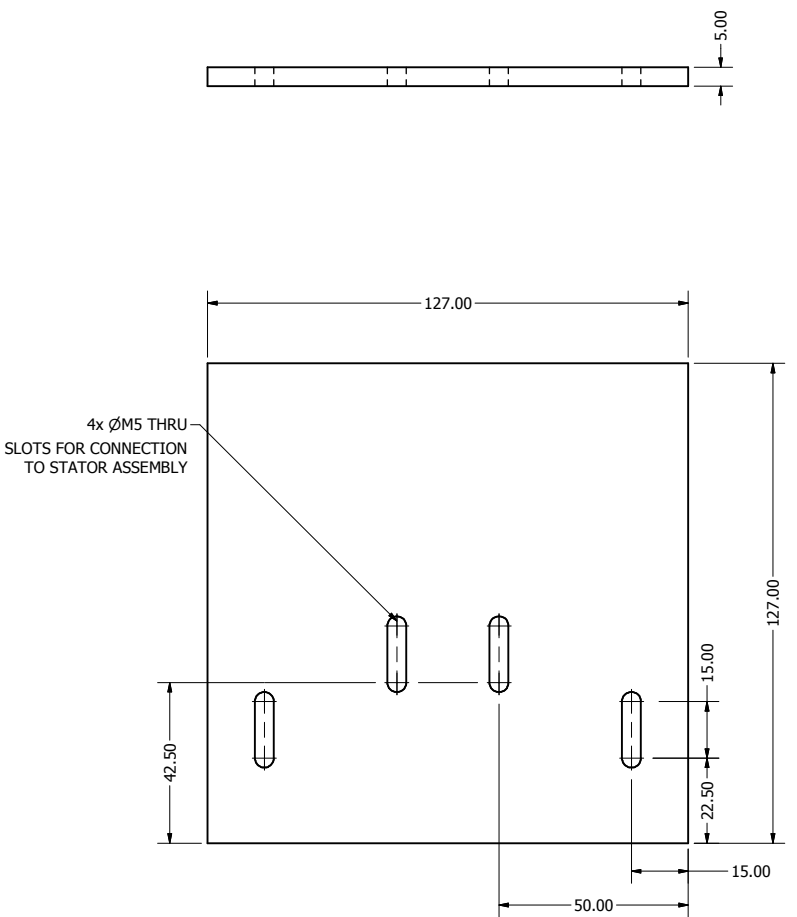
4

2

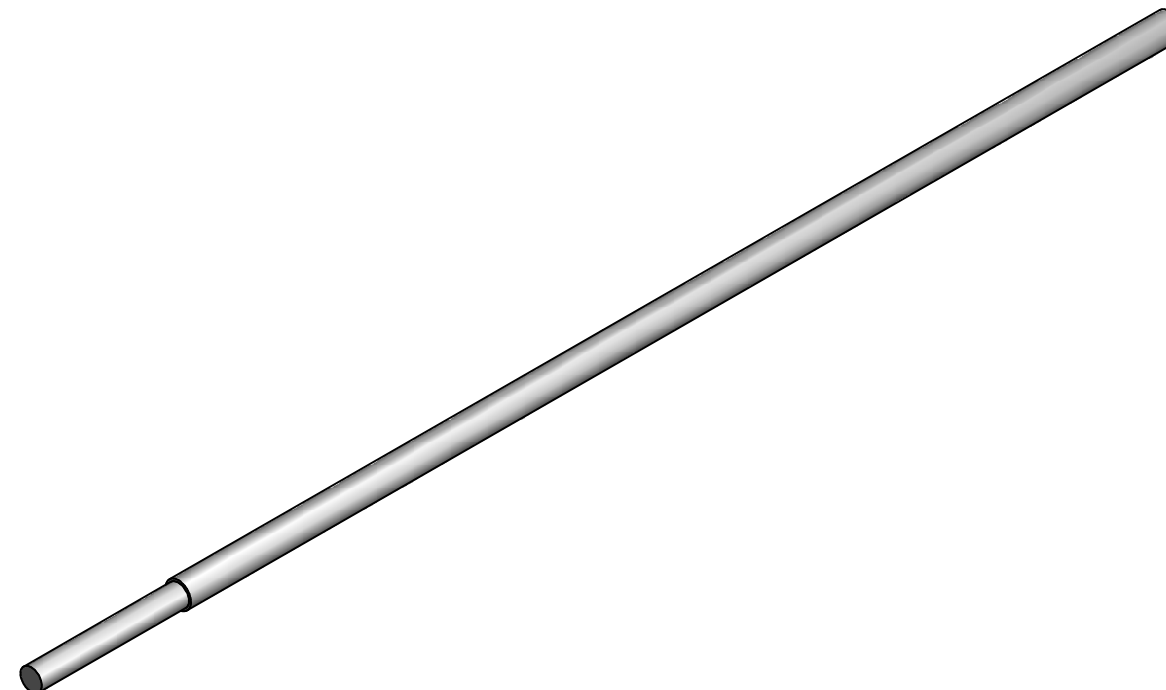
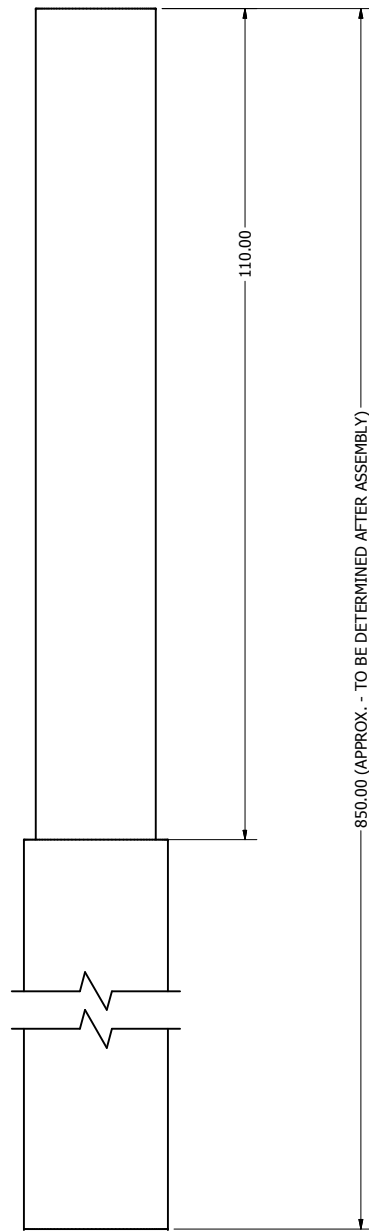
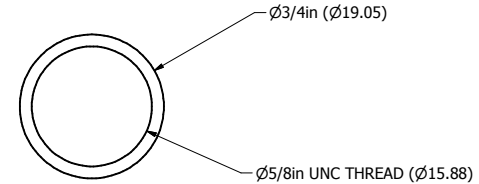
1



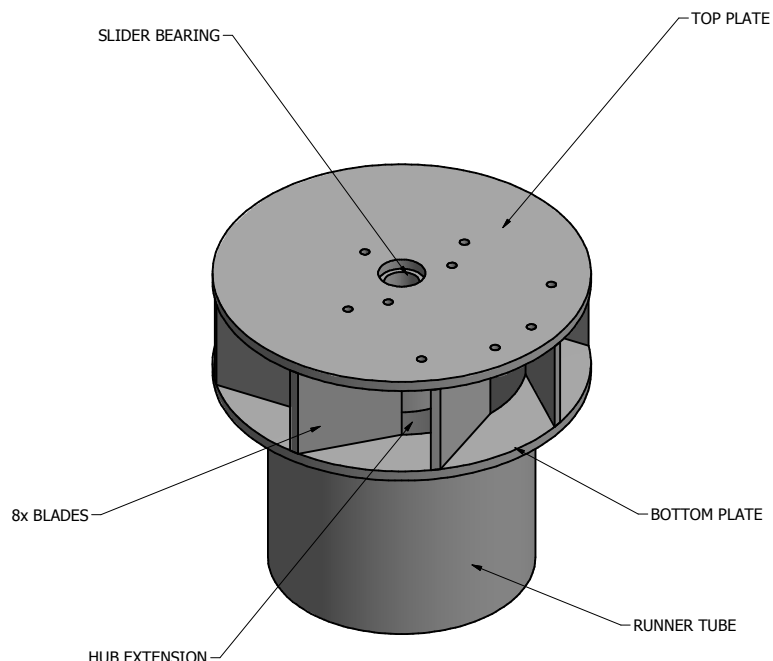
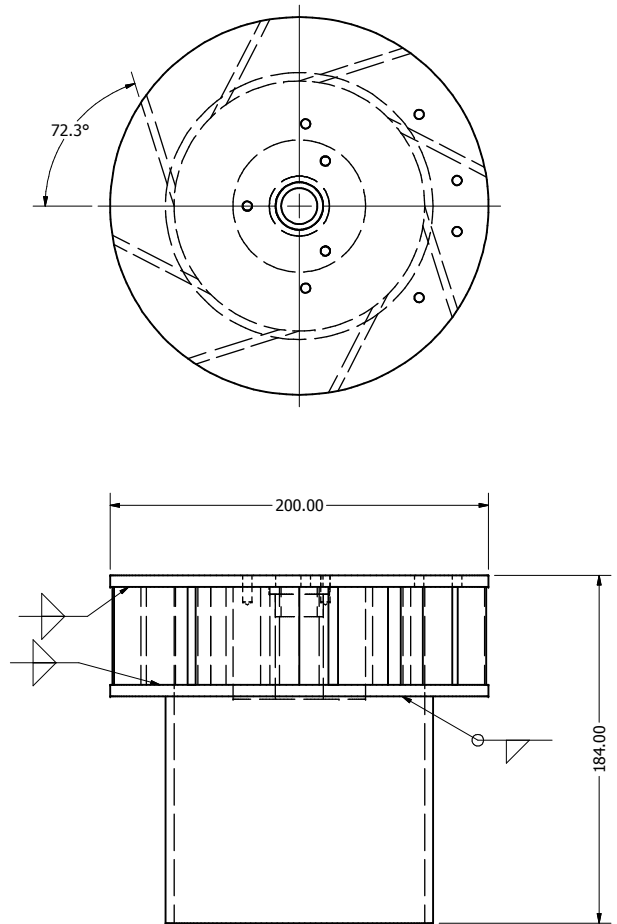
DRAWN BHY	04/08/2011	UNIVERSITY OF GUELPH		
CHECKED		TITLE		
QA		SPINE-I-BEAM (W5)		
MFG				
APPROVED		SIZE C	DWG NO D01-01	REV A
		SCALE MM		SHEET 1 OF 1



DRAWN BHY	04/08/2011	UNIVERSITY OF GUELPH		
CHECKED QA		TITLE		
MFG		SPINE-END PLATE		
APPROVED				
	SIZE C	DWG NO D01-02	REV -	
	SCALE MM			SHEET 1 OF 1

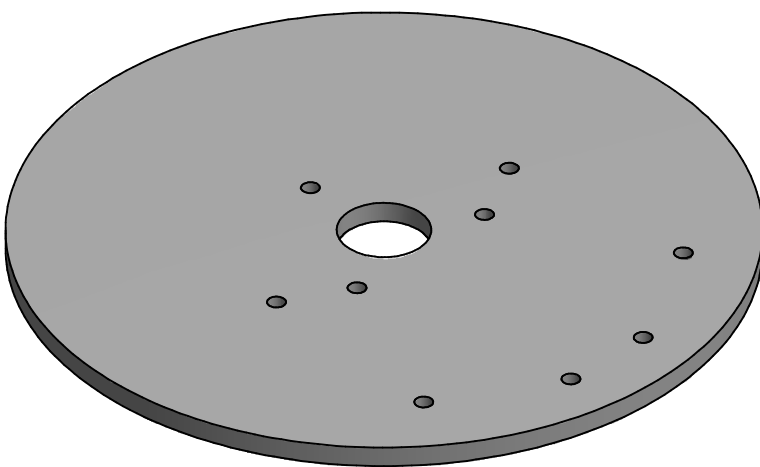
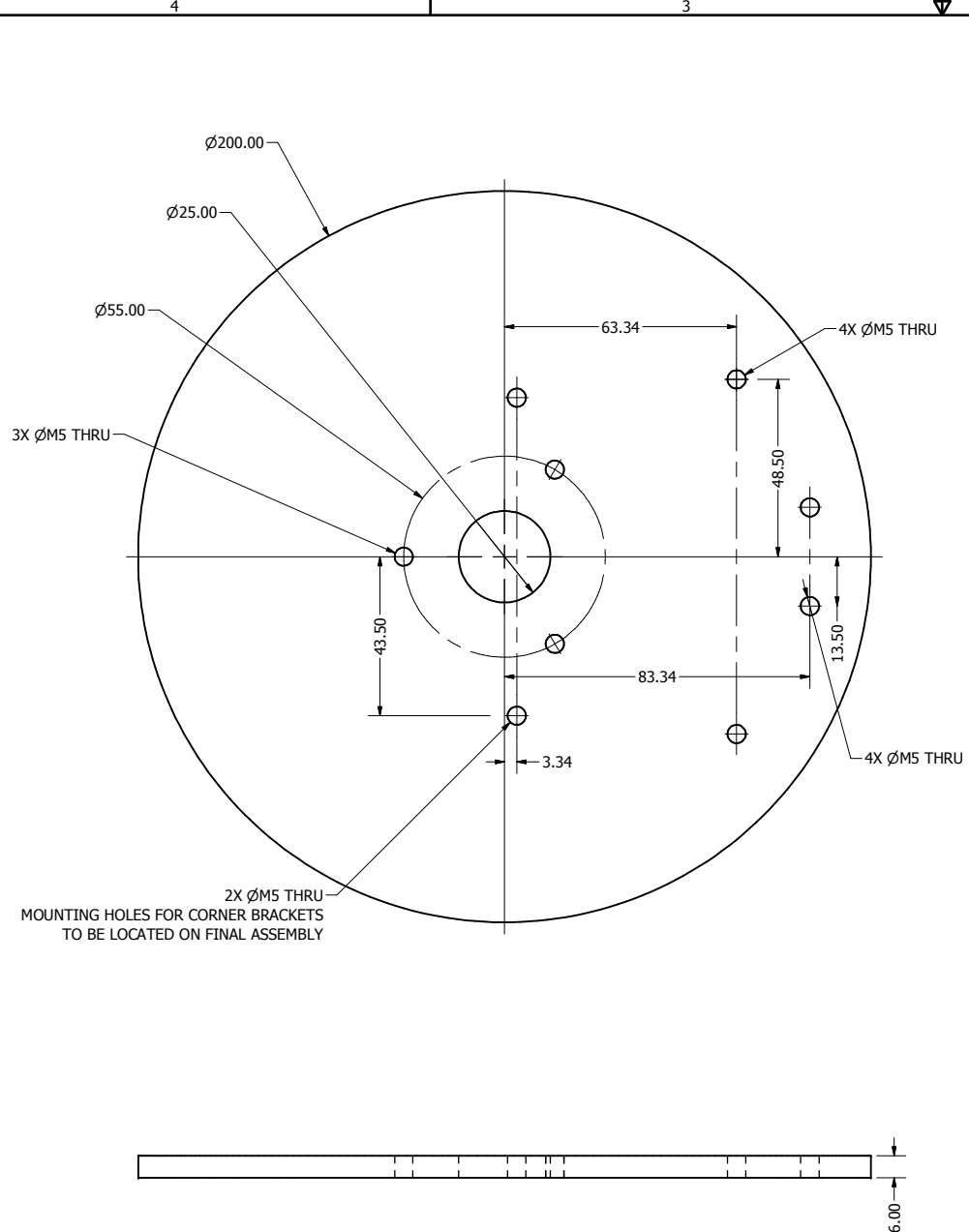


DRAWN BHY	04/08/2011	UNIVERSITY OF GUELPH		
CHECKED		TITLE		
QA		SHAFT		
MFG				
APPROVED		SIZE C	DWG NO D02-01	REV A
		SCALE MM		SHEET 1 OF 1



DRAWN BHY	04/08/2011	UNIVERSITY OF GUELPH		
CHECKED		TITLE		
QA		STATOR ASSEMBLY		
MFG				
APPROVED		SIZE C	DWG NO D03-00-A	REV A
		SCALE MM		SHEET 1 OF 1

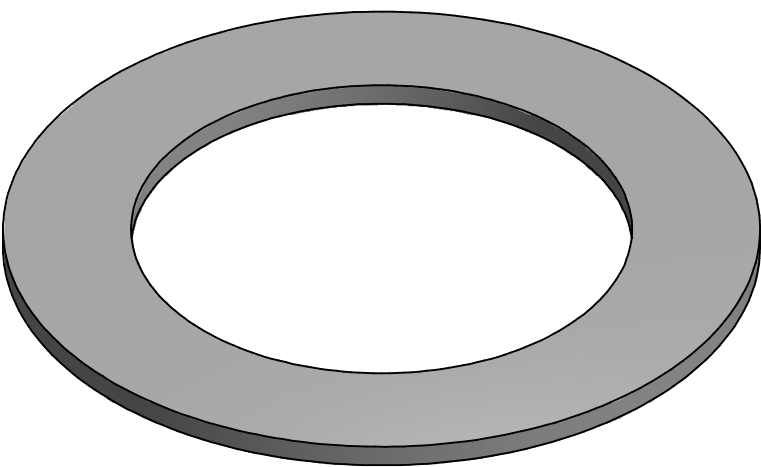
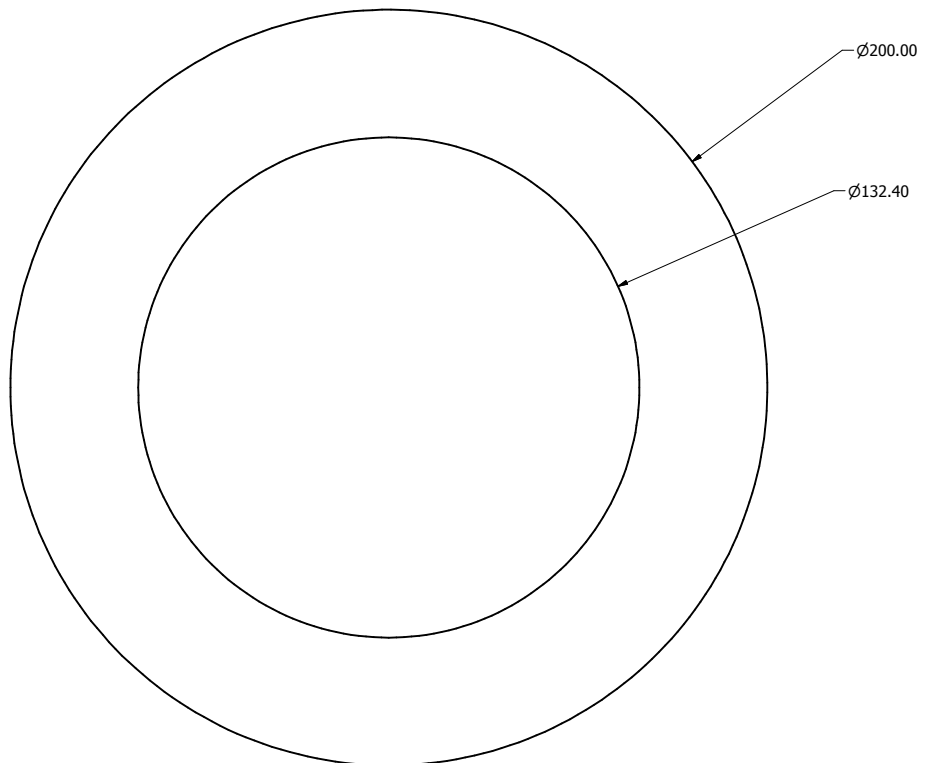
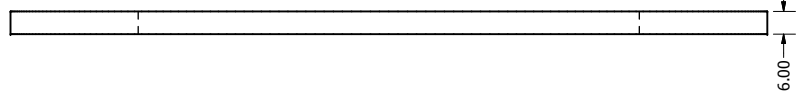
PRODUCED BY AN AUTODESK EDUCATIONAL PRODUCT



PRODUCED BY AN RUDI DESK EDUCATIONAL PRODUCT

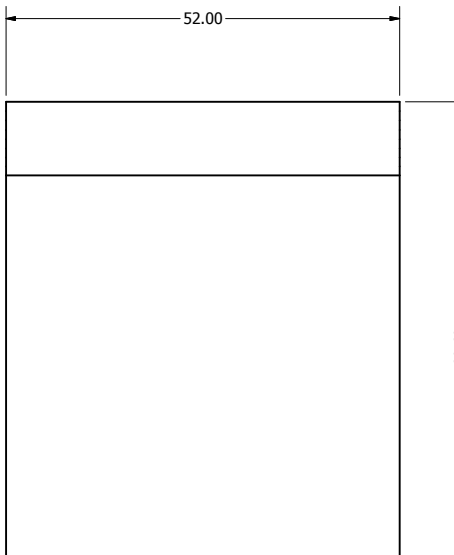
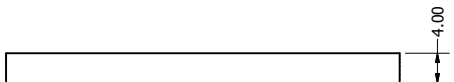
DRAWN BHY	04/08/2011	UNIVERSITY OF GUELPH		
CHECKED				
QA		TITLE STATOR-TOP PLATE		
MFG				
APPROVED		SIZE C	DWG NO D03-01	REV -
		SCALE	MM	SHEET 1 OF 1

PRODUCED BY AN AUTODESK EDUCATIONAL PRODUCT

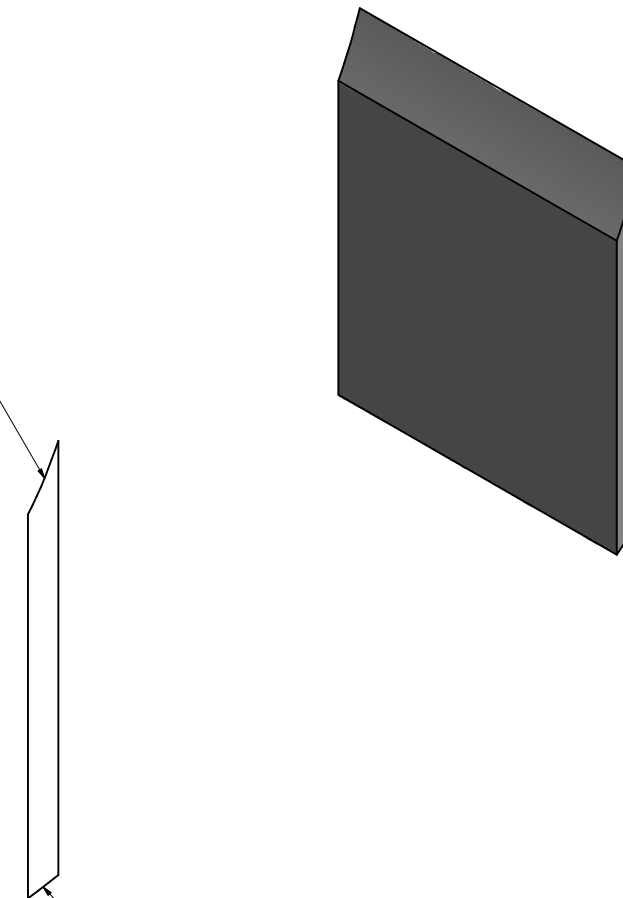


DRAWN BHY	04/08/2011	UNIVERSITY OF GUELPH		
CHECKED QA		TITLE		
MFG		STATOR-BOTTOM PLATE		
APPROVED		SIZE C	DWG NO D03-02	REV -
		SCALE MM		SHEET 1 OF 1

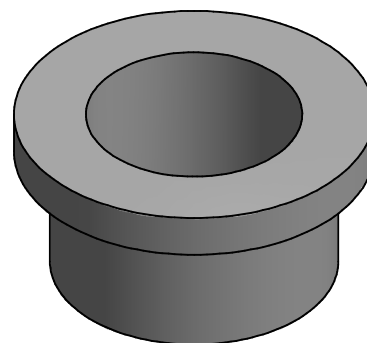
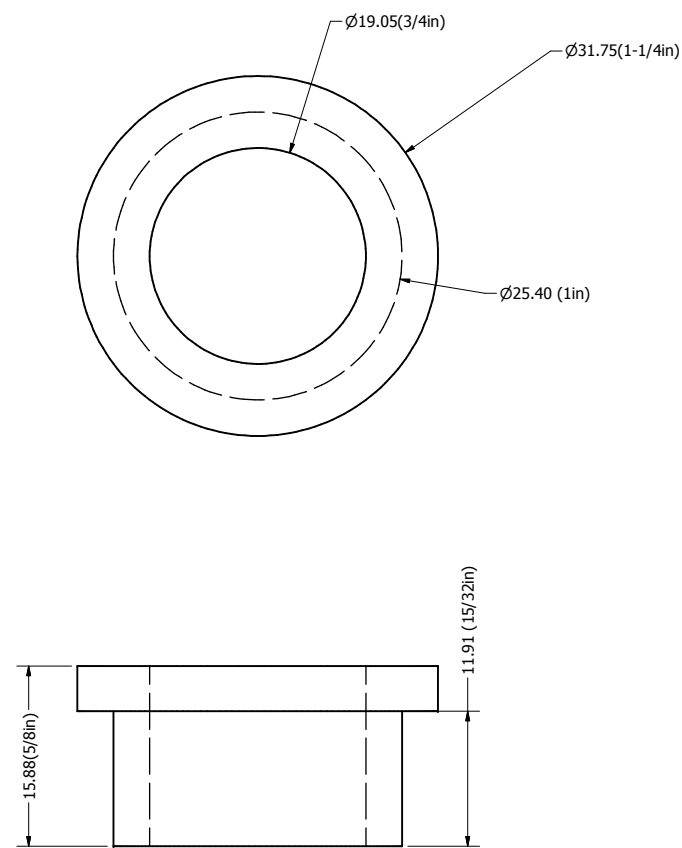
PRODUCED BY AN AUTODESK EDUCATIONAL PRODUCT



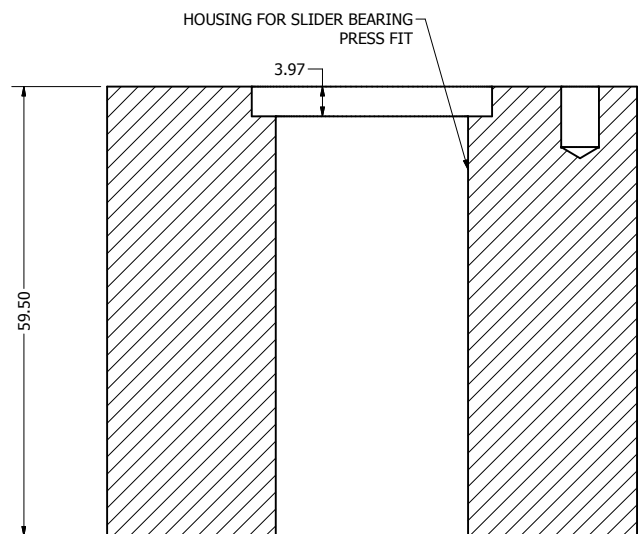
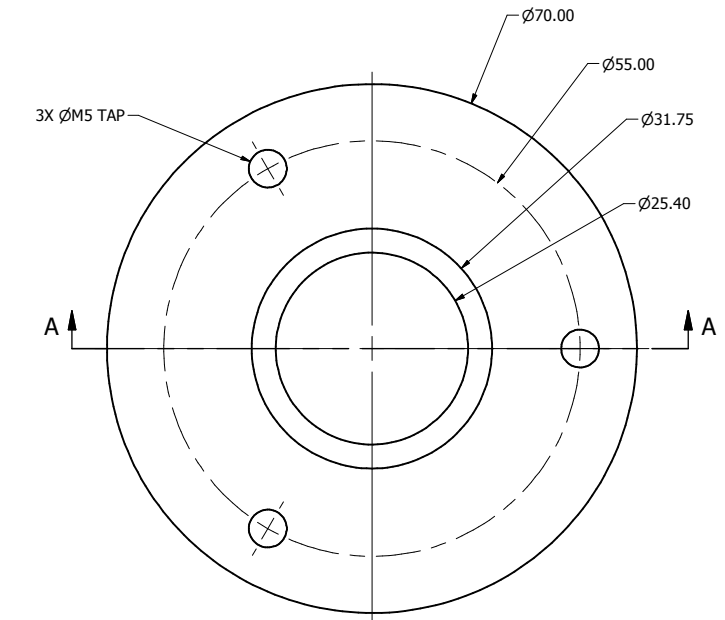
GRIND FLUSH WITH STATOR
BOTTOM PLATE INNER DIAMETER
AFTER PLACEMENT AND WELDING



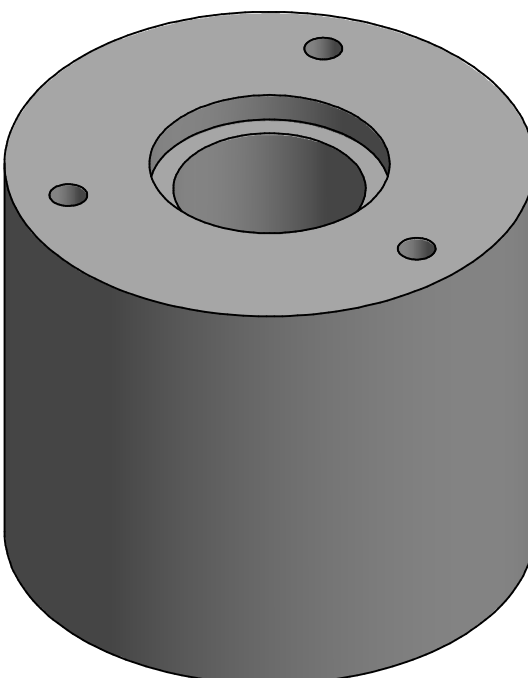
DRAWN BHY	04/08/2011	UNIVERSITY OF GUELPH		
CHECKED		TITLE		
QA		STATOR-BLADES		
MFG				
APPROVED		SIZE C	DWG NO D03-03	REV -
		SCALE MM		SHEET 1 OF 1



DRAWN BHY	04/08/2011	UNIVERSITY OF GUELPH		
CHECKED		TITLE		
QA		STATOR-SLIDER BEARING		
MFG				
APPROVED		SIZE C	DWG NO D03-04	REV A
		SCALE MM		SHEET 1 OF 1

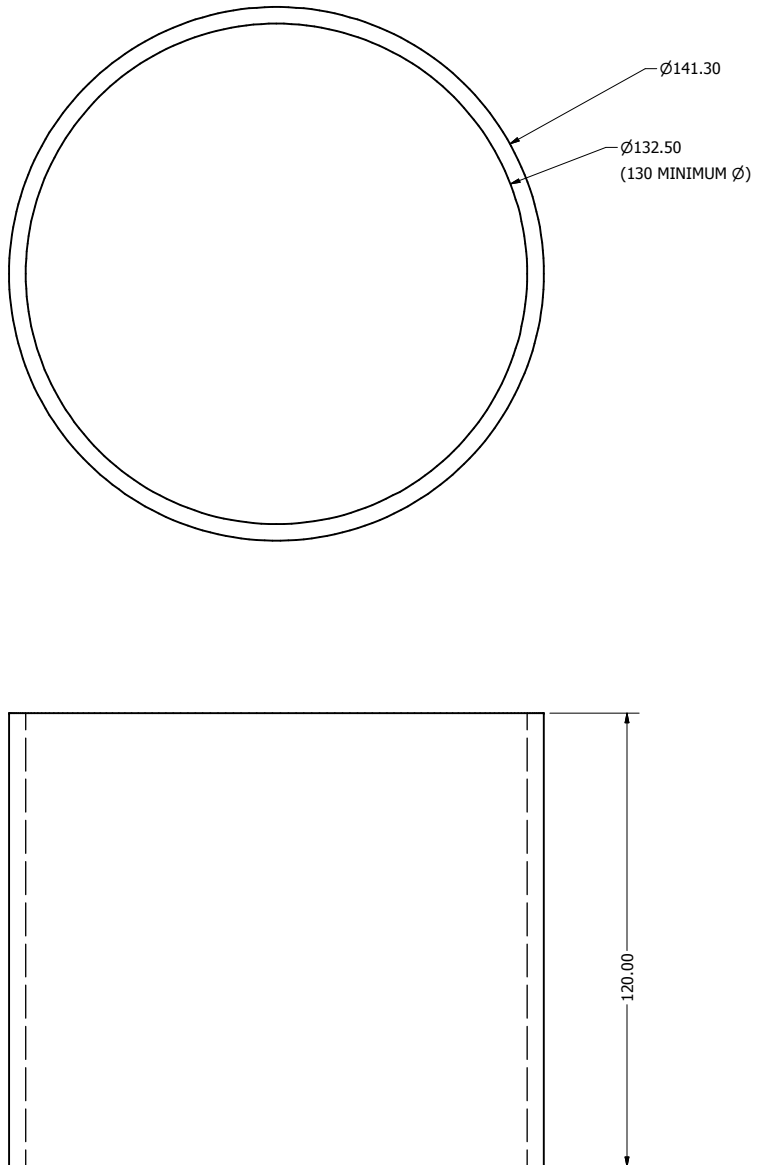


SECTION A-A
SCALE 2 : 1



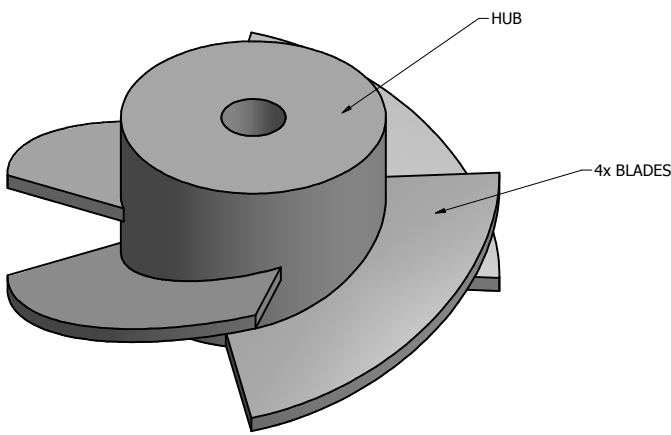
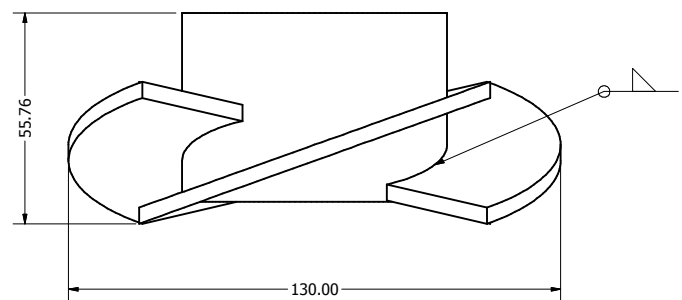
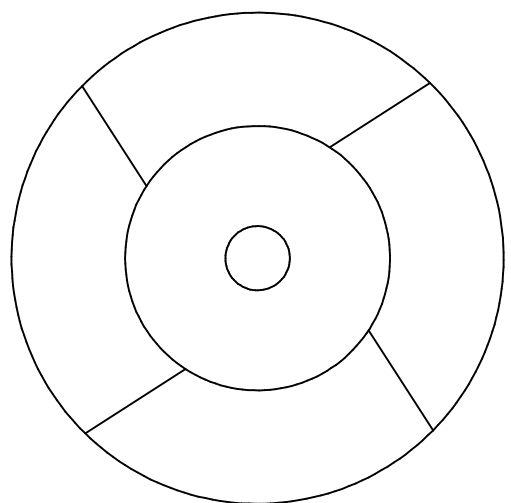
DRAWN BHY	04/08/2011	TITLE		
CHECKED		STATOR-HUB EXTENSION		
QA				
MFG		SIZE	C	DWG NO
APPROVED				D03-05
		SCALE	MM	REV -
				SHEET 1 OF 1

4 1 3 2 1

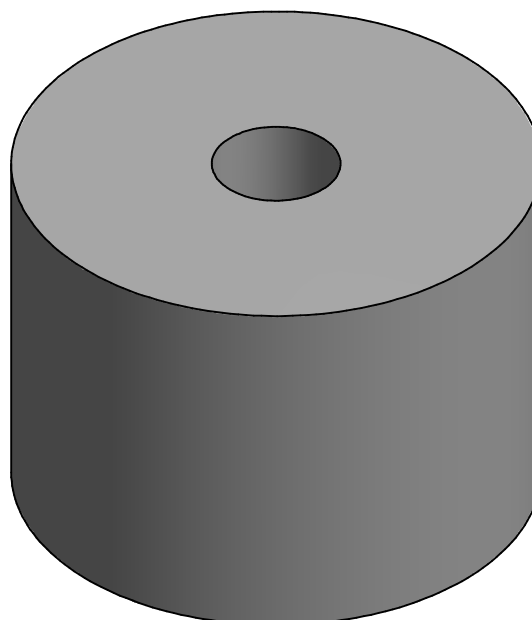
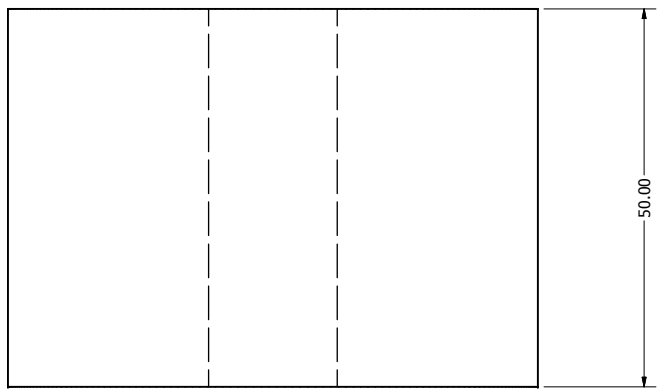
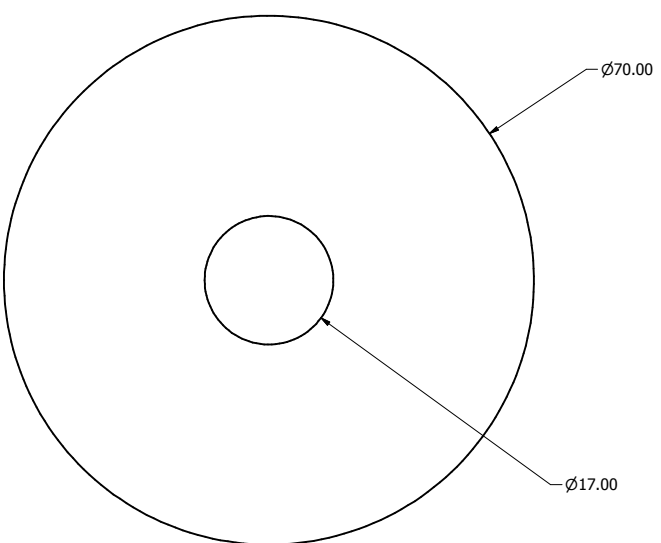


DRAWN BHY	04/08/2011	UNIVERSITY OF GUELPH		
CHECKED QA		TITLE		
MFG		STATOR-RUNNER TUBE		
APPROVED		SIZE C	DWG NO D03-06	REV A
		SCALE MM		SHEET 1 OF 1

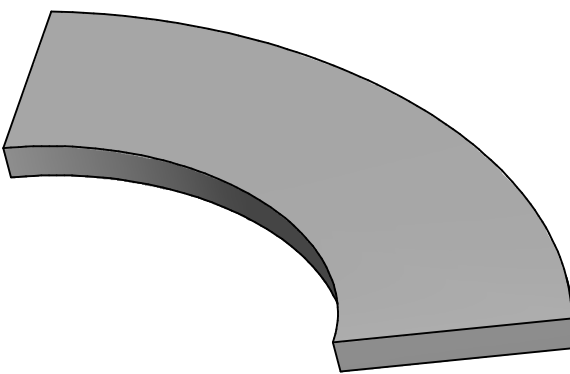
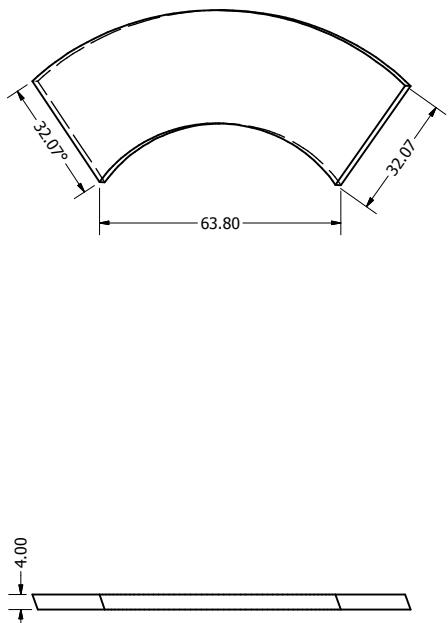
4 1 3 2 1



DRAWN BHY	04/08/2011	UNIVERSITY OF GUELPH		
CHECKED QA		TITLE		
MFG		RUNNER ASSEMBLY		
APPROVED		SIZE C	DWG NO D04-00-A	REV A
		SCALE MM		SHEET 1 OF 1

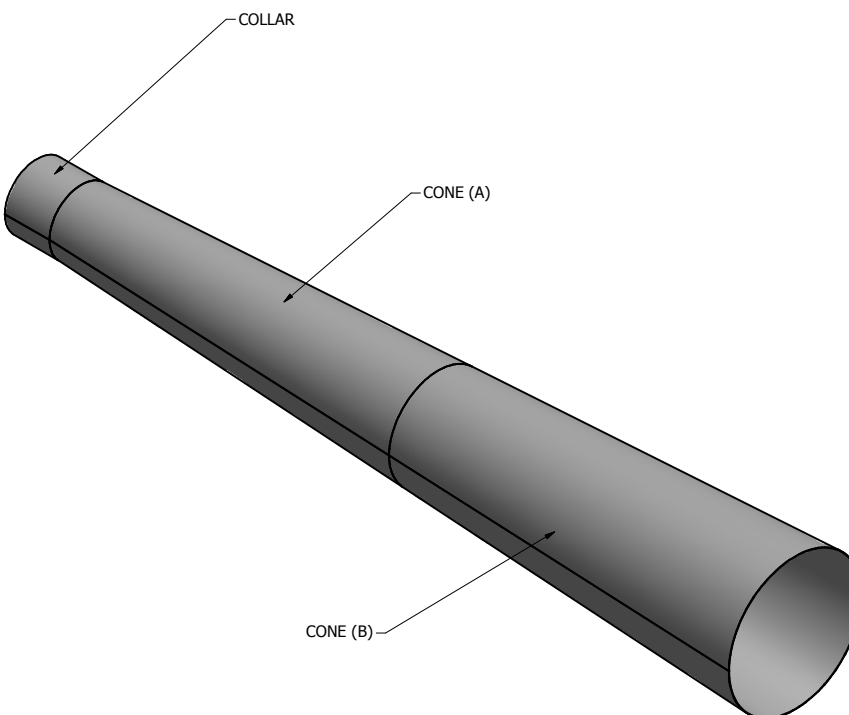
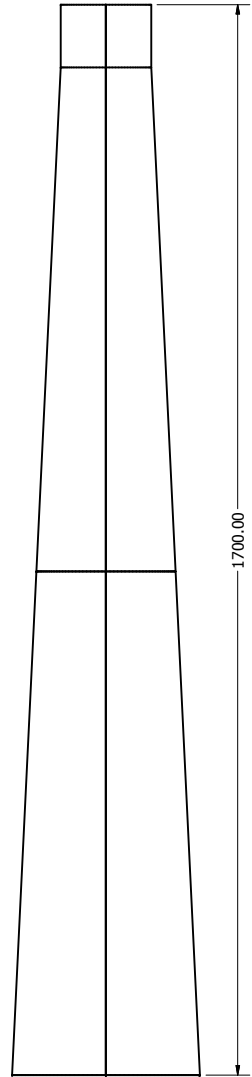
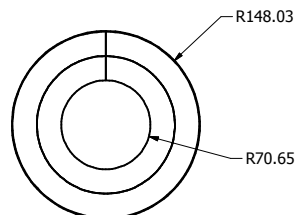


DRAWN BHY	04/08/2011	UNIVERSITY OF GUELPH		
CHECKED QA		TITLE		
MFG		RUNNER-HUB		
APPROVED		SIZE C	DWG NO D04-01-A	REV A
		SCALE MM		SHEET 1 OF 1

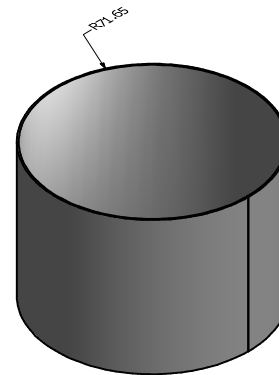
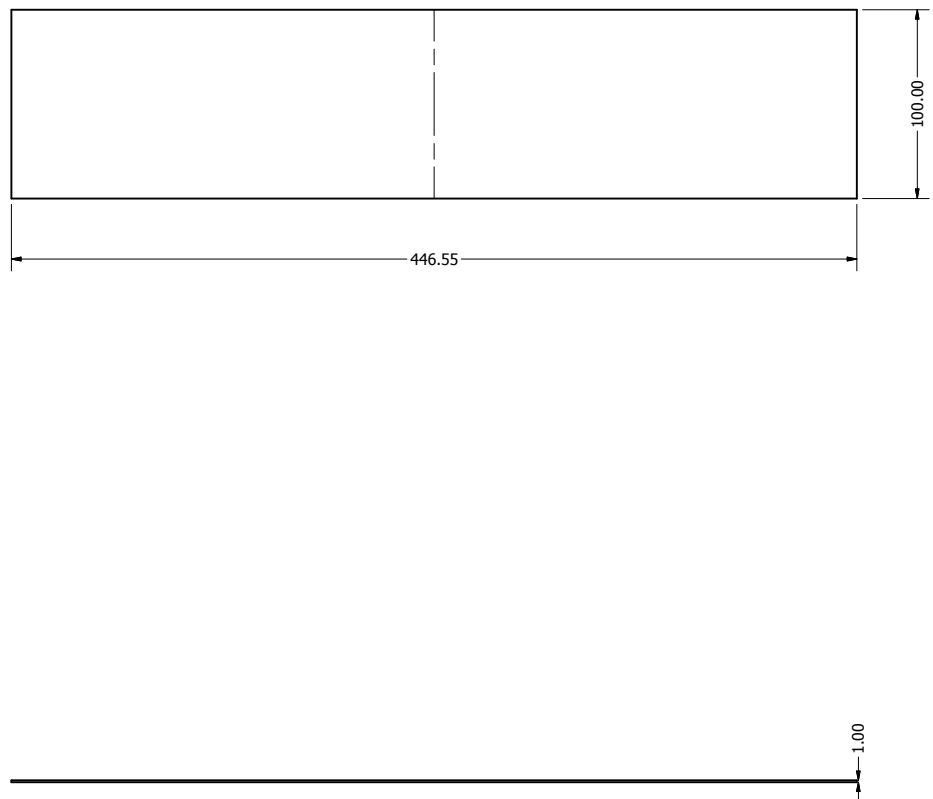


DUE TO COMPLEX SHAPES THIS DRAWING
IS TO BE PRINTED TO SCALE AND USED TO
TRACE SHAPE OF BLADE ON MATERIAL

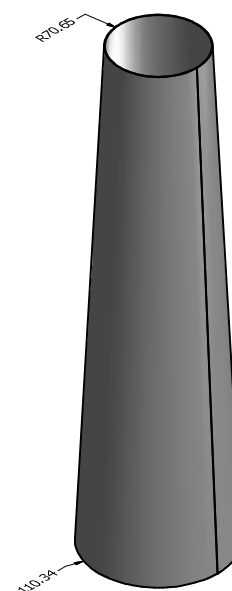
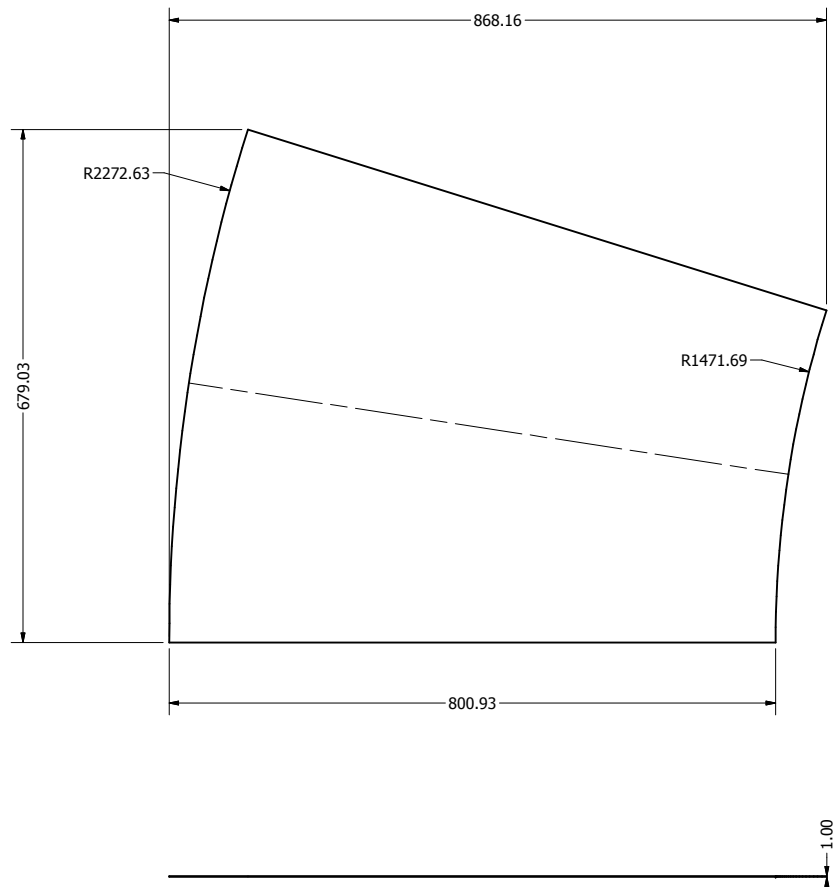
DRAWN BHY	04/08/2011	UNIVERSITY OF GUELPH		
CHECKED		TITLE		
QA		RUNNER-FLAT BLADE		
MFG				
APPROVED		SIZE C	DWG NO D04-02-A	REV A
		SCALE MM		SHEET 1 OF 1



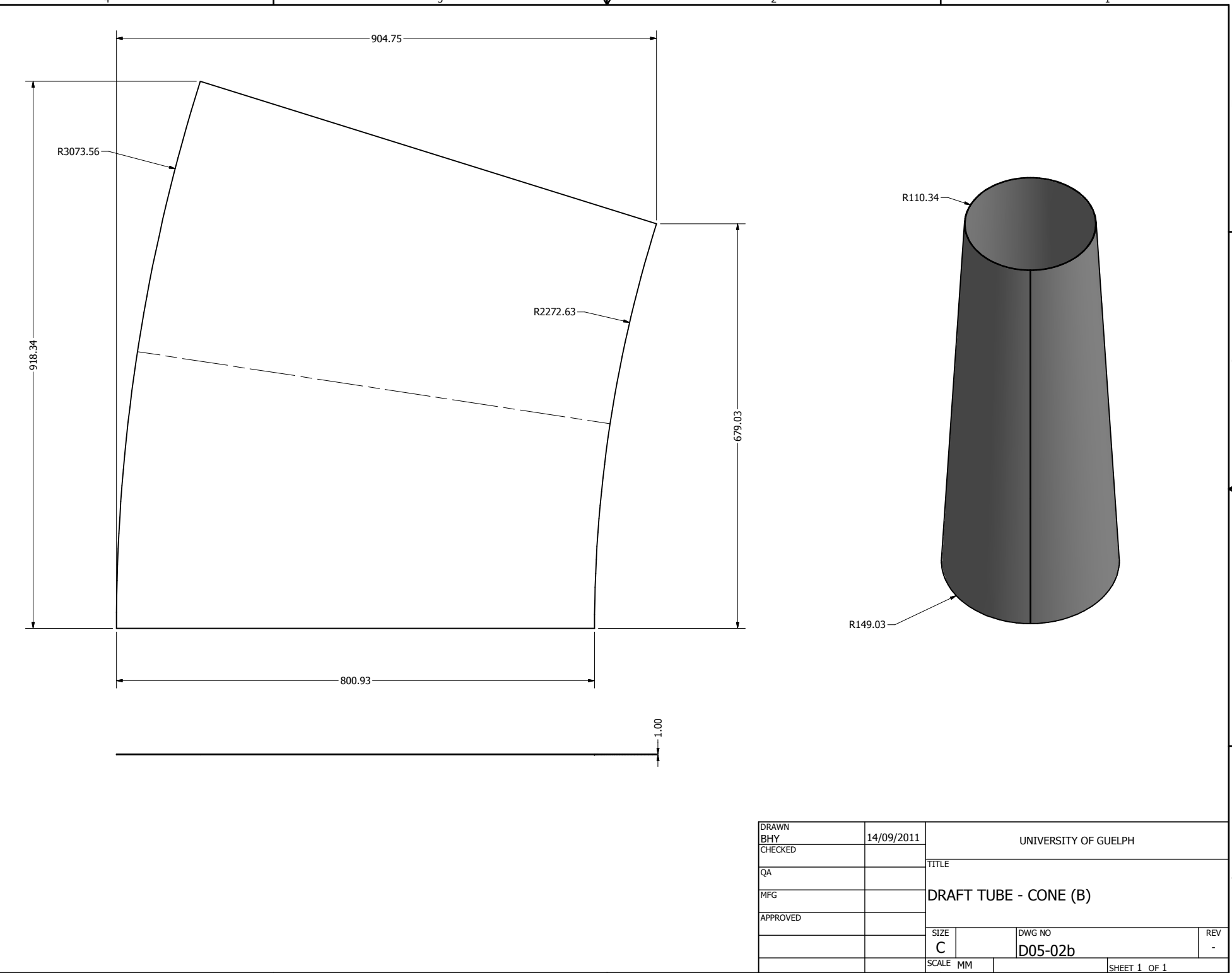
DRAWN BY	14/09/2011	UNIVERSITY OF GUELPH		
CHECKED		TITLE		
QA		DRAFT TUBE ASSEMBLY		
MFG				
APPROVED		SIZE C	DWG NO D05-00-B	REV B
		SCALE MM		SHEET 1 OF 1



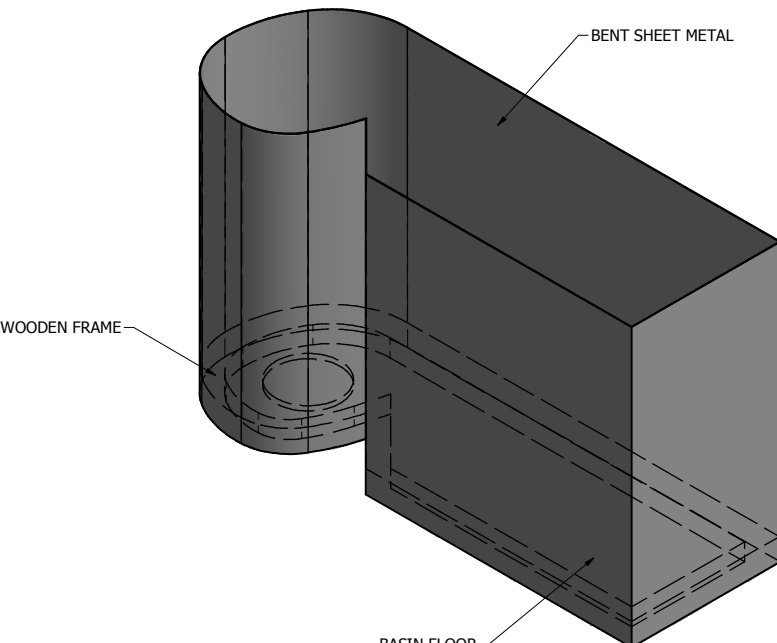
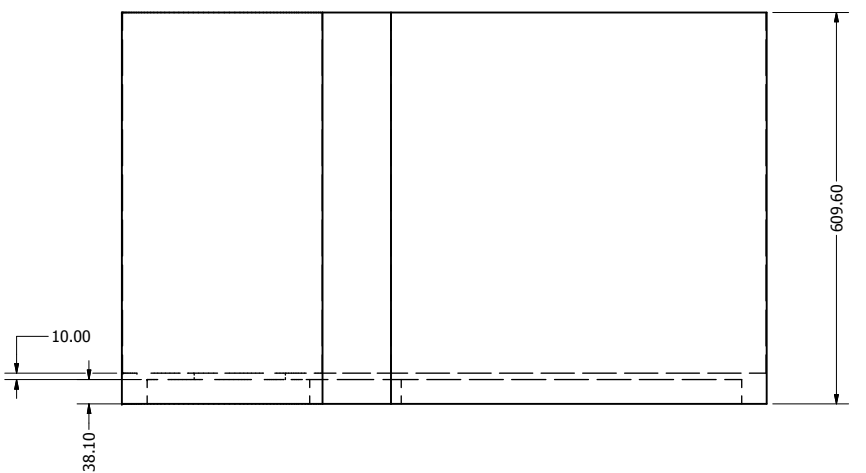
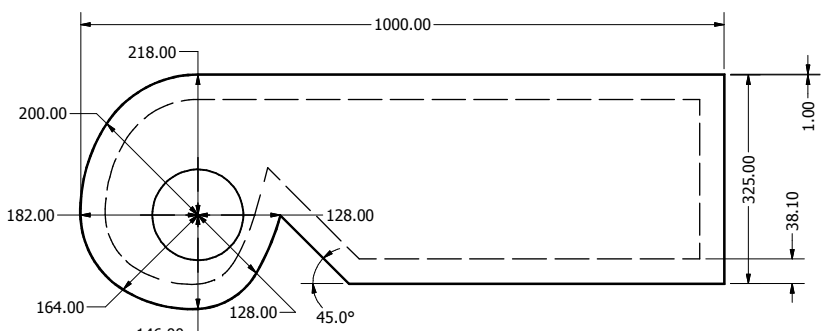
DRAWN BHY	24/08/2011	UNIVERSITY OF GUELPH		
CHECKED		TITLE		
QA		DRAFT TUBE-COLLAR		
MFG				
APPROVED		SIZE C	DWG NO D05-01	REV -
		SCALE MM		SHEET 1 OF 1



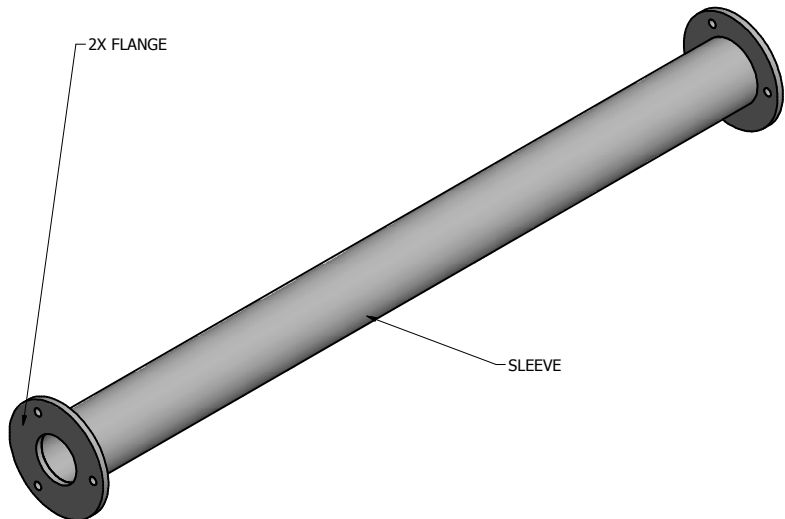
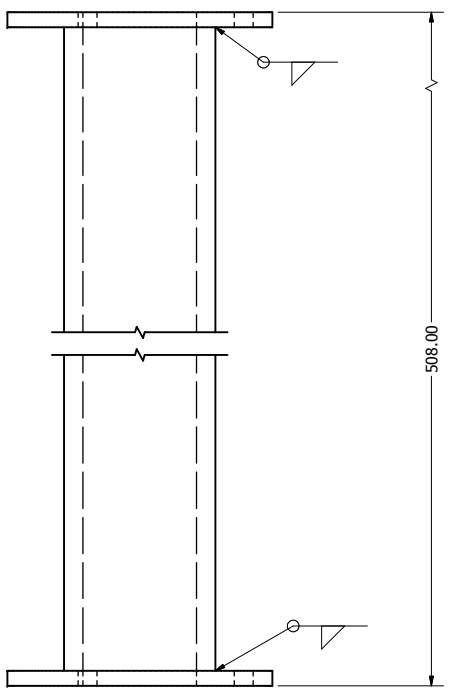
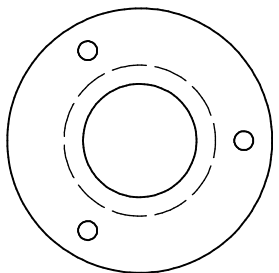
DRAWN BHY	14/09/2011	UNIVERSITY OF GUELPH			
CHECKED		TITLE			
QA		DRAFT TUBE - CONE (A)			
MFG					
APPROVED		SIZE C	DWG NO D05-02a	REV -	
		SCALE MM		SHEET 1 OF 1	



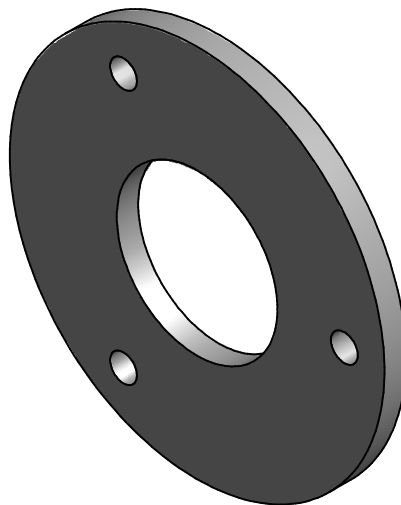
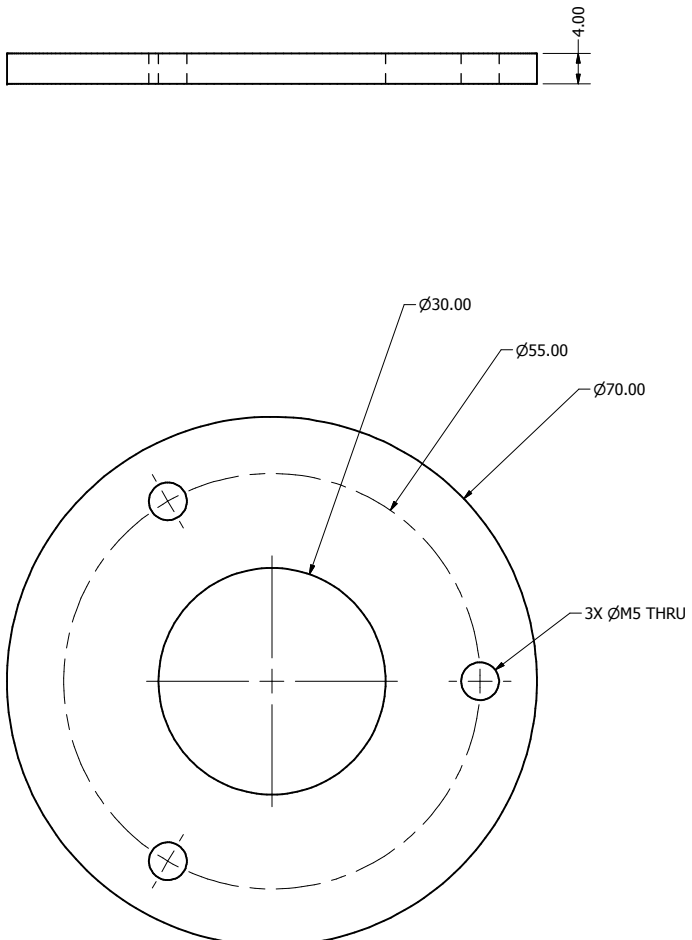
DRAWN BHY	14/09/2011	UNIVERSITY OF GUELPH		
CHECKED		TITLE		
QA		DRAFT TUBE - CONE (B)		
MFG				
APPROVED		SIZE C	DWG NO D05-02b	REV -
		SCALE MM		SHEET 1 OF 1



DRAWN BY BHY	30/08/2011	UNIVERSITY OF GUELPH			
CHECKED QA		TITLE			
MFG		INLET BASIN			
APPROVED		SIZE C	DWG NO D06-01	REV -	
		SCALE MM		SHEET 1 OF 1	

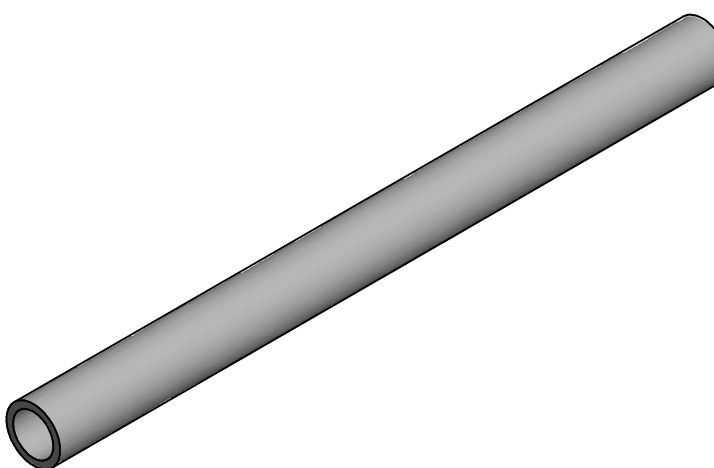
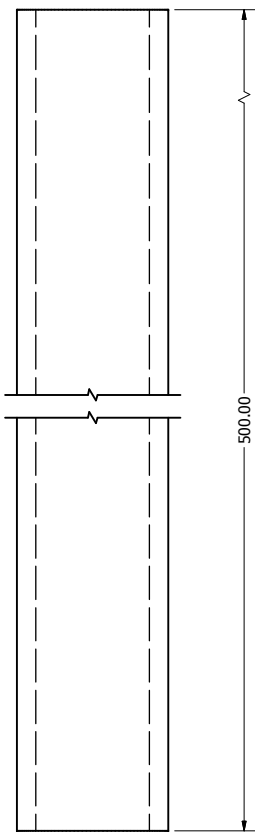


DRAWN BY	30/08/2011	UNIVERSITY OF GUELPH		
CHECKED		TITLE		
QA		HOUSING ASSEMBLY		
MFG				
APPROVED		SIZE C	DWG NO D07-00	REV -
		SCALE MM		SHEET 1 OF 1



DRAWN BY	30/08/2011	UNIVERSITY OF GUELPH		
CHECKED		TITLE		
QA		HOUSING-FLANGE		
MFG				
APPROVED		SIZE C	DWG NO D07-01	REV -
		SCALE MM		SHEET 1 OF 1

∅30.00
∅40.00



DRAWN BHY	30/08/2011	UNIVERSITY OF GUELPH		
CHECKED		TITLE		
QA		HOUSING - SLEEVE		
MFG				
APPROVED		SIZE C	DWG NO D07-02	REV -
		SCALE MM		SHEET 1 OF 1

Appendix C: Matlab Program Code - Detailed Design

This appendix includes the Matlab program code used for the detailed design of the camber-twist blade runner turbine, as discussed in Chapter 7.0.

```
%Multisection
%this is the matlab code for the design of a camber-twist blade runner
turbine

clear

%global constants
gravity=9.807    %gravity [m/s^2]
density=999       %density of water [kg/m^3]

%site conditions
head=2           %head pressure [m], USER INPUT
flow_rate=25     %volumetric flow rate [L/s], USER INPUT
rpm=1500         %desired angular velocity [rev/min], USER INPUT
omega=rpm*(2*pi)/60 %desired angular velocity [rad/s]
spec_speed_rpm_d=(rpm*sqrt(flow_rate/1000))/head^0.75  %specific speed
without gravity
hyd_eff_1=0.95-(13.2*flow_rate)^-0.32 %efficiency 1 (see Williams)
hyd_eff_2=hyd_eff_1+0.04-0.29*(0.32-log10(spec_speed_rpm_d*0.047))^2
%efficiency 2 (see Williams)
hyd_eff=(hyd_eff_1+hyd_eff_2)/2        %hydraulic efficiency, average of 1
and 2 USER INPUT
P_gross=head*(flow_rate/1000)*gravity*density
P_hyd=hyd_eff*P_gross %hydraulic power [W]

%overall design
d_t=0.13         %tip diameter [m], USER INPUT
d_h=0.07         %hub diameter [m], USER INPUT
d_h_d_t=d_h/d_t %hub diameter to tip diameter ratio

r_t=d_t/2         %tip radius [m]
r_h=d_h/2         %hub radius [m]
r_m=(r_t+r_h)/2 %mean radius [m]
num_sec=5         %number of sections
R=[r_h:(r_t-r_h)/(num_sec-1):r_t] %radial co-ordinates of sections
area=pi*((d_t/2)^2-(d_h/2)^2) %blade swept area [m^2]
circ_m=2*pi*r_m %mean circumference [m]
circ=2*pi*R %circumference [m]

%Velocity Triangles-Flow Conditions
U=(2*pi/60)*rpm*R %blade velocity [m/s]
C_x=(flow_rate/1000)/area %fluid absolute velocity, meridional/axial
component [m/s]
C_x=zeros(1,num_sec)+C_x

%Rotor Outlet
```

```

W_3=U      %fluid relative total velocity = blade velocity as per Nechleba
recommendation [m/s]
W_x3=C_x    %fluid relative axial velocity [m/s]
W_theta3=sqrt(W_3.^2-W_x3.^2) %fluid relative tangential velocity [m/s]
C_theta3=U-W_theta3 %fluid absolute axial velocity [m/s]
C_3=sqrt(C_theta3.^2+C_x.^2) %fluid absolute total velocity [m/s]
alpha_3=acosd(C_x./C_3) %flow angle between C and axial direction
beta_3=acosd(W_x3./W_3) %flow angle between W and axial direction
%Stator Outlet/Rotor Inlet
C_theta2=C_theta3+(gravity*hyd_eff*head./U) %define fluid absolute
tnagential velocity using Euler's equation
C_2=sqrt(C_theta2.^2+C_x.^2) %fluid absolute total velocity [m/s]
W_theta2=U-C_theta2 %fluid relative tangential velocity [m/s]
W_x2=C_x    %fluid relative axial velocity [m/s]
W_2=sqrt(W_theta2.^2+W_x2.^2) %fluid relative total velocity [m/s]
alpha_2=acosd(C_x./C_2) %flow angle between C and axial direction
beta_2=acosd(W_x2./W_2) %flow angle between W and axial direction

%Dimensionless Parameters
flow_coeff=C_x./U      %flow coefficient
load_coeff=(C_theta2-C_theta3)./U      %load coefficient
reaction=(W_3.^2-W_2.^2)./(W_3.^2-W_2.^2+C_2.^2-C_3.^2)      %reaction

%blade spacing calculation, but for some designs using other spacing
%recommendation rather than Zweifel
num_blades=4      %USER INPUT
s=circ./num_blades %pitch/blade spacing [m]
Zweifel_rotor=0.4./(cosd(beta_3).^2.* (tand(beta_2)+tand(beta_3)))
%space to chord ratio as per Zweifel for rotor
b=s./Zweifel_rotor %axial chord length [m]

%Nozzle Design as per Wright example PG 190
r_w=0.100 % USER INPUT - radius of nozzle [m]
h_w=0.4*d_t %height of nozzles/stator blades
alpha_w=atand(C_theta2/((flow_rate/1000)/(2*pi*r_w*h_w)))
%nozzle/stator blade angle
lambda=0.25*d_t %distance between base of nozzle blade and centre
height of rotor blades, as per Nechleba pg 342 recommendation

%Cavitation
%determine placement of runner within 2m head range
p_atm_sea=101330 %USER INPUT-atmospheric pressure at sea level and
15deg [Pa]
spec_weight_air=12.014 %USER INPUT-atmospheric specific weight at sea
level and 15deg [N/m^3]
z_site=2428 %USER INPUT-site elevation, M'muock Village, above sea
level [m]
z_sea=0 %sea level elevation above sea level [m]
p_atm_site=p_atm_sea-spec_weight_air*(z_site-z_sea) %ref fundamentals
of fluid mechanics pg 50 assume incompressible and isothermal
p_v=1783      %USER INPUT-water vapour pressure @15deg [Pa] ref
fundamentals of fluid mechanics pg 831]
z=1.5      %height difference between base of runner to surface of tail
water
P_spec_speed_omega=(omega*sqrt(P_hyd/density))/(gravity*head)^1.25
%power specific speed using rad/s

```

```

Thoma=((p_atm_site-p_v)/(density*gravity)-z)/head %Thoma coefficient

%Incidence and Deviation - ref Hothersall Pg 135
%deviation
stagger=0.5*(beta_2+beta_3) %stagger angle [deg] between mean camber
line and axial direction
stagger_H=90-stagger %stagger angle [deg] between mean camber line
and circumferential direction
camber_angle=beta_2-beta_3 %camber angle using angles wrt axial
camber_angle_H=beta_3-beta_2 %camber angle usually (leading edge-
trailing edge) but changed to match convention of Hothersall and angles
wrt circumference
L=0.127 %aligned chord length [m] based on chord length at hub USER
INPUT measured from drawings
m=[0.19, 0.195, 0.20, 0.20, 0.205] %Carters parameter, USER INPUT ref
Hothersall Pg 35 Fig 3.13 NOTE: Hothersall does angles wrt
circumference and not axis
deviation=m.*camber_angle_H.*s./L %[deg], ref Hothersall Pg 31 Eq
3.40
beta_3_f=beta_3+deviation %runner blade exit angle [deg] between W
and axial direction
%incidence
%refer to Hothersall Pg 34 Fig 3.12 (a&b)
t_blade=0.004 %blade thickness [m] as per Hothersall pg 138 Fig 14.3
USER INPUT
t_blade./L

inc_load=[5, 1.5, 1, 0.5, 0.5]
inc_block=[1, 1, 0.75, 0.5, 0.5]
incidence=inc_load-inc_block
beta_2_f=beta_2-incidence %runner blade inlet angle [deg] between W
and axial direction

```

Appendix D: Matlab Program Code - Flat Blade Runner Performance Prediction Model

This appendix includes the Matlab program code used for the performance prediction model of the flat blade runner, as described in Chapter 7.2.

```
%Flat Blade Performance Prediction Model
%this is the matlab code for the performance prediction model of a flat
%blade propeller runner

clear
%global constants
gravity=9.807      %gravity [m/s^2]
density=999         %density of water [kg/m^3]

%site conditions
head=2              %head pressure [m], USER INPUT
flow_rate_index=[5.6, 7.3, 11.1, 12.9, 15, 17.5, 20, 22.5, 25]
%volumetric flow rate [L/s], USER INPUT
for j=1:length(flow_rate_index)
    flow_rate=flow_rate_index(j)    %volumetric flow rate [L/s], USER
INPUT
    rpm=1500          %desired angular velocity [rev/min], USER INPUT
    omega=rpm*(2*pi)/60 %desired angular velocity [rad/s]
    spec_speed_rpm_d=(rpm*sqrt(flow_rate/1000))/head^0.75 %specific
speed without gravity
    hyd_eff_1=0.95-(13.2*flow_rate)^-0.32 %efficiency 1 (see Williams)
    hyd_eff_2=hyd_eff_1+0.04-0.29*(0.32-
log10(spec_speed_rpm_d*0.047))^2 %efficiency 2 (see Williams)
    hyd_eff=(hyd_eff_1+hyd_eff_2)/2        %hydraulic efficiency, average
of 1 and 2 USER INPUT
    P_gross=head*(flow_rate/1000)*gravity*density
    P_hyd=hyd_eff*P_gross %hydraulic power [W]

    %overall design
    d_t=0.13          %tip diameter [m], USER INPUT
    d_h=0.07          %hub diameter [m], USER INPUT
    d_h_d_t=d_h/d_t %hub diameter to tip diameter ratio

    r_t=d_t/2          %tip radius [m]
    r_h=d_h/2          %hub radius [m]
    r_m=(r_t+r_h)/2  %mean radius [m]
    num_sec=5          %number of sections for Blade Element Method
analysis
    R=[r_h:(r_t-r_h)/(num_sec-1):r_t]    %radial co-ordinates of
sections
    area=pi*((d_t/2)^2-(d_h/2)^2)    %blade swept area [m^2]
    circ_m=2*pi*r_m    %mean circumference [m]
    circ=2*pi*R %circumference [m]
    num_blades=4        %USER INPUT number of blades
```

```

%Nozzle Design as per Wright example PG 190
r_w=0.100 % USER INPUT - radius of nozzle [m] (same as powerpal)
h_w=0.4*d_t %height of nozzles/stator blades
gv_angle=72.3 %USER INPUT stator guide vane angle from drawings
C_theta2=tand(gv_angle)*((flow_rate/1000)/(2*pi*r_w*h_w)) %fluid
absolute velocity, tangential component [m/s]
C_theta2=zeros(1,num_sec)+C_theta2
C_x=(flow_rate/1000)/area %fluid absolute velocity,
meridional/axial component [m/s]
C_x=zeros(1,num_sec)+C_x
%in the stator design the guide vanes are set to achieve this
C_theta_2, so
%even though it is a function of "U" and we do a range of "U"s
below the
%stator is fixed and the approaching absolute fluid velocity is
defined
C_2=sqrt(C_theta2.^2+C_x.^2) %fluid absolute total velocity [m/s]
alpha_2=acosd(C_x./C_2) %flow angle between C and axial direction

rpm_test=[0:100:1500] %range of [rpm]
omega_test=rpm_test*(2*pi)/60 %range of [rad/s]

for n=1:num_sec
    U_test(:,n)=omega_test*R(n) %range of blade velocities [m/s]
end

for n=1:length(U_test)
    W_theta2_test(n,:)=U_test(n,:)-C_theta2 %range of tangential
relative flow speeds [m/s]
    W_2_test(n,:)=sqrt(W_theta2_test(n,:).^2+C_x.^2) %range of
relative fluid velocities [m/s]
    beta_2_test(n,:)=atand(W_theta2_test(n,:)./C_x) %range of flow
angles [deg]
end

dW=diff(R) %define blade section width [m]
dW(:,1)=[] %define blade section width [m]
dW=[dW(1)/2,dW,dW(end)/2] %define blade section width [m]
dA=dW.*circ %define planform area [m^2]

Angle_Attack=[0:10:90;] %define range of angle of attacks
C_N=[2*pi*sind(Angle_Attack)./(4*pi*sind(Angle_Attack))*1.98/0.88]
%Normal coefficient from Hoerners Lift
C_L=C_N.*cosd(Angle_Attack) %Lift coefficient (normal to flow) from
Hoerners Lift
C_D=C_N.*sind(Angle_Attack) %Drag coefficient (parallel to flow)
from Hoerners Lift
C_L2=2*sind(Angle_Attack).*cosd(Angle_Attack) %Lift coefficient
(normal to flow) from flat plate theory
C_D2=2*(sind(Angle_Attack)).^2 %Drag coefficient (normal to flow)
from flat plate theory

fig1=plot(Angle_Attack,C_L,Angle_Attack,C_L2,Angle_Attack,C_D,Angle_Attack,C_D2)

```

```

blade_set_angle=71 %define blade setting angle [deg] ref to axial

%define abs(delta)=abs(angle between blade and W)
[nrows,ncols]=size(U_test)
for r = 1:nrows
    for c = 1:ncols
        if beta_2_test(r,c)<=blade_set_angle && beta_2_test(r,c)>=0
%for case 0<=flow angle<=blade angle
            delta(r,c)=blade_set_angle-beta_2_test(r,c)
        elseif beta_2_test(r,c)>blade_set_angle      %for case flow
angle>blade angle
            delta(r,c)=beta_2_test(r,c)-blade_set_angle
        else beta_2_test(r,c)<0 %for case flow angle<0
            delta(r,c)=beta_2_test(r,c)*-1+blade_set_angle
        end
    end
end

%define lift coefficient and drag coefficient and assign direction
relative
%to +ve U dir
for r = 1:nrows
    for c = 1:ncols
        if beta_2_test(r,c)<=blade_set_angle && beta_2_test(r,c)>=0
%for case 0<=flow angle<=blade angle
            C_L_test(r,c)=interp1(Angle_Attack,C_L2,delta(r,c))
            C_D_test(r,c)=interp1(Angle_Attack,C_D2,delta(r,c))*-1
        elseif beta_2_test(r,c)>blade_set_angle      %for case flow
angle>blade angle
            C_L_test(r,c)=interp1(Angle_Attack,C_L2,delta(r,c))*-1
            C_D_test(r,c)=interp1(Angle_Attack,C_D2,delta(r,c))*-1
        elseif beta_2_test(r,c)<0 && delta(r,c)>=90 %for case flow
angle<0 && delta>=90
            C_L_test(r,c)=interp1(Angle_Attack,C_L2,delta(r,c)-90)*-1
            C_D_test(r,c)=interp1(Angle_Attack,C_D2,delta(r,c)-90)
        else beta_2_test(r,c)<0 && delta(r,c)<90      %for case flow
angle<0 && delta<90
            C_L_test(r,c)=interp1(Angle_Attack,C_L2,delta(r,c))
            C_D_test(r,c)=interp1(Angle_Attack,C_D2,delta(r,c))
        end
    end
end

for n=1:length(U_test)
    Lift_test(n,:)=0.5*density*W_2_test(n,:).^2.*dA.*C_L_test(n,:)
%calculate range of lift forces [N]
    Drag_test(n,:)=0.5*density*W_2_test(n,:).^2.*dA.*C_D_test(n,:)
%calculate range of drag forces [N]
end

Lift_proj=Lift_test.*cosd(abs(beta_2_test)) %project lift forces to
tangential axis
Drag_proj=Drag_test.*sind(abs(beta_2_test)) %project drag forces to
tangential axis

```

```

L_D_sum=Lift_proj+Drag_proj %sum lift and drag forces for each
section
Torque_sum_test=R*L_D_sum' %calculate torque for each section
Power_test=num_blades*Torque_sum_test.*omega_test %calculate
total power by multiplying by rotation speed and number of blades
for n=1:length(U_test) %set power=0 for negative power points
    if Power_test(n)<0
        Power_test(n)=0
    end
end

xls_out(:,j)=Power_test %output table of results

end
fig2=plot(rpm_test,xls_out) % plot results

```

Appendix E: Uncertainty Analysis

Experimental uncertainty was calculated for the mechanical power and hydraulic efficiency results of the performance tests. Methods by Coleman and Steele (Coleman & Steele, 1989) were followed. Uncertainty values are expressed at the 68% confidence level. The sources of uncertainty from the instrumentation are tabulated.

Table E1: Instrumentation uncertainty

Variable	Instrument	Uncertainty
Force 1, ΔF_1	Load cell LCDA-1	Varies with load (Figure E1)
Force 2, ΔF_2	Load cell LCDA-2	Varies with load (Figure E1)
Radius, Δr_{vp}	V-notched pulley	0.01 mm
Rotational speed, Δn	Hall effect sensor	6 rpm
Flow rate 1, ΔQ_1	Gas powered water pump 1	0.43 L/s
Flow rate 2, ΔQ_2	Gas powered water pump 2	0.73 L/s
Flow rate 3, ΔQ_3	Gas powered water pump 3	0.42 L/s
Head, ΔH	Meter scale	0.005 m

Repeated load cell measurements over a range of applied loads were conducted to determine the standard error of the load cells for a given applied load and illustrated for each device in Figure E1.

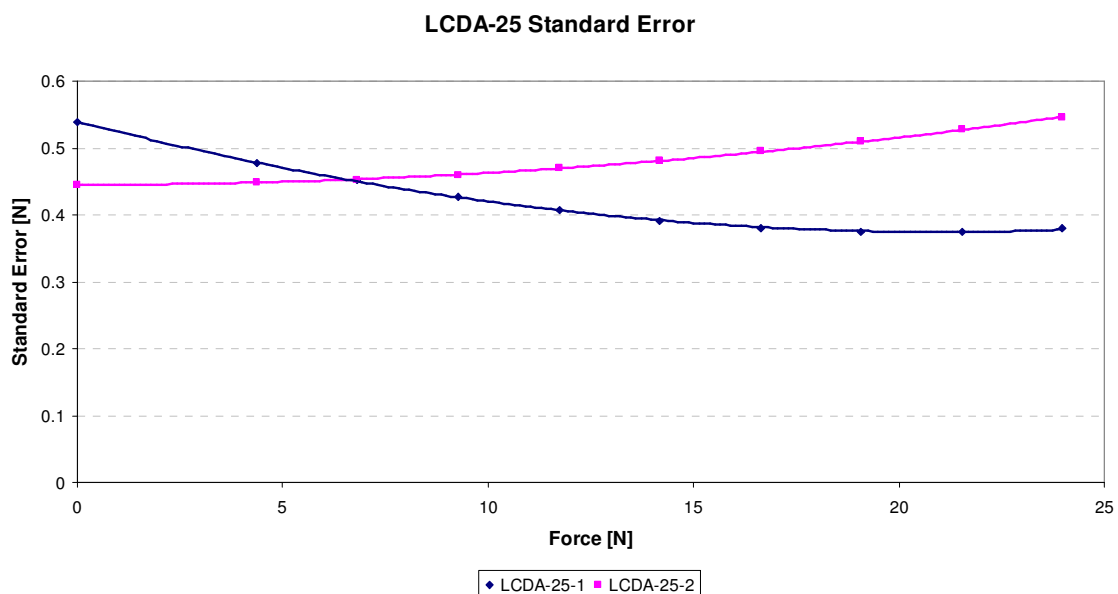


Figure E1: Load cell standard error versus applied load

Repeated radius measurements of the V-notch pulley using callipers were recorded to determine the uncertainty attributed to physical variation of the pulley, measurement misalignment, and instrument resolution.

The uncertainty of the rotation speed measurements using the Hall effect sensor was attributed to the resolution of the sensor and timing of the test sample. The pulses were counted in the 10 second test duration to determine rotation speed. The uncertainty of the rotation speed measurement was +/- 1 revolution per 10 second duration, or +/- 6 rpm.

Flow rates of the gas powered pumps were calculated by filling a known volume using each individual pump and measuring the time to completely fill the volume. This calculation involved sources of uncertainty from the volume measurements and the timing measurements. The volume measurement was due to instrument resolution, misalignment, and parallax. The timing measurements were due to lag time and personal error. These sources of uncertainty propagated through to the standard combined uncertainty of the flow rates. For the performance tests involving combination of pumps, the uncertainty values were also combined. The uncertainty of the head measurements was attributed to the resolution of the scale, parallax, and misalignment of the measuring scale.

Mechanical power, P , was calculated using equation (E.1).

$$P = \tau\omega = (F_1 - F_2)r_{vp}\omega \quad (\text{E.1})$$

The uncertainty in the mechanical power measurements, ΔP , was determined as follows:

$$\frac{\Delta P}{P} = \sqrt{\left(\frac{\Delta F_1}{F_1} + \frac{\Delta F_2}{F_2}\right)^2 + \left(\frac{\Delta r_{vp}}{r_{vp}}\right)^2 + \left(\frac{\Delta \omega}{\omega}\right)^2} \quad (\text{E.2})$$

Efficiency, η , was evaluated using equation (E.3).

$$\eta = \frac{P}{\rho g H Q} \quad (\text{E.3})$$

The uncertainty in the efficiency measurements, $\Delta\eta$, was calculated using (E.4).

$$\frac{\Delta\eta}{\eta} = \sqrt{\left(\frac{\Delta P}{P}\right)^2 + \left(\frac{\Delta H}{H}\right)^2 + \left(\frac{\Delta Q}{Q}\right)^2} \quad (\text{E.4})$$